Characterization and flow simulations of discrete fracture networks

Dissertation

der Mathematisch-Naturwissenschaftlichen Fakultät

der Eberhard Karls Universität Tübingen

zur Erlangung des Grades eines

Doktors der Naturwissenschaften

(Dr. rer. nat.)

vorgelegt von

Dipl.-Geol. Conny Zeeb

aus Nürtingen

Tübingen

2013

Tag der mündlichen Qualifikation:	18.07.2013
Dekan:	Prof. Dr. Wolfgang Rosenstiel
1. Berichterstatter:	Jun.-Prof. Dr. habil. Philipp Blum
2. Berichterstatter:	Prof. Dr. Paul D. Bons

Dedicated to Gabriela and Berthild.

Acknowledgements

First of all, I would like to thank Jun.-Prof. Dr. habil. Philipp Blum, Prof. Paul D. Bons and Dr. Enrique Gomez Rivas for their never-ending support and valuable help. Moreover I would like to thank the members of the FRACS group for the opportunity to work with them on this ambitious research project and the various support for my work. My PhD was carried out within the framework of DGMK (German Society for Petroleum and Coal Science and Technology) research project 718 "Mineral Vein Dynamics Modelling", which is funded by the companies ExxonMobil Production Deutschland GmbH, GDF SUEZ E&P Deutschland GmbH, RWE Dea AG and Wintershall Holding GmbH, within the basic research program of the WEG Wirtschaftsverband Erdöl- und Erdgasgewinnung e.V. I thank the companies for their financial support and their permission to publish my results. I am also thankful to all colleagues and friends for many fruitful discussions. They also often helped lift my spirit along the way.

Abstract

Fractures, such as joints, faults and veins, strongly influence the transport of fluids through rocks by either enhancing or inhibiting flow. Especially in rocks with negligible permeability fractures can act as major for fluid conduits. Therefore, the contribution of fracture networks to the overall flow behavior is of high interest to, for example, the hydrocarbon industry, the power generation using deep geothermal systems, the sustainable management of fractured rock aquifers, the planning of high risk waste repositories and geotechnical projects situated in fractured rock. The fluid transport through a fractured rock mass can be simulated by continuum, discrete fracture network (DFN) or hybrid models. Latter combines aspects of the continuum and the DFN approaches. Especially the DFN approach relies on a detailed knowledge of fracture network characteristics. In the subsurface fractures and fracture networks are typically characterized studying well cores and image logs, whereas at the surface outcropping subsurface analogues are studied. Especially outcrops provide valuable information such as fracture length and length distribution, which are important parameters for fluid transport simulations. The fracture networks encountered at outcrops are commonly analyzed applying the scanline sampling, window sampling, or the circular scanline and window method. These methods vary in their application and the parameters they provide. Therefore, each method has its specific advantages and limitations, which are summarized in a critical review.

In order to compare the application of the scanline sampling, window sampling, and the circular scanline and window methods, natural fracture networks outcrops of (1) Ignimbrites at Craghouse Park, UK, (2) the Wajid Sandstone in Saudi Arabia, and (3) Miocene limestone in the Oman Mountains, Oman are analyzed. Although, sampling biases such as orientation, truncation and size bias were accounted for, the network parameters calculated from different sampling methods show significant differences. Two plausible explanations for those differences exist: (1) a lack of measurements to adequately define the fracture network parameters, and (2) the influence of censoring bias on the estimated network parameters. Artificially generated orthogonal two-dimensional fracture networks (AFNs) with known input parameters were used two evaluate (1) the required minimum number of measurements for each sampling method, and (2) quantify the influence of censoring bias on the evaluation of fracture network parameters. The large numbers of

sampling areas investigated during this process were analyzed using the novel software FraNEP (Fracture Network Evaluation Program), which was developed as part of this thesis.

The lowest minimum number of measurements to adequately capture the statistical properties of fracture networks was found to be 110 for the window sampling method, followed by the scanline sampling method with 225. For the application of the circular scanline and window method at least 860 fractures should be present in a sampling area. Although, these numbers are not universally applicable, they may serve as a first guideline for the analyses of fracture populations with similar length distributions. The latter resemble those reported for typical natural fracture networks. Furthermore, the window sampling method proved to be the method that is least sensitive to censoring bias. Reevaluating the natural fracture networks proved that the existing percentage of censored fractures significantly influences the accuracy of inferred fracture network parameters.

Zusammenfassung

Klüfte haben einen starken Einfluss auf den Fluidtransport im Festgestein, da sie diesen verstärken oder verringern können. Vor allem in Gesteinen mit geringer Permeabilität sind Klüfte häufig die einzigen Transportwege für Fluide. Aus diesem Grund sind Kluftnetze von großem Interesse für den Fluidtransport, z. B. in der Kohlenwasserstoffindustrie, der geothermischen Energieerzeugung, der nachhaltigen Nutzung von Grundwasser aus geklüfteten Aquiferen, der Planung von nuklearen Endlagern sowie bei geotechnischen Projekten in geklüftetem Fels. Der Fluidtransport in geklüftetem Festgestein kann mithilfe von Kontinuums-, diskreten Kluftnetzwerk (DFN)-, oder Hybrid-Modellen simuliert werden. Dabei ist speziell der DFN-Ansatz auf ein detailliertes Wissen über die Klufteigenschaften angewiesen. Im Untergrund werden Klüfte und Kluftnetze typischerweise anhand von Bohrkernen und Aufnahmen der Bohrlochwand charakterisiert, während man an der Oberfläche zum Untergrund analoge Aufschlüsse untersucht. Vor allem diese Aufschlüsse liefern wichtige Informationen zu Kluftlängen und deren statistischer Verteilung. Diese Parameter sind sehr wichtig für die numerische Simulation des Fluidtransports. Kluftnetze in Aufschlüssen werden typischerweise mithilfe der "*Scanline Sampling*", der "*Window Sampling*", oder der "*Circular Scanline and Window*" Methoden untersucht. Diese Aufnahmemethoden unterscheiden sich in ihrer Anwendung und den bestimmten Parametern. Daher hat jede dieser Methoden spezifischen Vor- und Nachteile. Die Methoden werden eingehend beschrieben und deren Vor- und Nachteile diskutiert.

Um die Anwendung der drei Methoden zu vergleichen, wurden natürliche Kluftnetze in Aufschlüssen (1) von Ignimbriten nahe "*Craghouse Park*", GB, (2) des "*Wajid Sandstone*" in Saudi Arabien, und (3) von Miozänen Kalken in den "*Oman Mountains*", Oman untersucht. Obwohl die Messunsicherheiten, wie "*Orientation Bias*", "*Truncation Bias*" und "*Size Bias*" berücksichtigt wurden, unterscheiden sich die berechneten Parameter deutliche in Abhängigkeit der angewandten Methode. Hierfür gibt es zwei mögliche Gründe: (1) die Anzahl der Messwerte war zu gering um die Parameter adäquat zu bestimmen, und (2) die berechneten Parameter sind von "*Censoring Bias*" beeinflusst. Künstliche Kluftnetze (AFN) mit bekannten Eingabeparametern wurden benutzt, um (1) die benötigte minimale Anzahl von Messwerten für jede Methode abzuschätzen, und (2) den Einfluss von "*Censoring*

Bias" auf die Berechnung der Parametern zu quantifizieren. Die große Anzahl der untersuchten Arbeitsgebiete wurde mithilfe der im Rahmen dieser Arbeit entwickelten Software FraNEP (Fracture Network Evaluation Program) analysiert.

Die kleinste benötigte minimale Anzahl von Messwerten zur adäquaten Auswertung der statistischen Eigenschaften eines Kluftnetzes ist 110 für die "*Window Sampling*" Methode, gefolgt von der "*Scanline Sampling*" Methode mit 225. Für die Anwendung der "*Circular Scanline and Window*" Methode sollten mindestens 860 Klüfte im Untersuchungsgebiet vorhanden sein. Obwohl diese Werte nicht universell anwendbar sind, stellen diese einen Richtwert für die Auswertung von Kluftdaten mit einer vergleichbaren Längenverteilung dar. Darüber hinaus erwies sich "*Window Sampling*" als die am wenigsten für "*Censoring Bias*" anfällige Methode. Eine erneute Auswertung der natürlichen Kluftnetze zeigte, dass die prozentuale Anzahl der zensierten Klüfte einen deutlichen Einfluss auf die Genauigkeit der berechneten Kluftparameter hat.

Content

Abbreviations

1D	One-dimensional
2D	Two-dimensional
3D	Three-dimensional
AFN	Artificial fracture network
CE	Circular estimator (or: circular scanline and window method)
DFN	Discrete fracture network
EPM	Equivalent porous media
FraNEP	Fracture Network Evaluation Program
LIDAR	Light detection and ranging
MSE	Maximum-squared-error
RMSE	Root-mean-squared-error
SLS	Scanline sampling
SSE	Sum of squared errors
UK	United Kingdom
UTM	Universal Transverse Mercator
VBA	Visual Basic for Applications
WS	Window sampling

Nomenclature

A	area [m²]
a_h	hydraulic fracture aperture [m]
a_m	mechanical fracture aperture [m]
d	maximum distance used to evaluate the lower cut-off for truncation bias applying the chord method [-]
E	exponent of a power-law function [-]
E_{2D}	exponent of a power-law function evaluated from fracture lengths measured by window sampling [-]
f	scaling factor for hydraulic apertures [-]
g	gravitational acceleration [m s^{-2}]
i	designator for individual fractures [-]
I	fracture intensity:
$P10$	linear fracture intensity (1D) [m^{-1}]
$P21$	areal fracture intensity (2D) [m m^{-2}]
$P32$	volumetric fracture intensity (3D) [m^2 m^{-3}]
j	designator for individual fracture sets [-]
JRC	joint roughness coefficient [-]
k	hydraulic conductivity [m s^{-1}]
k_{eff}	effective hydraulic conductivity (matrix + fractures) [m s^{-1}]
$k_{eff\ (max)}$	maximum effective hydraulic conductivity [m s^{-1}]
$k_{eff\ (mean)}$	mean effective hydraulic conductivity [m s^{-1}]
$k_{eff\ (min)}$	minimum effective hydraulic conductivity [m s^{-1}]
k_m	hydraulic conductivity of the matrix [m s^{-1}]
$k_{m\ (max)}$	maximum hydraulic conductivity of the matrix [m s^{-1}]
$k_{m\ (mean)}$	mean hydraulic conductivity of the matrix [m s^{-1}]
$k_{m\ (min)}$	minimum hydraulic conductivity of the matrix [m s^{-1}]
k_f	hydraulic conductivity of the fracture network [m s^{-1}]
$k_{f\ (eva)}$	evaluated hydraulic conductivity of the fracture network [m s^{-1}]
l	fracture (trace) length [m]
l_0	lower cut-off length [m]
l_m	mean fracture length [m]
L	length of a scanline [m]

L	is an arbitrary unit of length
m	number of fracture endpoints inside a circular scanline [-]
n	number of fracture intersections with a circular scanline [-]
N	total number of sampled fractures [-]
o	strike (2D) or orientation (3D) of a fracture [°]
o_m	mean fracture strike (2D) or mean fracture orientation (3D) in a fracture set [°]
o_{max}	maximum fracture strike (2D) or maximum fracture orientation (3D) in a fracture set [°]
o_{min}	minimum fracture strike (2D) or minimum fracture orientation (3D) in a fracture set [°]
$Occurrence$	frequency of an individual fracture [-]
p	fracture density:
$P20$	areal fracture density (2D) [m^{-2}]
$P30$	volumetric fracture density (3D) [m^{-3}]
Q	fluid flow [m^2 s^{-1}]
r	radius of a circular scanline [m]
S	fracture spacing (distance between two adjacent fractures) [m]
S_A	apparent spacing between two adjacent fractures [m]
S_{2D}	true spacing between two adjacent fracture traces [m]
S_{3D}	true spacing between two adjacent fracture planes [m]
UCS	uniaxial compressive strength [Pa]
X	x-coordinate
X_{dir}	direction along x-axis
Y	y-coordinate
Y_{dir}	direction along y-axis
α	dip direction [°]
β	dip [°]
η	fluid viscosity [kg m^{-2} s^{-1}]
θ	angle between a scanline and the pole of a fracture [°]
θ_{2D}	angle between the normal of a fracture trace and a scanline [°]
θ_{3D}	angle between the normal of a fracture plane and a scanline [°]
λ	decay rate of a negative exponential function [-]

μ	mean of the natural logarithm of l in a log-normal cumulative distribution function [-]
ρ	fluid density [kg m^{-3}]
σ^2	standard deviation of the natural logarithm of l in a log-normal cumulative distribution function [-]
∇h	hydraulic head [m m^{-1}]

1. Introduction

Mechanical discontinuities such as fractures significantly influence the fluid transport in geologic formations, especially in rocks with negligible permeability. Therefore, an accurate description of individual fracture and fracture network parameters is essential for simulating the hydraulic behavior of fractured rock masses. In hydrocarbon reservoirs, especially in the unconventional ones, fractures can completely control well productivity. The productivity can be higher due to an increased influx of hydrocarbons into a borehole, but also lowered if a breakthrough of water occurs (e.g. Belayneh et al., 2009). Similar considerations have to be taken into account when extracting heat from deep geothermal systems. The aim is a high productivity without the risk of a thermal breakthrough (e.g. Blöcher et al., 2010). With a changing climate, managing water resources is becoming more and more crucial. Especially in arid and semiarid regions aquifers are often situated in fractured rock masses. For sustainable water management detailed knowledge about these fracture aquifers is required (e.g. Zeeb et al., 2010). Another research topic is the security assessment of high-risk waste repositories. Here fractures can make the difference whether particles from a repository reach the biosphere in decades, millennia or never at all (e.g. Blum et al., 2005). Above examples illustrate well the importance of an as accurate as possible fracture and fracture network analysis.

In the sections below an overview is provided on the characterization of fractured rock masses. The introduction briefly summarizes: (1.1) fracture mechanics, (1.2) the concepts of simulating fluid transport in a fractured rock mass, (1.3) the methodology of discrete fracture network (DFN) generation, (1.4) fracture and (1.5) fracture network parameters, (1.6) difficulties and biases associated with fracture sampling, and (1.7) commonly used sampling methods.

1.1. Fracture mechanics

Fractures are the result of brittle failure of rock due to stress. The Mohr-Griffith-Coulomb failure criterion is usually used to explain the different failure modes and orientations of resulting fractures (Bons et al., 2012). Mechanical failure occurs as a result of principal stresses, their orientations and the mechanical properties of the

failing material (Brace, 1960; Phillips, 1972; Price and Cosgrove, 1990; Sibson, 1998; Laubach et al., 2009; Cox, 2010; Bons et al., 2012). The rocks strength to withstand fracturing is a function of the rocks tensile strength, its cohesion and its internal angle of friction. As soon as the effective stress (principal stresses minus pore fluid-pressure) exceeds this rock strength, fracturing occurs.

An extensive terminology exists to describe mechanical defects in rocks and the related notations often adhere to the process, which led to the formation of the defect. For example, Van der Pluijm & Marshak (2004) describe 16 different forms of brittle deformation. Three end-member brittle failure modes are described by Pollard and Segall (1987) and Scholz (2002): (Mode I) opening mode failure, (Mode II) in-plane shear or sliding mode failure, and (Mode III) out-of-plane shear or tearing mode failure. In geology, we commonly distinguish between extensional and shear fractures (Bons et al., 2012). The terminology presented by Bons et al. (2012) distinguishes between three types of fractures: (1) extensional fractures, (2) obliquely opening or hybrid fractures and (3) shear fractures. Extensional fractures form with an opening vector perpendicular to the fracture plane. Hybrid fractures have an opening vector at an oblique angle to the fracture plane. Shear fracture do not exhibit an opening mode component. Syn- and post-tectonic processes, such as changes in the stress field or mineral precipitation on fracture walls, can lead to a closure of fractures. Fractures filled by mineral precipitates are typically referred to as veins (e.g. Bons et al., 2012). In this manuscript however the general term “fracture” is used.

1.2. Simulation of fluid transport

Fluid transport in a fractured medium can be simulated using (1) a continuum approach, in which a volume of rock is treated as an equivalent porous media (EPM), (2) a DFN approach, in which each fracture is represented as a discrete feature, or (3) a hybrid approach, which combines both previous concepts. A detailed review of these concepts as well as the characterization of flow and transport behavior in fractured media is provided, for example, by Neuman (2005).

In DFN models each fracture is individually represented with all its geometric parameters (i.e. fracture length and aperture), which are translated into equivalent

fluid flow properties (i.e. permeability, hydraulic conductivity or hydraulic fracture aperture). The DFN concept generally depends on the geometric and hydraulic properties of the fracture network (e.g. Lee and Farmer, 1993; Dershowitz et al., 2000) and models are typically treated in a stochastic framework (Berkowitz, 2002), meaning that multiple realizations of fracture networks are studied using Monte Carlo analysis (e.g. Blum et al., 2005; 2009). Based on the results of such an analysis a 2D or 3D permeability tensor is calculated, which can be used for the subsequent upscaling of the fracture network hydraulic properties in an EPM (e.g. Blum et al., 2009). The latter can be used, for example, in a continuum model.

1.3. Discrete fracture network generation

DFN are typically generated based on the statistical parameters calculated by analyzing natural fracture networks. In this section the concept of the DFN generator FracFrac (Blum et al., 2005) is described. FracFrac is developed in Visual Basic for Applications (VBA) in Microsoft® Excel. For the generation of a DFN fractures are typically grouped into sets. Each set is defined by (1) averaged fracture orientation, (2) fracture density, and (3) fracture length distribution. Based on the input fracture density, fracture centers are commonly placed in a predefined generation region using a random Poisson distribution model. Depending on the probability of a fracture length to be present in the generation region a length is assigned to each fracture center. The probability is described by the cumulative distribution of fracture lengths. The orientation of the fracture equals the input mean orientation.

In the current study a truncated power-law is used to describe the cumulative distribution of fracture lengths. The truncated power-law is given by (Blum et al., 2005; Riley, 2005):

$$f(l) = 1 - \left(\frac{l}{l_0}\right)^{-E} \quad (1)$$

where l is the fracture length, l_0 the lower cut-off length and E the exponent of the power-law function. The lower cut-off is required to constrain the range of fracture lengths in a DFN and is commonly related to a specific case study, the scale of observation or truncation bias (section 1.6).

1.4. Fracture parameters

Individual fractures are commonly described by (1) the wall rock rheology, (2) size, (3) orientation, (4) aperture, (5) displacement, and (6) filling (e.g. Lee and Farmer, 1993; Barton and Quadros, 1997; Renshaw et al., 2000; Laubach 2003; Laubach and Ward, 2006). Table 1 provides a short summary of above parameters.

Wall rock rheology encompasses the properties of the fracture wall, such as its uniaxial compressive strength UCS and the joint roughness coefficient JRC. The UCS describes the strength of the fracture wall to withstand loading. The JRC is a dimensionless value that can be used to describe the asperities (roughness) of a fracture wall. As an example, both parameters are used to model fracture closure under load (Barton & Bandis, 1980; Barton et al., 1985).

Table 1. Parameters of individual fractures required to adequately simulate fluid flow through fractured rocks (modified from Zeeb et al., 2013a; Copyright AAPG 2013, reprinted by permission of the AAPG).

Parameter		Definition
Filling		The filling of the fracture void determines whether a fracture acts as conduit or prevents fluid flow.
Displacement		The displacement of fracture walls against each other.
Wall rock rheology		The uniaxial compressive strength (UCS) and the joint roughness coefficient (JRC) influence fracture closure under increased loading. Furthermore, JRC also controls hydraulic fracture aperture.
Orientation		Orientation (3D, defined by dip and dip direction) or strike (2D) of a fracture [°]
Aperture	Mechanical (a_m)	Real distance between the two walls of a fracture.
	Hydraulic (a_h)	Effective hydraulic fracture aperture according to the cubic law.
Size	Length (l)	The length of the fracture trace on a sampling plane [m]
	Area	The area of the fracture plane [m^2]
	Volume	The volume of the fracture void [m^3]

The size of a fracture is the trace length l on an outcrop, the area of the fracture plane or the volume of the fracture void. Since fracture sampling at outcrops is often restricted to two dimensions, the trace-length of a fracture is commonly used to describe fracture size and size distribution.

The orientation (3D) or strike (2D) can be used to reconstruct the palaeo-stressfield, which led to the formation of the fracture (e.g. Bons et al., 2012).

Orientation is also often used as an indicator to group fractures into sets. Moreover, longer fractures tend to follow a preferential orientation more closely than smaller ones.

For the description of fracture aperture we distinguish between the mechanical aperture a_m, which is the actual distance between fracture walls, and the hydraulic aperture a_h, which is used for fluid flow calculations and is smaller than the mechanical aperture. Latter can be thought of as a mean value that does not account for asperities or flow channeling. The hydraulic aperture is typically used in the parallel plate or cubic law assumption, which describes the fluid transport in a fracture as laminar flow between two smooth parallel plates (Snow, 1965). Hydraulic and mechanical aperture can be related to each other by (Barton and de Quadros, 1997):

$$a_h = \frac{{a_m}^2}{JRC^{2.5}} \tag{2}$$

Displacement describes the offset of fracture walls against each other. This offset can cause a channeling of fluid flow (e.g. Schwarz & Enzmann, 2013) and also a self-propping effect of fractures under high confining pressures (Durham & Bonner, 1994).

The filling of the fracture void determines whether a fracture acts as a conduit or prevents fluid flow. Fluids typically transport minerals, which can precipitate on the fracture walls. This process leads to a reduction of fracture aperture or even to the complete closure of a fracture, which would then be referred to as a vein (e.g. Bons et al., 2012).

1.5. Fracture network parameters

Fracture networks are commonly described by: (1) fracture density, (2) fracture intensity, (3) fracture spacing, (4) fracture mean length and (5) fracture length distribution (e.g. Priest, 1993; Narr, 1996; Mauldon et al., 2001; Castaing et al., 2002; Ortega et al., 2006; Blum et al. 2007; Neuman, 2008). Table 2 summarizes above parameters.

Table 2. Definition of fracture density p, intensity I, spacing S and mean length lm and governing equations to calculate these parameters using the scanline sampling, window sampling and circular estimator methods. The latter is based on Rohrbaugh et al. (2002). The definitions of fracture length distributions and orientations evaluated by the scanline sampling and window methods are also included. Dershowitz (1984) introduced notations to distinguish between linear, areal and volumetric fracture densities and intensities ($P20$, $P30$, etc.) (modified from Zeeb et al., 2013a; Copyright AAPG 2013, reprinted by permission of the AAPG).

Parameter		Definition	SLS	WS	CE
Density (p)	Areal ($P20$)	Number of fractures per unit area [m^{-2}]	-	$p_{WS} = \frac{N}{A}$	$p_{CE} = \frac{m}{2\pi r^2}$
	Volumetric ($P30$)	Number of fractures per unit volume [m^{-3}]	-	-	-
Intensity (I)	Linear ($P10$)	Number of fractures per unit length [m^{-1}]	$I_{SLS} = \frac{N}{L}$	-	-
	Areal ($P21$)	Fracture length per unit area [m m^{-2}]	-	$I_{WS} = \frac{\sum l}{A}$	$I_{CE} = \frac{n}{4r}$
	Volumetric ($P32$)	Fracture area per unit volume [m m^{-2}]	-	-	-
Spacing (S)	Linear	Spacing between fractures [m]	$S = 1/I_{SLS}$	-	-
Mean length (l_m)	Linear	Mean fracture length [m]	$l_{m;\,SLS} = \frac{\sum l}{N}$	$l_{m;\,WS} = \frac{\sum l}{N}$	$l_{m;\,CE} = \frac{\pi r}{2}\frac{n}{m}$
Length distribution	1D	Fractures intersecting with a scanline	yes	-	-
	2D	Fractures intersecting with a sampling area	-	yes	-
Orientation	2D	Orientation of a fracture on a sampling plane	yes	yes	-
	3D	Orientation of a fracture in a sampling volume	(yes)[a, b]	(yes)[b]	-

N is the total number of sampled fractures, L is the scanline length, A is the sampling area, r is the radius of the circular scanline, l is the fracture length, n and m are the number of intersections with a circular scanline and the number of endpoints in a circular window enclosed by the circular scanline.

[a] Borehole: possible for oriented well cores and image logs.

[b] Outcrop: possible for 3D outcrop settings.

Fracture density p describes the number of fractures in a sampling area ($P20$) or a sampling volume ($P30$). Fracture intensity I denotes the number of fractures along a line ($P10$) the total length of fractures in a sampling area ($P21$) or the total area of fracture planes in a rock mass volume ($P32$). Fracture intensity $P10$ is often also referred to as fracture frequency. The fracture intensity can be estimated by the product of fracture density and fracture mean length. Fracture spacing S is the average distance between adjacent fractures and is equal to $1/P10$. Fracture mean length l_m is the average length of fractures in an area.

The distribution of fracture lengths describes the probability of a certain fracture length to be present in an area. Fracture length distributions are typically evaluated by fitting a function to the measured length data. Common length distributions of natural fracture networks reported in literature are: (1) truncated power-law, which is the most often reported (e.g. Pickering et al., 1995; Odling 1997; Blum et al., 2005; Tóth, 2010; LeGarzic et al., 2011), (2) log-normal (e.g. Priest and Hudson, 1981), and (3) exponential (Cruden, 1977).

1.6. Sampling difficulties and biases

Sampling difficulties and biases can lead to a significant under- or overestimation of statistical parameters, and can thus potentially prejudice the characterization of fracture networks (Zhang and Einstein, 1998). In this section typical problems and biases associated with fracture sampling are summarized.

Data collected directly in the subsurface provides valuable in-situ information on fracture aperture, spacing, orientation and cementation (e.g. Olson et al., 2009). However, the problem of fracture sampling in the subsurface is the limitation to well cores and image logs from boreholes. Moreover, fracture sampling strongly depends on borehole inclination and fracture orientation, which significantly reduces potential data for fracture sets parallel to a borehole. Some parameters, such as average fracture spacing (Narr, 1996) and fracture frequency (Ortega and Marrett, 2000) can be estimated irrespectively of borehole inclination. Other parameters, such as fracture size cannot be measured directly. Examples for indirect methods to estimate fracture size in the subsurface encompass ground penetration radar, electrical resistance tomography and seismics (e.g. Sudha et al., 2011; Forte et al., 2012;

Jeanne et al., 2012). Drawbacks of these methods are the limitations in penetration depth and resolution. Another possibility to estimate fracture length is the use of relationships between aperture and length for opening-mode fractures (e.g. Olson, 2003; Scholz, 2010). However, these relationships are still under debate (e.g. Olsen & Schultz, 2011). Therefore, the analysis of outcropping subsurface analogues is important for the characterization of a fractured rock mass, especially if data on fracture length and their distribution are required.

Fracture length and their distribution are important parameters for the simulation of fluid flow in fractured rocks (e.g. Philip et al., 2005). However, the definition of lengths using outcrops can be difficult. For example, fractures identified as single strands at one scale of observation (e.g. satellite image), may be seen as linked segments when changing the scale of observation (e.g. at ground level) (Zeeb et al., 2013a). Moreover, the intersection of different fractures (e.g. Ortega and Marrett, 2000) and fracture cementation (e.g. Olson et al., 2009; Bons et al., 2012) add significant complexity to the identification of individual fractures. Thus, an important key factor for fracture network analysis is linking observations made in the subsurface to those obtained from outcrops.

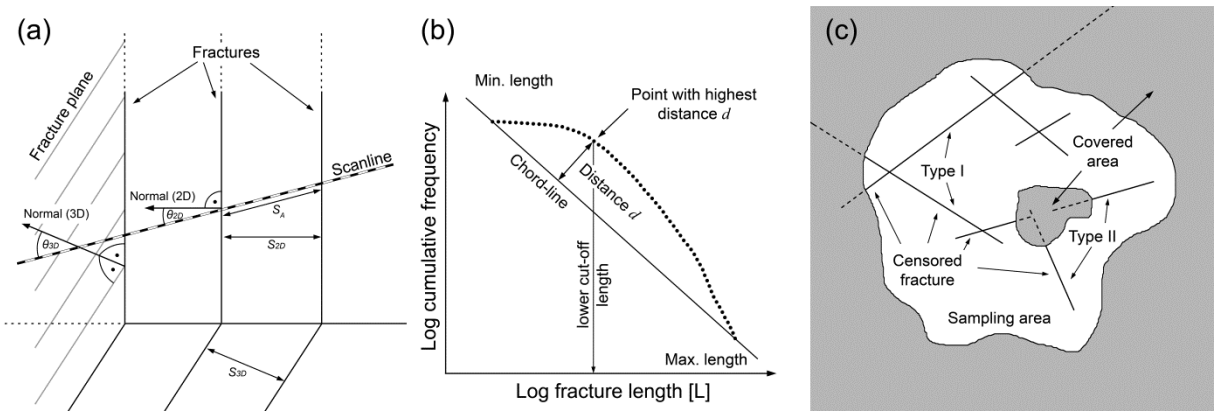

Fig. 1. (a) Sketch illustrating orientation bias and the definition of the variables required to calculate the factor for the Terzaghi correction (Eq. 1). S_A is the apparent spacing measured along a scanline, S_{2D} is the true spacing between two fracture traces and S_{3D} is the true spacing between two fracture planes. θ_{2D} and θ_{3D} are the angles between the normal to a fracture trace, or a fracture plane respectively, and a scanline. (b) Illustration of the Chord method (Pérez-Claros et al., 2002; Roy et al., 2007). (c) Censoring bias caused by the boundaries of a sampling area (Type I) and covered parts in an outcrop (Type II) (Zeeb et al., 2013a; Copyright AAPG 2013, reprinted by permission of the AAPG).

Orientation bias

Fractures rarely intersect an outcrop surface or scanline at perpendicular angles. Therefore, an apparent spacing S_A is measured for two adjacent fractures. This orientation bias causes an overestimation of fracture spacing, or respectively an underestimation of fracture frequency (Fig. 1a). The biased fracture spacing is corrected by applying the Terzaghi correction (Terzaghi, 1965; Priest, 1993), which provides the true spacing S:

$$S = S_A \times \cos\theta_{2D} \tag{3}$$

where θ_{2D} is the acute angle between the normal to a fracture trace and a scanline. In three dimensions $\cos\theta_{3D}$ is given by (Hudson and Priest, 1983):

$$\cos\theta_j = \cos(\alpha - \alpha_j)\cos\beta\cos\beta_j + \sin\beta\sin\beta_j \tag{4}$$

where α and β are the dip direction and dip of the scanline, α_j and β_j the dip direction and dip of the j-th fracture set normal, and θ_{3D} is the angle between the normal to a fracture plane and a scanline. For the application of the Terzaghi correction fractures need to be grouped into sets. Lacazette (1991) presented an alternative technique where orientation bias is corrected for each individual fracture:

$$Occurence = 1 \div (L \times \cos\alpha) \tag{5}$$

where *Occurrence* may be thought of as the frequency of an individual fracture, L is the length of a scanline and θ is the angle between the pole to the fracture and the scanline. The fracture frequency of a set is the sum of the *Occurrence* parameters calculated for the individual fractures in this set. Orientation bias can be reduced or even avoided by placing a scanline perpendicular to a fracture set. If necessary, several scanlines can be used in outcrops to capture different fracture sets.

Truncation bias

Truncation bias is caused by unavoidable resolution limitations, which depend on the used detection device (e.g. satellite image, human eye or microscope) and the contrast between the host rock and fractures. Parameters such as fracture length or width are not detectable below a certain scale. Moreover, as fracture size approaches the detection limit, the actual number of recognized fractures significantly decreases (e.g. Zeeb et al., 2013a). Thus, defining a lower cut-off of fracture size based on data resolution is needed to correct truncation bias (Nirex, 1997b). The truncation bias of sampled fracture lengths can be corrected by applying the Chord

method (Fig. 1b) (Pérez-Claros et al., 2002; Roy et al., 2007). In a log-log plot of fracture length against cumulative frequency, the line through the data point with the shortest length and the data point with the longest length is calculated. The fracture length from the data point with the highest distance d to this line is used as lower cut-off for the truncation bias.

Size bias

Size bias is related to scanline sampling (Bonnet et al., 2001; Manzocchi et al., 2009). The probability of a fracture to intersect a scanline is proportional to fracture length and therefore shorter fractures are underrepresented in the length data acquired by scanline sampling (Fig. 2a) (Priest, 1993; LaPointe, 2002). The correction of size bias depends on certain assumptions concerning the fracture shape, the spatial distribution of fractures and their length distribution (e.g. Hatton et al., 1993; LaPointe, 2002; Darcel et al., 2003; Barthélémy et al., 2009; Zeeb et al., 2013a).

Censoring bias

Censoring bias is typically related to limited outcrop size (Type I: Fractures with one or both ends outside the sampling area), uneven outcrops (e.g. erosion features) and coverage by overlaying rock layers or vegetation (Type II: Fractures with both ends inside the sampling area, but partly hidden from observation) (Fig. 1c) (Priest, 1993; Pickering et al., 1995; Zhang and Einstein, 2000; Bonnet et al., 2001; Rohrbaugh et al., 2002; Fouché and Diebolt, 2004). A typical effect of this censoring bias is an overestimation of fracture density (Kulatilake and Wu, 1984; Mauldon et al., 2001). Correction techniques for censoring bias rely on assumptions of fracture shape (e.g. disc, ellipsoid or rectangle) and size distribution (Priest, 2004), as well as on their spatial distribution (Riley, 2005). However, the use of such assumptions may also influence the results. Therefore, it is important to systematically quantify the influence of censored fractures to assess the uncertainty of the measured fracture network parameters (Zeeb et al., 2013a).

1.7. Fracture sampling

In this section three commonly used methods for fracture sampling from outcrops, well cores or image logs are presented: (1) the scanline sampling, (2) the window sampling and (3) the circular estimator method. Previous studies by Rohrbaugh et al. (2002), Weiss (2008), Belayneh et al. (2009) and Manda and Mabee (2010) compare these sampling methods for specific case studies. However, a comprehensive analysis including (1) the application of all three sampling methods to the same case, (2) their verification using AFNs with known input parameters, and (3) the use of a power-law to describe the distribution of fracture lengths is still lacking. A main issue is also the lack of a general consensus regarding the minimum number of length measurements required to adequately determine the length distribution of a fracture network. According to Priest (1993) the sampling area should contain between 150 and 300 fractures, of which about 50% should have at least on end visible. Furthermore, Bonnet et al (2001) suggested the sampling of a minimum of 200 fractures to adequately define exponents of power-law length distributions.

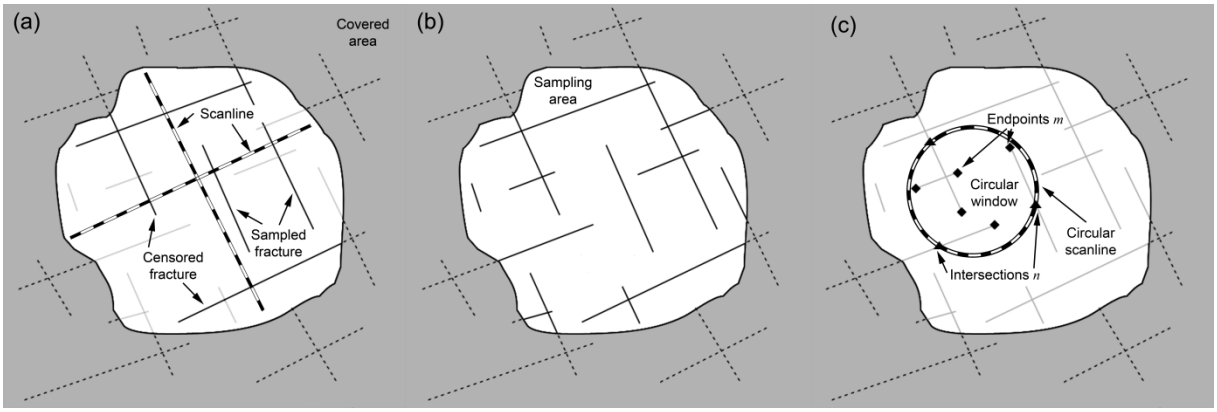

Fig. 2. (a) Window sampling, (b) scanline sampling, and (c) circular estimator method (modified from Rohrbaugh et al., 2002). Solid black lines indicate sampled fractures, light gray lines indicate non-sampled fractures and dashed lines non-observable (censored) parts of fractures (Zeeb et al., 2013a; Copyright AAPG 2013, reprinted by permission of the AAPG).

Scanline sampling method

Scanline sampling (Fig. 2a; Table 2) allows quick measurement of fracture characteristics along a survey line in the field or from well cores and image logs (e.g. Priest and Hudson, 1981; Priest, 1993; Bons et al., 2004; Zeeb et al., 2013a). The method provides one dimensional parameters of fracture networks (Table 2) and is affected by: (1) orientation bias, (2) truncation bias, (3) censoring bias and (4) size bias.

Window sampling method

Window sampling (Fig. 2b; Table 2) estimates the parameters of a network by measuring the characteristics from all fractures present within a sampling window (Pahl, 1981; Wu and Pollard, 1995). The method is typically applied to analyze outcropping subsurface analogues (Belayneh et al., 2009) or remote sensing data from satellite images or aerial photographs (Koike et al., 1995; Becker, 2006; Holland et al., 2009a; Zeeb et al., 2010). Three types of sampling bias affect window sampling: (1) orientation, (2) truncation and (3) censoring biases.

Circular estimator method

The circular estimator uses a combination of circular scanlines and windows (Mauldon et al., 2001; Fig. 2c) and is a maximum likelihood estimator (Lyman, 2003). Therefore, the method is not subject to sampling biases. The circular estimator uses statistical models instead of measuring fracture parameters (e.g. orientation, length or aperture) directly (Mauldon et al., 2001). Based on (1) the number of intersections n between a circular scanline and fractures, and (2) the number of fracture endpoints m in a circular window formed by this scanline, fracture density, intensity and mean length are calculated (Table 2). Rohrbaugh et al. (2002) provide a guideline for the application of the circular estimator method, which assures an accuracy of the results of 15% or higher. Following this guideline at least ten circular scanlines, with m-counts higher than 30, should be applied to a sampling area.

2. Objectives

The following objectives and research questions are addressed in this thesis:

- Several sampling methods exist to characterize fracture networks. Each of these methods has advantages and limitations. The first objective is to provide an overview and a critical evaluation of the (1) scanline sampling, (2) window sampling, and (3) circular estimator methods. Moreover, descriptions as well as correction techniques for (1) orientation bias, (2) truncation bias, (3) size bias and (4) censoring bias are provided.

- Each sampling methods allows the characterization of fracture networks. However, the number of measurements required to obtain accurate results is typically unknown. Is it possible to define a minimum number of required measurements for DFN characterization?

- Sampling biases have a significant influence on inferred fracture network parameters. To what degree are the scanline sampling, window sampling and circular estimator methods influenced by censoring bias?

- The analysis of fracture networks can be time consuming and tedious. Can the development of a novel software, which allows application of scanline, window or circular estimator sampling, help reduce the time required to characterize a 2D fracture network?

- The final objective is the analysis of fracture networks from real outcrops of (1) Ignimbrites at Craghouse Park, UK, (2) the Wajid Sandstone in Saudi Arabia, and (3) Miocene limestone in the Oman Mountains, Oman. Hence, what is the impact of different sampling methods and censoring bias for the characterizations of real fracture networks?

3. Results

3.1. Analysis of natural fracture networks

In this section the analyses of three natural fracture networks are presented and discussed: (1) fractures at outcrops of the Wajid Sandstone, Saudi Arabia (section 3.1.1), (2) fractures at outcrops of ignimbrites in Craghouse Park, Uk (section 3.1.3), and (3) vein networks at outcrops of Miocene limestones in the Oman Mountains, Oman (section 3.1.2).

3.1.1. Fractures in the Wajid Sandstone, Saudi Arabia

The fractured aquifer north-east of the studied outcrops is formed by the Wajid Sandstone formation and is the main source of water in the area (GTZ/DCo, unpublished report, 2010). The fracture networks at three outcrops of the Wajid Sandstone are analyzed to assess the contribution of the fractures to the overall flow transport in the fracture rock aquifer (Zeeb et al., 2010). The evaluated hydraulic conductivity tensors are compared with in-situ hydraulic pumping tests and matrix conductivities to estimate in-situ hydraulic fracture apertures. In the sections below the methodology and results are summarized. A more detailed description of the research is published in Zeeb et al. (2010).

Study area

Fig. 3 shows the location and the geology of the study area. The outcropping parts of Wajid Sandstone formation are located in the southern part of Saudi Arabia, approximately 300 km east of the Red Sea and 100 km north-east of the city of Khamis Mushaat. Most of the area is covered by sand and therefore only three outcrops could be studied: (1) Al Jufrah in the southern part, (2) Uruq Khurb in the northern part and (3) Jabal al Bara'im in the far north (Fig. 3). The Wajid sandstone consists of four different members separated by unconformities with a combined thickness of approximately 550 m. Two aquifers are situated within the Wajid Sandstone, of which the Upper Wajid aquifer is investigated in the current study. The

whole formation gently dips to the east. Detailed geologic descriptions of the Arabian Peninsula and the study area are provided, for example, by Kellogg et al. (1986), Evans et al. (1991), Konert et al. (2001).

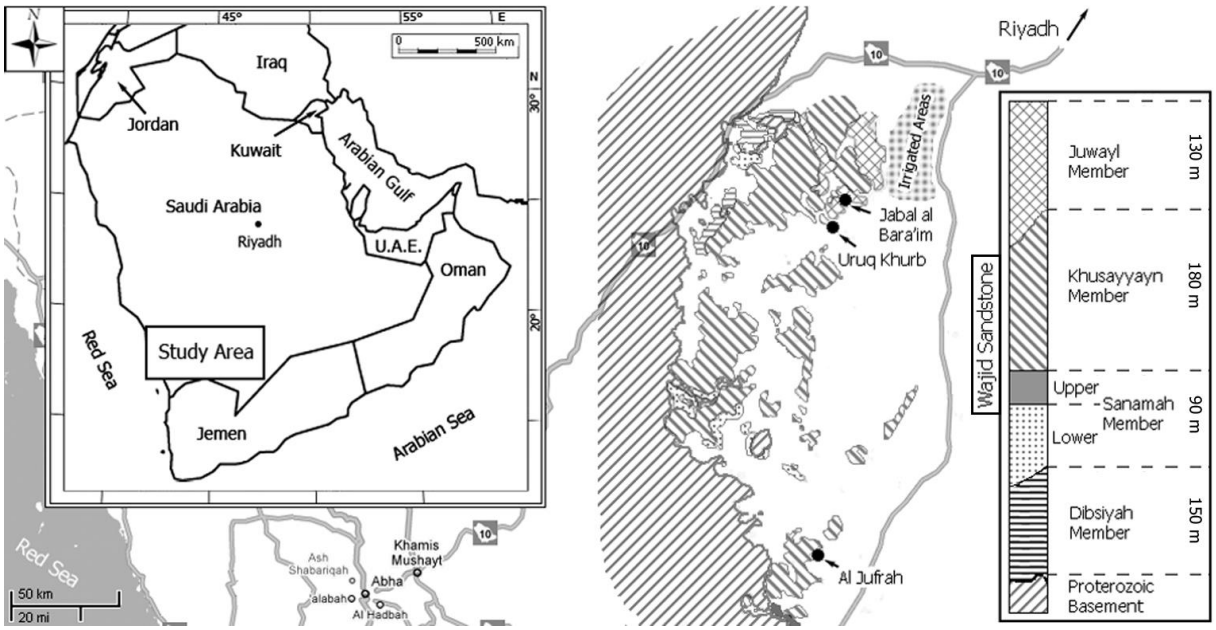

Fig. 3. Location and geology of the study area (Zeeb et al., 2010; Copyright Springer-Verlag 2010, with kind permission of Springer Science & Business Media).

Methodology

Fracture trace-line maps of the three studied outcrops are analyzed to evaluate the 2D conductivity tensors of the fracture networks. The trace-line maps were generated by combining Landsat ETM+ data, Saudi Geological Survey aeromagnetic data and field measurements. Unfortunately, the analyses of these data did not provide enough information to treat the transport simulations in a stochastic framework. Therefore, a deterministic approach is used to generate the DFN required for the transport simulations. Three DFN are “cut-out” from areas with a high fracture density (Fig. 4).

FRAC2D (Blum et al., 2005) is used for the hydraulic simulations of the fluid transport in the fracture network. The program calculates the flow across the boundaries of a DFN by applying the cubic law assumption (Snow, 1965; Louis, 1967) to each fracture:

$$Q = \frac{\rho g}{12\eta} a_h \nabla h \qquad (1)$$

where Q is the flow through a single fracture, ρ is the fluid density, g is the gravitational acceleration, η is the fluid viscosity and ∇h is the hydraulic head. A hydraulic gradient is applied and rotated around the center of the DFN. Since in-situ hydraulic apertures were not known, apertures are assumed to be 200 µm. Assuming Darcian flow, the conductivity tensor is calculated for the DFN (Jackson et al., 2000; Blum et al., 2007).

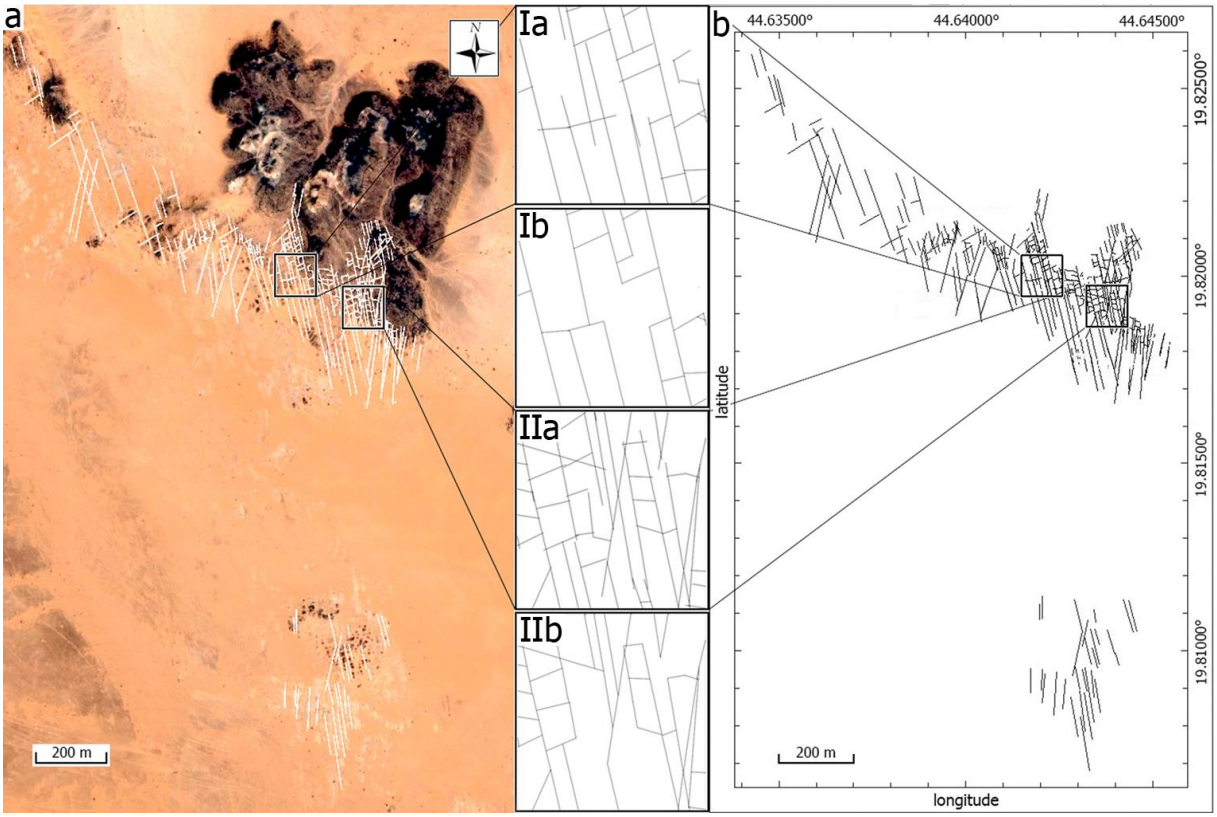

Fig. 4. a Satellite image taken from Google Earth (modified from Google, DigitalGlobe). **b** Fracture trace line map from combined remote sensing and field data for the outcrop at Jabal al Bara'im. White (**a**) and black lines (**b**) indicate the identified fracture traces and black squares indicate the chosen cut-out areas with an extent of 100 m × 100 m. **Ia** and **IIa** show the chosen DFN in more detail, **Ib** and **IIb** the backbone of the DFN (black lines indicate fracture traces) (Zeeb et al., 2010; Copyright Springer-Verlag 2010, with kind permission of Springer Science & Business Media).

Several pumping tests were carried out to measure the transmissivity of the Upper Wajid aquifer after the methods proposed by Butler (2009). The corresponding hydraulic conductivities k vary between 1.0×10^{-5} and 2.3×10^{-4} m s^{-1} with a geometric mean of 8.3×10^{-5} m s^{-1} (Al Ajmi et al., 2009). The matrix permeabilities of the different Wajid Sandstone members were measured from plug samples using the

method after Hornung (1999). The mean hydraulic matrix conductivity of the Upper Wajid aquifer is calculated from these permeability measurements and estimated to be 7.3×10^{-6} m s^{-1} (Dirner & Filomena, University of Tübingen, unpublished data). The relationship between effective conductivity k_{eff}, matrix conductivity k_m and fracture conductivity k_f is given by (Toublanc et al., 2005):

$$k_{eff} = k_m + k_f \tag{2}$$

A scaling factor, which provides a relationship between hydraulic apertures and therefore also between hydraulic conductivities, is used to calculate the in-situ hydraulic apertures of the fracture network (Blum et al., 2007):

$$f = \left(\frac{a_{h\,(new)}}{a_{h\,(old)}}\right)^3 = \left(\frac{k_{(new)}}{k_{(old)}}\right)^3 \tag{3}$$

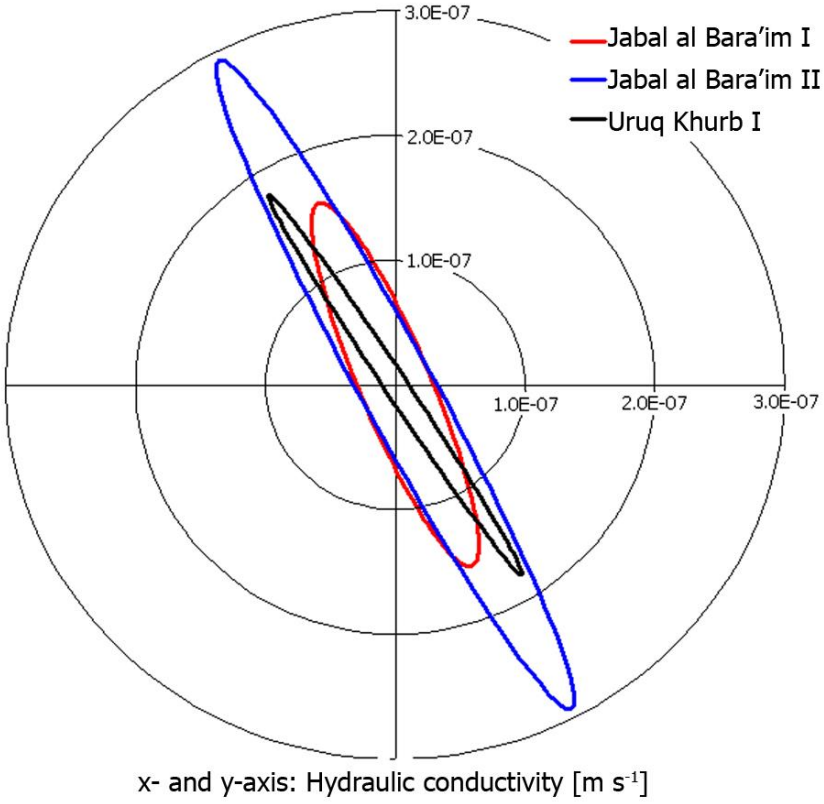

Fig. 5. Hydraulic conductivity tensors for the studied DFN's using a constant hydraulic aperture of 200 µm at Uruq Khurb I (black) and at Jabal al Bara'im I (red) and II blue) (Zeeb et al., 2010; Copyright Springer-Verlag 2010, with kind permission of Springer Science & Business Media).

Results and discussion

Fig. 5 shows the hydraulic conductivity tensors calculated for the three studied DFN's. The orientations of maximum conductivity coincide well with the orientation of the main fracture sets. The observed differences from those main fracture sets of 12° up to 27° are most likely caused by fluid flow along the subordinate fracture sets.

Fig. 6 illustrates the relationship between hydraulic aperture and hydraulic conductivity. Applying equation 7 the fracture conductivity is estimated to be 7.6×10^{-5} m s^{-1} for the Upper Wajid aquifer. The in-situ hydraulic apertures are calculated using equation 8. At Uruq Khurb the hydraulic fracture aperture in the aquifer is approximately ~1,500 µm and at Jabal al Bara'im the apertures are in between ~1,300 µm (DFN 1) and ~1,700 µm (DFN 2). Although laboratory (e.g. Yeo et al. 1998) and other field-scale studies (e.g. Steele et al. 2006) show smaller fracture apertures (<1,000 µm) for sandstones, field observations at the Wajid Sandstone outcrops indicate even larger open fracture apertures (>>1 mm). The hydraulic conductivity ratio k_f / k_m of 10.4 is an indication that the overall flow is influenced by the fracture network, but not entirely dominated by it (Castaing et al., 2002).

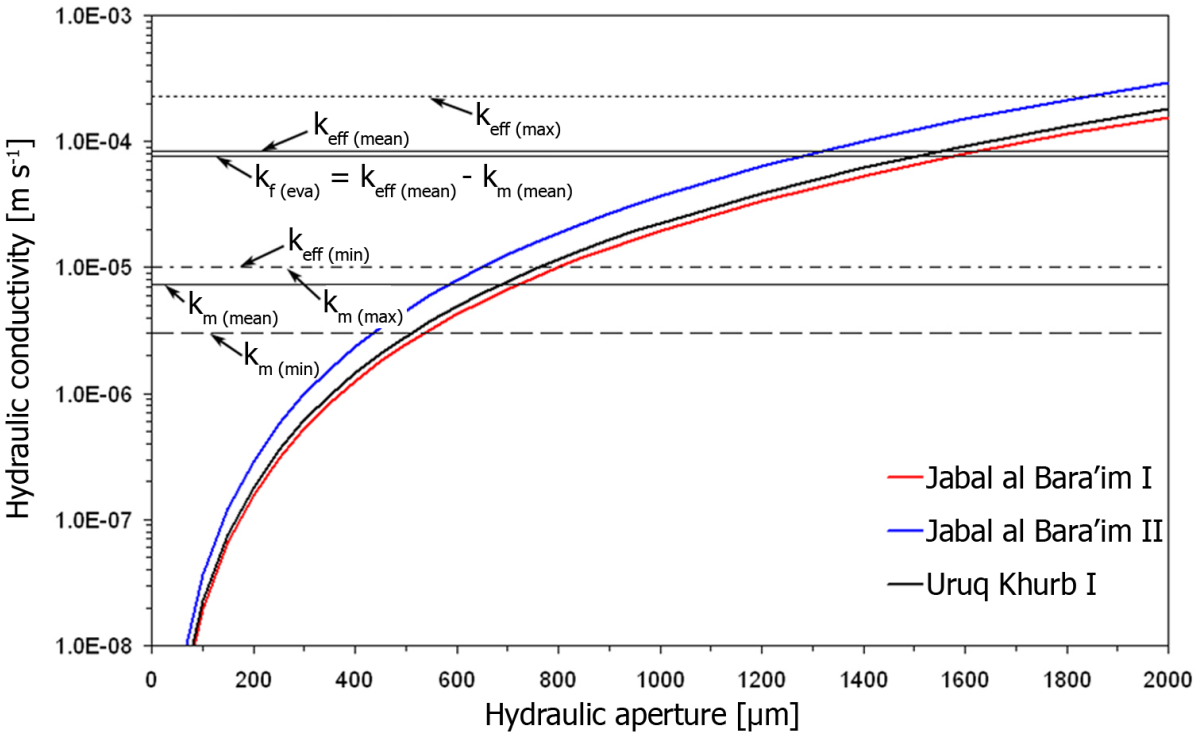

Fig. 6. Hydraulic conductivities determined for the three studied DFN's - Jabal al Bara'im I (red) and II (blue), and Uruq Khurb I (black). The matrix conductivity is denoted as k_m, with the mean, the maximum and the minimum values $k_{m\ (mean)}$, $k_{m\ (max)}$ and $k_{m\ (min)}$. The bulk effective hydraulic conductivity based on pumping test data is denoted as k_{eff}, with the mean, the maximum and the minimum values $k_{eff\ (mean)}$, $k_{eff\ (max)}$ and $k_{eff\ (min)}$. The evaluated fracture hydraulic conductivity is shown as $k_{f\ (eva)}$ (Zeeb et al., 2010; Copyright Springer-Verlag 2010, with kind permission of Springer Science & Business Media).

3.1.2. Fracture networks in ignimbrites, Craghouse Park, UK

The trace-line map of fractures in ignimbrites (Fig. 7a, b) near Craghouse Park, UK (Nirex, 1997a; Blum et al., 2007) is analyzed using FraNEP (section 3.5). The sampling area at the outcrop has a size of approximately 19 m^2 and contains a total of 288 visible fractures with lengths ranging between 0.05 and 4.0 m, of which 30% are biased by censoring. The lower cut-off length for truncation bias is 0.8 m.

Results and discussion

Fig. 7 presents the fracture lengths measured by applying two scanlines (Fig. 7c) and by window sampling (Fig. 7d). Table 3 summarizes the fracture network parameters assuming a power-law length distribution. Such an assumption is valid (and necessary), if an upscaling of the results is intended. If the length distribution at

the scale of observation is evaluated, then a log-normal distribution might be a better choice. However, the length measurements should not be corrected for truncation bias, since the procedure removes the short fracture lengths, which are essential for the definition of a log-normal distribution. The values calculated for fracture density, intensity, mean length and length distribution by applying (1) the scanline sampling, (2) the window sampling and (3) the circular estimator method significantly differ from each other. Whether these differences are due to a lack of measurements or are caused by censoring bias is discussed in sections 3.2 and 3.3 respectively.

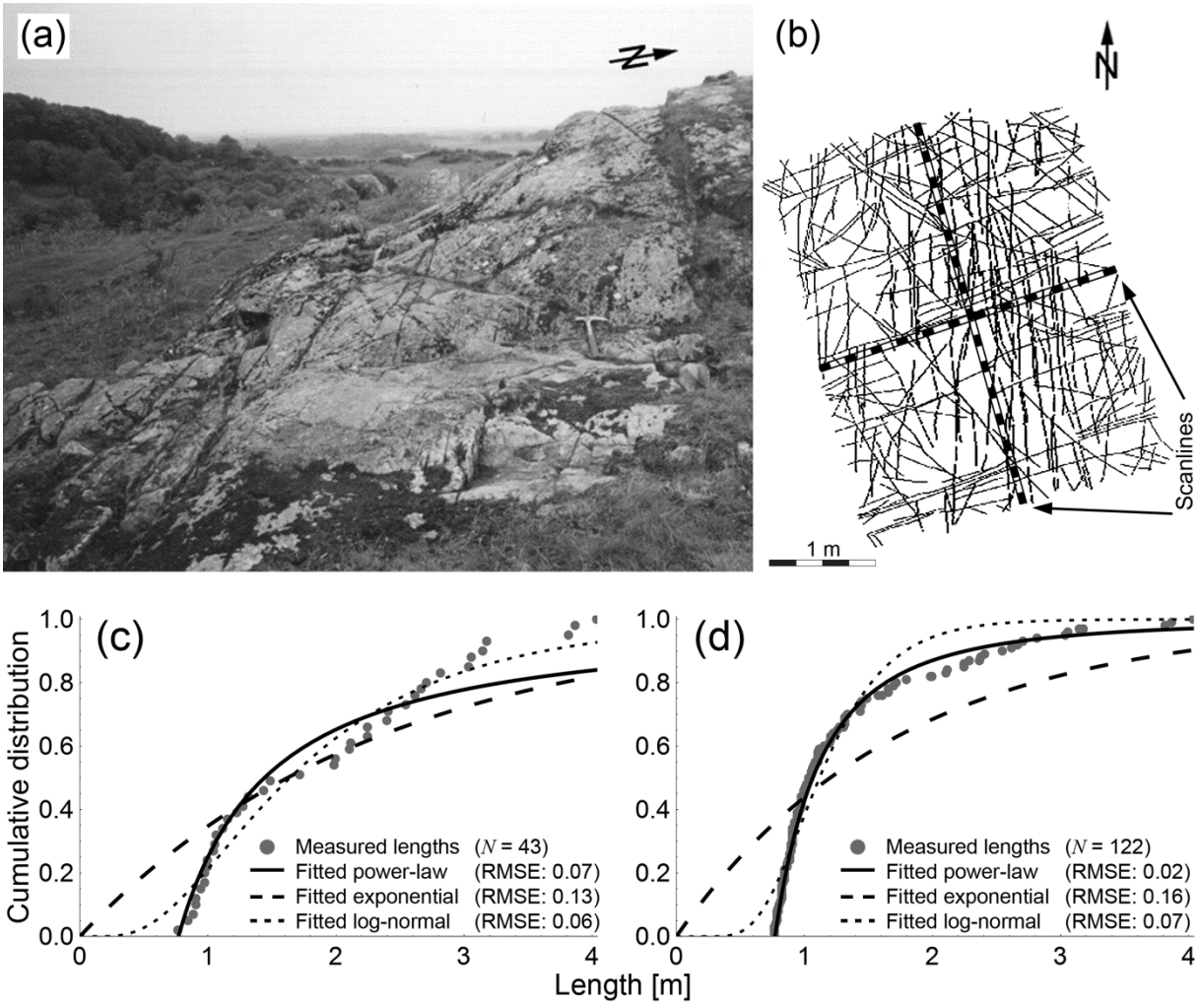

Fig. 7. (a) Photo of the investigated outcrop at Craghouse Park, UK (geologic hammer for scale). (b) Trace-line map of the cleaned outcrop. (c) and (d) show a plot of fracture lengths (gray dots) against the cumulative distribution measured by (c) two scanlines and (d) one window sampling of the whole study area (a). The solid, dashed and dotted black lines indicate power-law, exponential and log-normal fits. The fitting accuracy is given by the RMSE (Zeeb et al., 2013a; Copyright AAPG 2013, reprinted by permission of the AAPG).

Table 3. Parameters calculated for the fracture network in outcropping ignimbrites near Craghouse park, UK. The results are corrected for orientation, truncation and size bias (modified from Zeeb et al., 2013a; Copyright AAPG 2013, reprinted by permission of the AAPG).

Parameter	SLS	WS	CE
Number of measurements [-]	43	122	-
Length range [m]	0.8 – 4.0	0.8 – 4.0	-
Radius [m]	-	-	1.6
Censored fractures [%]	11	30	-
Density [m^{-2}]	3.5	5.4	2.8
Intensity [m m^{-2}]	5.1	7.4	3.6
Mean length [m]	1.5	1.4	1.3
Power-law Exponent [-]	2.1	2.2	-

3.1.3. Fracture networks in Miocene limestones, Oman Mountains, Oman

A trace-line map of lineament data (fractures, faults, joints, veins, etc.) is analyzed (Fig. 8a, b). The lineaments were extracted by optical picking from a Quickbird satellite image of the southern flank of the Jabal Akhdar dome in the Oman Mountains, Oman (Hilgers et al., 2006; Holland et al., 2009a, b). The parameters of the fracture network are calculated using FraNEP (section 3.5). The studied sampling area has an extent of 120,000 m^2, in which 650 lineaments with lengths ranging between 3 and 179 m could be identified by optical picking. The cut-off length for truncation bias is 23.3 m. Approximately 5% of the fractures in the sampling area appear to be censored.

Results and discussion

Fig. 8 presents the fracture lengths measured by applying two scanlines (Fig. 8c) and by window sampling (Fig. 8d). Table 4 summarizes the parameters of the fracture network. As was already observed in section 3.1.2, significant differences exist between the values calculated for fracture intensity, mean length and length distribution. The deviation between the results for the power-law exponents of the length distribution might be due to difficulties when interpreting fracture lengths in the satellite image. A lineament interpreted as one fracture in the satellite image might be

a series of fracture segments when studied at the ground level. Moreover, some fractures are separated by erosion features. What is interpreted as two individual fractures might also be partly unobservable long fracture. The possible impact of a lack of measurements and the influence of censoring bias are discussed in sections 3.2 and 3.3 respectively.

Table 4. Parameters calculated for the fracture network in outcropping limestones at the southern flank of the Jabal Akhdar dome in the Oman Mountains, Oman. The results are corrected for orientation, truncation and size bias (modified from Zeeb et al., 2013a; Copyright AAPG 2013, reprinted by permission of the AAPG).

Parameter	SLS	WS	CE
Number of measurements [-]	51	268	-
Length range [m]	25.6 – 179	23.3 – 179	-
Radius [m]	-	-	100
Censored fractures [%]	0	5	-
Density [m^{-2}]	0.002	0.002	0.002
Intensity [m m^{-2}]	0.07	0.09	0.10
Mean length [m]	39.7	41.6	53.9
Power-law Exponent [-]	2.8	2.2	-

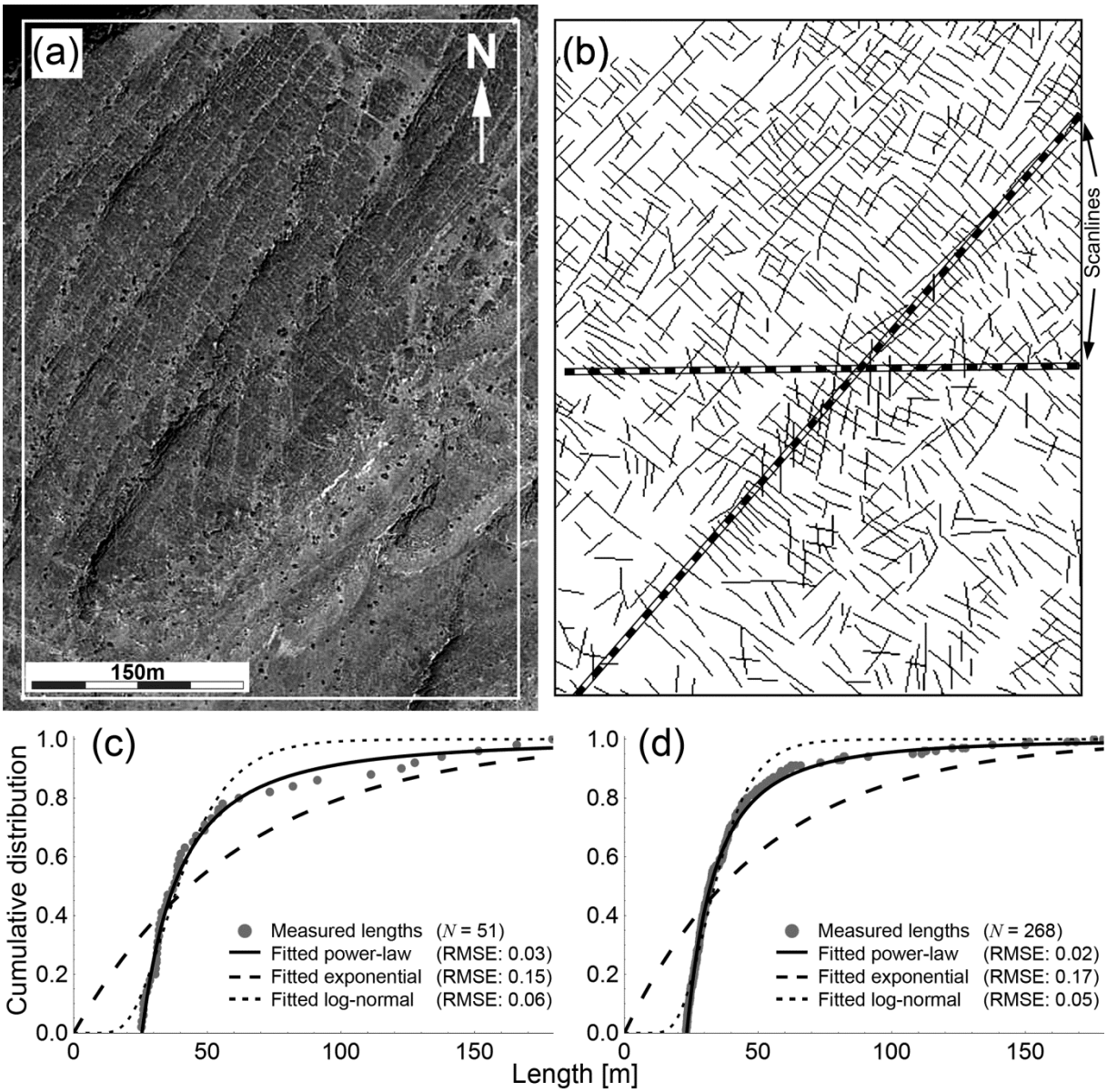

Fig. 8. (a) Satellite image from the southern flank of the Jabal Akhdar dome in the Oman Mountains, Oman (modified after Google, DigitalGlobe). (b) Interpretation of the fractures in the white rectangle in (a) after correction of truncation bias (modified after Holland et al., 2009a). UMT coordinates of the lower left and upper right corners are 40N 525496 2562373 and 40N 525799 2562760. Please note that the satellite image and the trace line map are not to scale due to the slope of the flank. (c) and (d) show a plot of fracture lengths (gray dots) against the cumulative distribution measured by (c) two scanlines and (d) one window sampling of the whole study area (a). The solid, dashed and dotted black lines indicate power-law, exponential and log-normal fits. The fitting accuracy is given by the RMSE (Zeeb et al., 2013a; Copyright AAPG 2013, reprinted by permission of the AAPG).

3.2. The required minimum number of measurements

A certain number of measurements are required to adequately determine the parameters of a fracture network, for example the distribution of fracture lengths. However, no general consensus exists regarding the minimum number of measurements required for the application of the (1) scanline sampling, (2) window sampling, and (3) circular estimator methods. According to Priest (1993) a sampling area used to characterize a fracture network should contain between 150 and 300 fractures, of which about 50% should have at least on end visible. Furthermore, Bonnet et al (2001) suggested the sampling of a minimum of 200 fractures to adequately define exponents of power-law length distributions. However, these numbers only apply to specific case studies. Therefore, the required minimum number of measurements to apply a sampling method is evaluated. A detailed description of the methodology and the results is provided by Zeeb et al. (2013a).

3.2.1. Methodology

In this section the methodology used to evaluate the required minimum number of measurements is described. The numbers are assessed using AFNs. Below the generation of these AFNs and the criteria applied to evaluate the required minimum number of measurements are described.

Artificial fracture networks

The fracture network generator FracFrac (section 1.3), is used to generate nine 2D AFNs. For the fracture density three values with p = 0.5 m^{-2}, p = 1.0 m^{-2} and p = 1.5 m^{-2} are assumed. The fracture lengths are described using the cumulative distribution function of a truncated power-law (Eq. 1), with exponents of E = 1.5, E = 2.0 and E = 2.5. These power-law exponents correspond well to values reported for natural fracture systems, which are typically in the range between 0.8 and 3.5 with the majority actually around 2 (Bonnet et al., 2001). The lower cut-off length l_0 is set to one meter. Two sets of perfectly parallel fractures are defined with orientations of 0° and 90°. A summary of the input parameters is provided in Table 5. Fig. 9a shows nine 20 m × 20 m sampling areas, one for each of the nine AFNs. The generation area of each AFN is 300 m × 300 m. In this whole area, a total of 146 squared

sampling areas are defined (one area with an edge length of 200 m, four with 100 m, 16 with 50 m and 25 sampling areas with edge lengths of 40 m, 30 m, 20 m, 10 m and 5 m), providing a total of 1314 sampling areas for all nine AFNs (Fig. 9b). Fractures are treated as censored, if one or both ends intersect with a boundary of the sampling area (Fig. 9c). The percentage of censored fractures is calculated from the total number of fractures in a sampling area and the number of fractures that are censored. The percentage of censored fractures increases for smaller sampling areas and for higher values of the power-law exponent (Fig. 9d). Each sampling area is analyzed using FraNEP (section 3.5). Note that the same AFNs and sampling areas are also used in section 3.3.

Evaluation criteria

The criteria for the evaluation of the required minimum number of measurements are defined in such a way that each sampling method sufficiently captures the statistical properties. For the scanline and window sampling methods the criterion is defined as the number of measurements, above which a power-law always provides the best fit to the fracture length measurements. The criterion of the circular estimator method is defined as the number of fractures in a sampling area, above which a circular window always contains 30 or more fracture endpoints.

Table 5. Summary of the fracture network parameters for the nine generated AFNs (modified from Zeeb et al., 2013a; Copyright AAPG 2013, reprinted by permission of the AAPG).

Parameter	AFN								
	1	2	3	4	5	6	7	8	9
Density p [m^{-2}]	0.5	1.0	1.5	0.5	1.0	1.5	0.5	1.0	1.5
Intensity I [$m\ m^{-2}$]	1.5	3.0	4.5	1.0	2.0	3.0	0.8	1.7	2.5
Mean length l_m [m]	3.0	3.0	3.0	2.0	2.0	2.0	1.7	1.7	1.7
Exponent E_{2D} [-]	1.5	1.5	1.5	2.0	2.0	2.0	2.5	2.5	2.5

Each of the 1314 sampling areas is analyzed by applying the three sampling methods. Then the criteria are applied to the data and two numbers are evaluated for each sampling method: (1) the highest number of measurements that does not satisfy the criterion, and (2) the lowest number of measurements above which the criterion is always satisfied. The required minimum number of measurements, which is universally applicable to all nine studied AFNs, is the lowest number of (2), which is also higher than all numbers of (1).

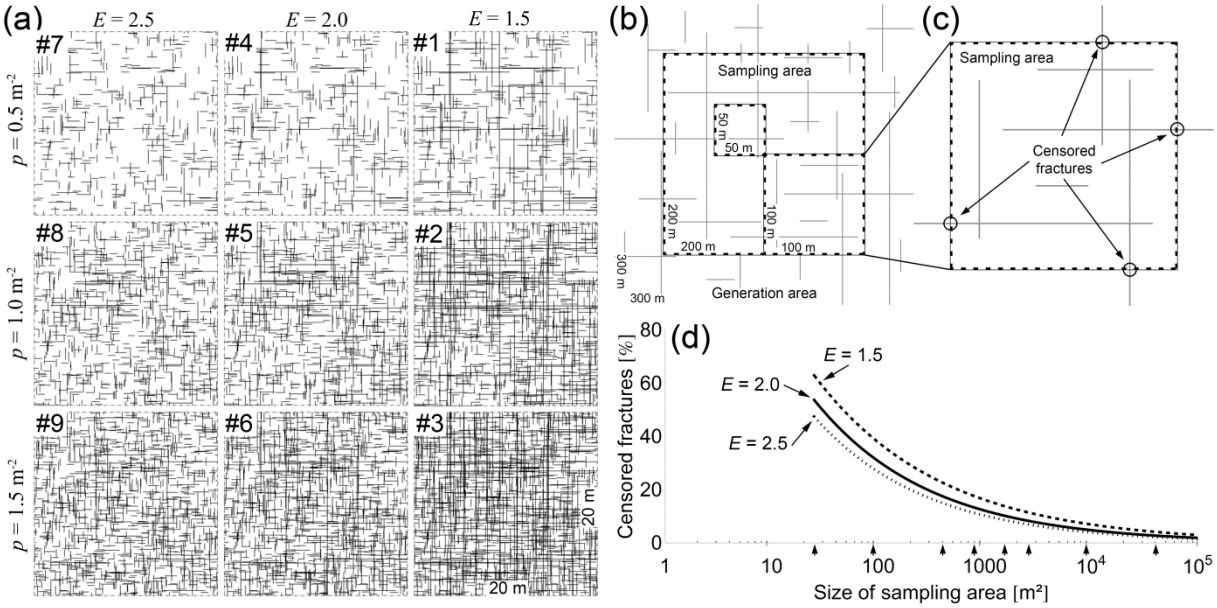

Fig. 9. (a) Examples of a 20 m × 20 m sampling areas from each of the nine 2D AFNs. The numbering of the AFN corresponds to those in Table 5. (b) Sketch illustrating the generation area and the definition of sampling areas. (c) Definition of the censored fractures in a sampling area. (d) The relationship between the size of the sampling area and the average percentage of censored fractures for the three power-law length distributions. The black arrows on the x-axis indicate the size of the sampling areas analyzed in this study (Zeeb et al. 2013a; Copyright AAPG 2013, reprinted by permission of the AAPG).

3.2.2. Results and discussion

In this section the required minimum numbers of measurements are provided and discussed. To define a power-law distribution at least 110 fracture lengths should be measured applying the window sampling and 225 applying the scanline sampling method. Since only the fractures intersecting with a line are considered when applying the scanline sampling method, significantly more fractures have to be present in a sampling area to measure 225 fractures. The size of a sampling area,

and therefore the fracture density, does not directly influence the definition of a length distribution. However, a small sampling area may cause more fractures to be censored, which would lead to a more complex fracture network. For the application of the circular estimator method we found that ~ 860 fractures should be present in a sampling area to always sample a minimum of 30 fracture endpoints. This minimum number depends on the radius of the circular scanline and decreases for larger radii. Note that the required minimum corresponds to the number of measurements after accounting for truncation bias.

An universally applicable minimum number is probably impossible to obtain since each case study may require a different number of measurements depending on the studied network itself. However, the power-law exponents used to generate the AFNs represent those commonly reported for natural networks (Bonnet et al., 2001). Therefore, above numbers allow a better estimate on the number of measurements necessary to adequately capture fracture statistics. For other length distributions, complex fracture networks or complex sampling area geometries more fracture lengths should be measured.

3.3. The influence of censoring bias

The effects responsible for censoring bias are well known and correction techniques are available in literature (e.g. Priest, 2004; Riley, 2005). The application of these techniques is only possible when making certain assumptions regarding fracture shape (e.g. disc, ellipsoid or rectangle) and fracture-size distribution (Priest, 2004), as well as their spatial distribution (Riley, 2005). However, the use of such assumptions may also influence the results. The actual influence of censored fractures on estimates of fracture network parameters has not been comprehensively investigated. In the present study the influence is assessed for: (1) fracture density, (2) intensity, (3) mean length, and (4) length distribution. In the sections below the methodology used to assess the influence of censoring bias on above parameters is presented and the results are summarized and discussed. A detailed description is provided by Zeeb et al. (2013a).

3.3.1. Methodology

The fracture networks and sampling areas described in section 3.2.1 are also used to assess the influence of censoring bias on inferred fracture network parameters. For each sampling area, which contains the necessary minimum number of fractures to apply the respective sampling method (section 3.2), the difference between estimated and input value is calculated for: (1) fracture density, (2) fracture intensity, (3) fracture mean length and (4) power-law exponent of the fracture length distribution. The percentage of censored fractures in a sampling area is plotted against the difference in percent for each parameter and sampling method. Fig. 10 shows an example of the observed differences when estimating fracture density applying the window sampling method. The plot illustrates the maximum difference observed for increasing percentages of censored fractures. The range of potential differences between those maximum differences is referred to as the uncertainty.

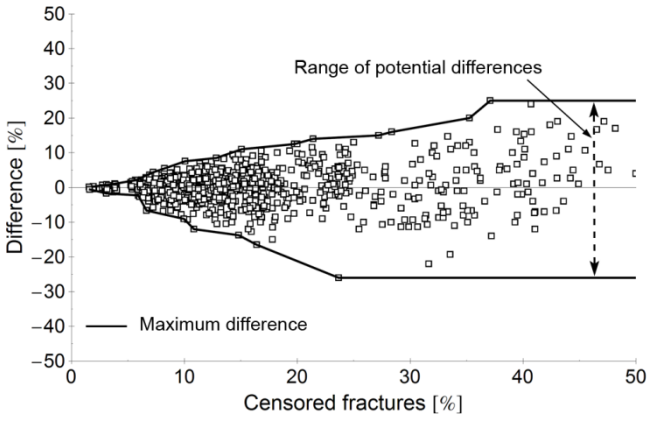

Fig. 10. Plot of censored fractures (in percent) against the difference (in percent) between estimated and input fracture density for window sampling. Each point represents a sampling area from the nine AFNs. The maximum difference is highlighted by the two solid black lines. The range of potential differences between those two lines represents the uncertainty of a result for a specific sampling area with the percentage of censored fractures (Zeeb et al., 2013a; Copyright AAPG 2013, reprinted by permission of the AAPG).

3.3.2. Results and discussion

For all sampling methods and parameters the uncertainty of the measured values clearly increases with the percentage of censored fractures (Fig. 11). In general, the results based on the window sampling method indicate the lowest uncertainty. However, all sampling methods show a high uncertainty for estimates of fracture intensity. Although, the circular estimator highly overestimates fracture intensity, the method exhibits the lowest uncertainty.

The results estimated by scanline sampling are within an 80% confidence interval. However, estimates of fracture density and mean length depend on the correct estimate of a power-law length distribution (Zeeb et al., 2013a). Therefore, only data sets with 225 measurements or more can be used for the calculations, and thus can be carried out for the cases of 0 - 5% censored fractures only.

The AFNs used in the current study are simple and natural examples are often much more complex. Hence, it is likely that more fractures are censored. However, since we use percentages of censored fractures, the approach to evaluate the uncertainty is also applicable to natural fracture networks.

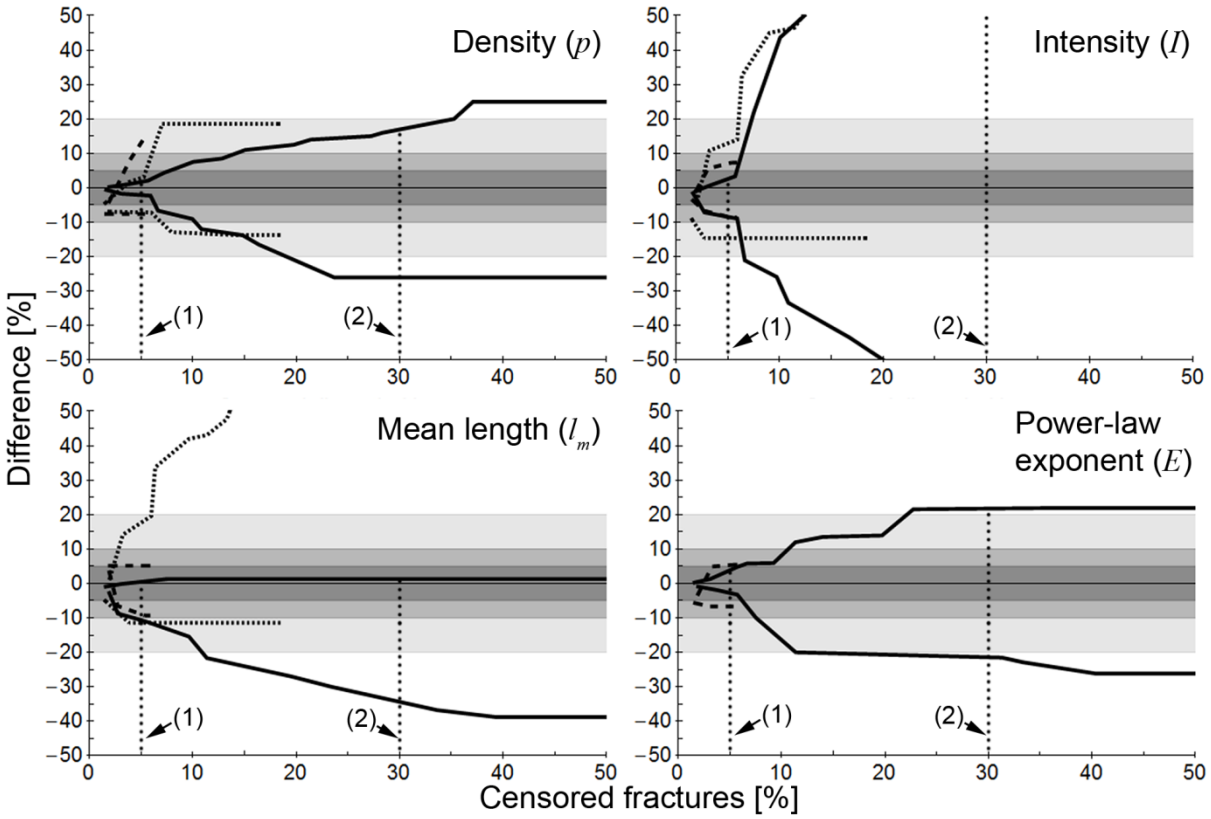

Fig. 11. Summary of potential differences evaluated for scanline sampling (dashed), window sampling (solid) and circular estimator (dotted) methods, illustrated as lines of maximum difference (Fig. 10). The areas highlighted in dark grey, grey and light grey represent the 95%, 90% and 80% confidence intervals of the true value. The vertical dotted lines indicate the percentage of censored fractures for the studied natural fracture networks: (1) Craghouse Park (section 3.1.2), and (2) the Oman Mountains (section 3.1.3) (Zeeb et al., 2013a; Copyright AAPG 2013, reprinted by permission of the AAPG).

3.4. Application of the results

The results from sections 3.2 and 3.3 are applied to reevaluate the natural fracture networks described in sections 3.1.2 and 3.1.3. Both, the required minimum number of measurements and the uncertainty due to censoring bias indicate that the window sampling method is the most suitable to analyze these fracture networks. Table 6 summarizes the measured fracture network parameters and their uncertainty, based on the evaluation in Fig. 11. The ranges of possible true values presented in Table 6 (values in brackets) emphasize the necessity of the present study.

Table 6. Fracture network parameters evaluated for the two natural fracture networks. The values in brackets indicate the range of possible true values due to the uncertainty (modified from Zeeb et al., 2013a; Copyright AAPG 2013, reprinted by permission of the AAPG).

Parameter	*Craghouse Park* (*UK*)		*Oman Mountains (Oman)*	
Number of fractures [-]	122		268	
Length range [m]	0.76 - 4.04		23.3 - 179	
Censored fractures [%]	30		5	
Density p [m^{-2}]	5.44	(4.52 - 6.80)	0.002	(insignificant)
Intensity I [m m^{-2}]	7.40	(<< 3.70 >> 11.1)	0.09	(0.09 - 0.10)
Mean length l_m [m]	1.36	(1.33 - 1.84)	41.6	(41.6 - 46.2)
Exponent E_{2D} [-]	2.17	(1.69 - 2.65)	2.15	(2.06 - 2.21)

The reevaluated results (Table 6) for the natural fracture network at Craghouse Park, UK (Fig. 7; section 3.1.2) illustrate the high uncertainty of fracture characteristics calculated for such a small outcrop. For the power-law exponent a value of E = 2.17 is obtained. However, since 30% of the fractures are censored the potential true value ranges between 1.69 and 2.65, which covers approximately 70% of the values reported by Bonnet et al. (2001). Unfortunately, outcrops with a limited number of measurable fractures, a small sampling area and a high percentage of censored fractures are often the only option for the characterization of subsurface fracture networks. Therefore, additional outcrops and a cross-correlation with borehole data should be considered to improve the characterization of the subsurface.

The uncertainty due to censoring bias is rather low for the parameters of the fracture network at the southern flank of the Jabal Akhdar dome (Fig. 8, section 3.1.3). However, the resolution limitations of satellite images cause a significant truncation bias. Hence, correcting the fracture length data for this sampling bias is required to attain distributions closer to the real one.

3.5. Fracture Network Evaluation Program - FraNEP

Several techniques allow a quick acquisition of fracture network data, such as (1) the automatic detection of lineaments from satellite images and aerial photographs, (2) LIDAR technologies or (3) borehole televiewers. The analysis of such data is often performed manually or with different analysis software, which can be time-consuming and tedious. In this section, a novel program for the analysis of large amounts of fracture data called FraNEP (Fracture Network Evaluation Program) is presented. A detailed description of the program is provided by Zeeb et al. (accepted for publication). The program was developed using Visual Basic for Applications in Microsoft Excel™ and combines features from different existing software and characterization techniques. FraNEP is a time-efficient tool for the characterisation of fracture network parameters, such as fracture density, intensity, mean length and length distribution. The software allows the application of the (1) scanline sampling, (2) window sampling or (3) circular estimator method, without the need of switching programs. Below a short program description is provided and the application of FraNEP is illustrated by analyzing a trace-line map of lineaments from the southern flank of the Jabal Akhdar dome in the Oman Mountains, Oman. Finally the advantages of FraNEP over other existing software are discussed.

3.5.1. Program description

For the characterisation of a fracture network three steps of input need to be defined: (1) data input, (2) sampling and (3) options for the analysis.

Data input

Data input encompasses the following information (Table 7): (1) the endpoint coordinates of each fracture, (2) the number of fracture sets as well as their strike spread (minimum and maximum value) and (3) the dimension of the study area. The fracture endpoints are imported as points with coordinates (*X1*, *Y1*) and (*X2*, *Y2*). From the endpoint coordinates the length and strike of each fracture is automatically calculated. The sum of fracture lengths divided by the number of fractures provides a first estimate of mean fracture length. The definition of the fracture sets automatically provides the mean strike and the number of fractures for each set. If the definition of

fracture sets is unclear, the input data can also be treated as one single set with strikes that range from 0° to 180°. The study area's location and size is defined by the coordinates of its lower-left corner and the extension in the *X*- and *Y*-directions. Once the study area is defined FraNEP automatically calculates the size, the fracture density and the fracture intensity. The definition of a study area is not necessarily required for the fracture network characterization and can be skipped. The preliminary results calculated for fracture mean length, density and intensity should be always treated carefully.

Table 7. Input data and governing equations for the calculation of individual fracture and the preliminary fracture network characteristics (modified from Zeeb et al., 2013b).

Input	Parameter	Equation
Endpoint coordinates		
$(X1_i, Y1_i)$ $(X2_i, Y2_i)$	Length, l_i [L]	$l_i = \sqrt{(X2_i - X1_i)^2 + (Y2_i - Y1_i)^2}$
	Mean length, l_m [L]	$l_m = \frac{1}{N}\sum_{i=1}^{N} l_i$
	Strike, O_i [°]	$O_i = \tan^{-1}\left(\frac{X1_i - X2_i}{Y1_i - Y2_i}\right)$ $\quad 0° \leq O_i \leq 180°$
Fracture sets		
Set j $\quad O^j_{min} \leq O_i < O^j_{max}$	Mean strike, O^j_m [°]	$O^j_m = \frac{1}{N}\sum_{i=1}^{N} O_i$
	Fractures per set, N_j [-]	$N_j = \sum_{i=1}^{N} o_i$
Dimension of the study area		
Point of origin (X, Y) Extension (X_{dir}, Y_{dir})	Study area size, A [L^2]	$A = X_{dir} \times Y_{dir}$
	Fracture density, p [L^{-2}]	$p = \frac{N}{A}$
	Fracture intensity, I [L L^{-2}]	$I = \frac{\sum_{i=1}^{N} l_i}{A}$

i designates individual fractures, *j* designates different fracture sets and L is an arbitrary unit of length.

FraNEP includes the possibility to generate and display a trace-line map from the imported fractures and a rose diagram plot of fracture strikes. Latter can be used to distinguish between different sets of fractures and can be drawn with or without fracture-length weighting.

Sampling

Fracture networks are analysed by applying one of three different sampling methods (section 1.7): (1) scanline sampling, (2) window sampling or (3) circular estimator. Scanlines are defined by the coordinates of their start- and endpoints. The sampling areas for the application of the window sampling and circular estimator methods are defined by a point of origin (lower left corner) and the extension of the area in X- and Y-directions. Fractures intersecting a boundary of the selected sampling area are considered censored and the intersection point is used to calculate the length of the censored fracture. The circular scanlines used by the circular estimator method are defined by (1) their centres, which are defined by their X- and Y-coordinates and can be placed either manually or randomly, and (2) their radii. The minimum distance between the boundaries of a sampling area and the centres is equal to the radius plus a small constant value of 0.1 to avoid interactions. It is possible to place up to 200 sampling areas and/or scanlines anywhere within the study area.

Options

Three categories of options are available to select (1) the correction methods, (2) define the analysis to be performed with the acquired data and (3) the visualization of results. A summary and short description of these options is provided in Table 8.

Table 8. Options for correction methods, data analysis and visualization of results. The symbols "+" and "–" indicate whether an option is applicable to the chosen sampling method or not (modified from Zeeb et al., 2013b).

Category	Option	Description	WS	SLS	CE
Correction methods	Fracture density	Reduces the overestimation of fracture density due to censoring bias.	+	–	–
	Lower uncensored cut-off length	Corrects artificial censoring bias (removes fractures smaller then smallest uncensored fracture).	+	+	–
Data analysis	Length fit	Defines the fitting for fracture lengths (power-law, lognormal, exponential).	+	+	–
	Circular scanlines	Defines the total number of circular scanlines placed in each sampling area.	–	–	+
Visualization	Diagram type	Creates a plot of sampled fracture lengths (cumulative frequency or cumulative distribution).	+	+	–
	Scanline combination	Combines the results from two and/or all scanlines.	–	+	–
	Write strikes	Write strikes in the output-sheets.	+	+	–
	Rose diagram	Plots the fracture strikes in a rose diagram (cumulative number per bin or length wieghted).	+	+	–
	Visualization	Creates a trace-line map of the sampled fractures.	+	–	–

3.5.2. Application example

A field case example from the Oman Mountains (Holland et al., 2009a) is used to illustrate the application of FraNEP. The investigated study area (Fig. 12) is a small part of a polyline shape file containing approximately 157 000 lineaments, which were identified by manual interpretation of a Quickbird satellite image with a panchromatic resolution of 0.7 m (Holland et al., 2009b). These lineaments actually correspond to veins, fractures and joints measured from an outcrop surface.

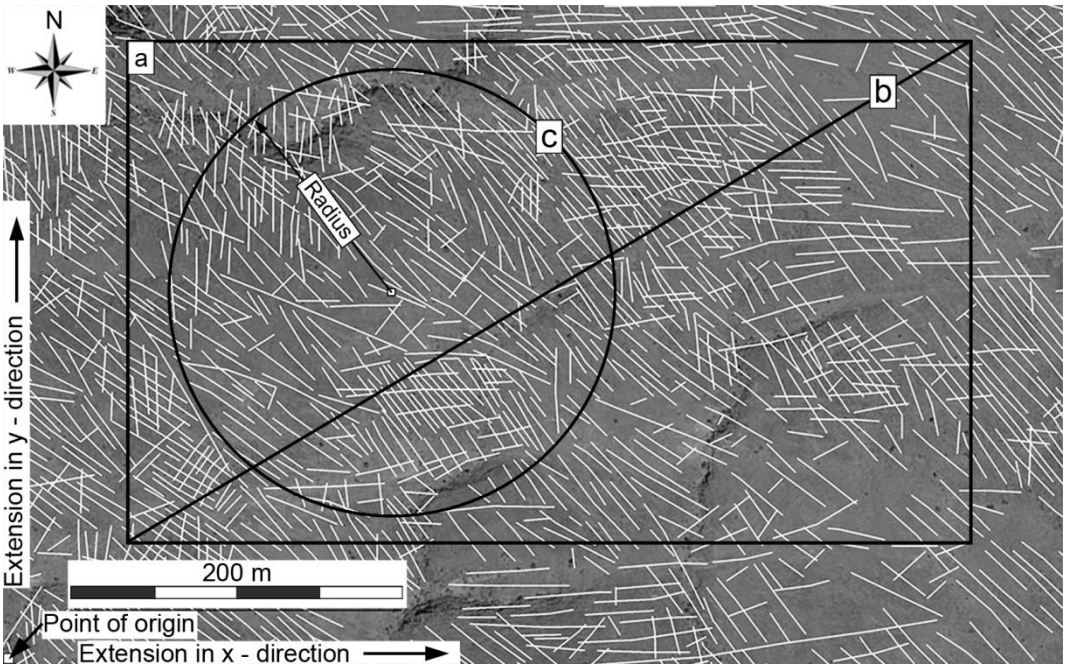

Fig. 12. Satellite image (modified from Google, DigitalGlobe) and size of the study area at the southern flank of the Jabal Akhdar dome in the Oman Mountains (Holland et al., 2009b). Lineaments identified by manual interpretation are represented by white lines. (a) Sampling area analysed using the window sampling and circular estimator method, (b) sampling line analysed using the scanline sampling method and (c) example of a circular scanline. The UTM coordinates of the lower left corner are 40N 517744 2564259 (Zeeb et al., 2013b).

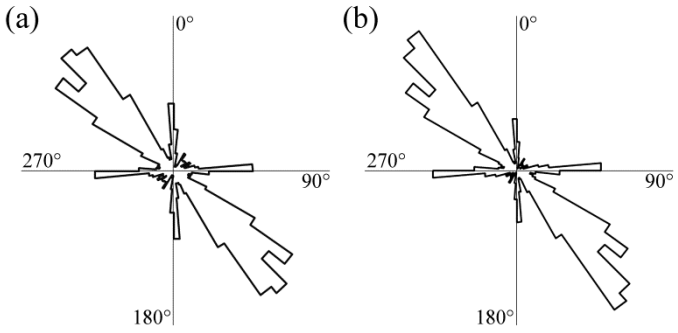

Fig. 13. Rose diagram (bin size of 5°) of the fracture strikes, with (a) the cumulative-number plot and (b) the length-weighted plot (Zeeb et al., 2013b).

Fracture network characteristics

The endpoints of 1236 fractures are imported to FraNEP as UTM coordinates. Three fracture sets are identified in the plot of fracture strikes in a length-weighted rose diagram (Fig. 13b). The locations for the application of the window sampling (Fig. 12a), the scanline sampling (Fig. 12b), and the circular estimator (Fig. 12c) methods are shown in Fig. 12. Fig. 14 shows the cumulative distribution of the fracture lengths sampled by window and scanline sampling. Moreover, the fits of a truncated power-law, a log-normal and an exponential equation are presented. For both sampling methods the best fit to the measured fracture lengths is found to follow a log-normal distribution. In Table 9 the calculated fracture network characteristics are summarized.

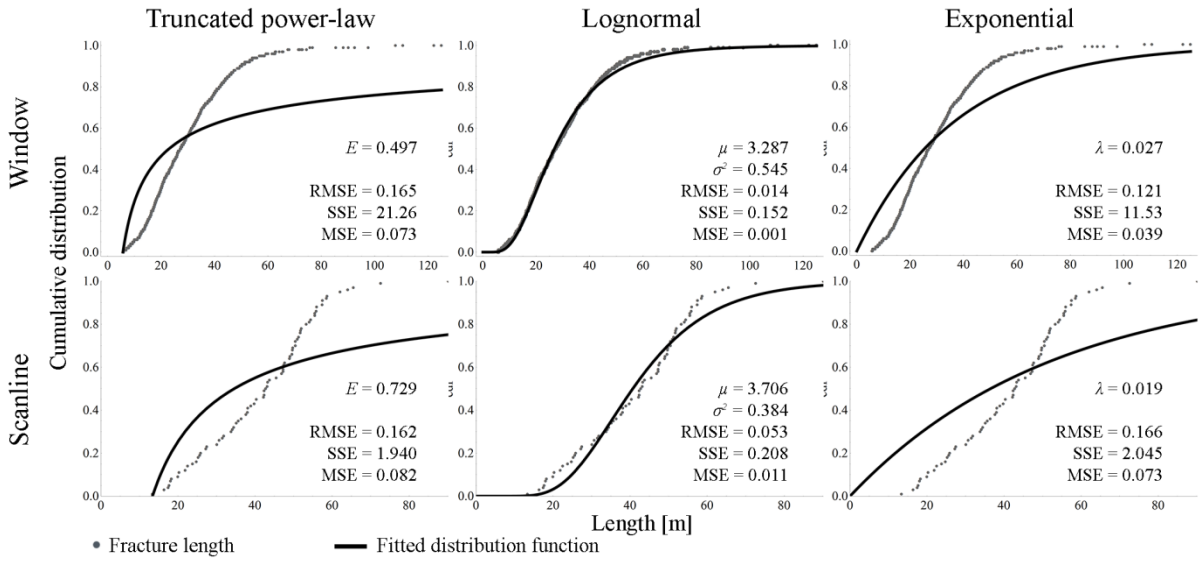

Fig. 14. Cumulative distribution of fracture lengths sampled by the scanline and window sampling methods, as well as the fits of a truncated power-law, log-normal and exponential function. E, μ, σ^2 and λ are the fitted parameters of the corresponding distribution functions. The accuracy of the fits is provided as RMSE, SSE and MSE (Zeeb et al., 2013b).

Table 9. Fracture network characteristics of the field example evaluated by the three sampling methods (Fig. 12) (Zeeb et al., 2013b).

Parameter		Window	Scanline	Circular
Sampled area [m²] or length of the scanline [m]		1.5×10^5	583	1.5×10^5
Number of fractures [-]		785	74	–
Fracture density [m^{-2}]		0.005	–	0.004
Fracture intensity [m m^{-2}] or fracture frequency (scanline) [m^{-1}]		0.15	0.13	0.17
Mean fracture length [m]		29.4	41.8	44.5
Number of censored fractures [-]		144	0	–
Number of fractures shorter than lower uncensored cut-off length [-]		23	0	–
Best fitted length distribution		log-normal	log-normal	–
Accuracy of the best fit	RMSE	0.014	0.053	–
	SSE	0.152	0.208	–
	MSE	0.001	0.011	–
Fitted parameter 1 (E, μ, λ)		μ = 3.287	μ = 3.706	–
Fitted parameter 2 (σ^2)		σ^2 = 0.545	σ^2 = 0.384	–

"–" Method provides no information.

Discussion

The software FraNEP automatically analyses the statistical properties of 2D fracture networks based on 2D trace-line maps in a time-effective and user-friendly way. The program is developed to quickly evaluate large amounts of fracture data, thus closing the gap between the automatic detection of lineaments and DFN modeling. A main novelty of FraNEP is the characterization of fracture networks applying the (1) scanline sampling, (2) window sampling or (3) circular estimator method, without the need of switching programs. Sampling methods can be applied to the entire study area or to specific sampling locations. Hence, the most appropriate sampling method can be used to analyse the most representative part of a study area.

FraNEP calculates the main network statistics, including the length and strike of each fracture, estimates for fracture density, intensity, mean length and length distribution, and information on the number of censored fractures. Rose diagrams with adjustable bin size provide information on fracture strikes and allow a quick identification of fracture sets. The strikes in each bin can be plotted either as their cumulative number or by the sum of their fracture lengths. The evaluation of the

fracture length distribution is done either automatically, or by choosing one of three distribution functions (truncated power-law, log-normal and/or exponential). Existing software often uses histograms and probability density plots to describe fracture length distributions. In FraNEP the cumulative distribution is used to determine the best fit, which avoids problems related to binning.

FraNEP is developed in Visual Basic for Applications in Microsoft Excel™, which makes the program easy-to-use and enables a post-processing of the results without the need to export data to other software. Moreover, the program code is organized in modules, which makes it easy to extend FraNEP to personal and site-specific requirements.

4. Conclusions

One objective of this thesis was the analysis of three natural fracture networks using outcrop and satellite-image data. The fracture networks of the Wajid sandstone were studied using a deterministic approach. It was found that the orientation of maximum hydraulic fracture conductivity follows the orientation of the main fracture sets. Moreover, the calculated in-situ hydraulic fracture apertures range between 1.3 to 1.7 mm and coincide with observed apertures in the field (>> 1 mm). The ratio between k_f / k_m with 10.4 indicates that overall fluid transport in the Wajid sandstone is influenced by the fracture network.

The fracture networks at Craghouse Park, UK and Oman Mountains, Oman were analysed applying various sampling techniques, such as scanline sampling, window sampling and circular estimator methods. Each applied sampling method provided different values for fracture density, intensity, mean length and length distribution. Since orientation, size and truncation biases were accounted for, these differences are either caused by a lack of measurements or by censoring bias. Hence, two other main objectives were therefore (1) the evaluation of the minimum number of required measurements for each sampling method and (2) the quantification of the influence of censoring bias on fracture network characterization.

For reasonable estimation of a power-law fracture length distribution at least 110 fractures should sampled using the window sampling method. Applying the scanline sampling method at least 225 fracture lengths should be measured. For the application of the circular estimator method a minimum of 860 fractures should be present in a sampling window to assure reasonable results. However, an universally applicable minimum number is almost certainly impossible to obtain. The suggested minimum numbers of required measurements were evaluated using artificial fracture networks with fracture lengths following power-law distributions. The range of exponents for this applied power-law distributions is equal to those commonly reported for natural fracture networks. Thus, the proposed numbers enable a better estimate of the required number of measurements for the characterization of natural fracture networks.

Investigating the influence of censoring bias on the characterization of fracture networks, it was found that for all sampling methods and parameters the uncertainty of measured values clearly increases with the percentage of censored fractures. In

general, the results based on the window sampling method indicate the lowest uncertainty. However, all sampling methods show a high uncertainty for estimates of fracture intensity. Although, the circular estimator highly overestimates fracture intensity, the method exhibits the lowest uncertainty. The artificial fracture networks used in the current study are simple and natural examples are often much more complex. Hence, it is likely that even more fractures are censored. However, since we use percentages of censored fractures, the approach to evaluate the uncertainty is also applicable to natural fracture networks.

A large amount of fracture networks were analysed within the framework of this thesis. Since the characterization of fracture networks by hand is tedious and time-consuming, a novel software was developed. The software FraNEP automatically analyses the statistical properties of 2D fracture networks based on 2D fracture trace-line maps in a time-effective and user-friendly way. A main novelty of FraNEP is the characterization of fracture networks using (1) scanline sampling, (2) window sampling and/or (3) circular estimator method, without the need of switching programs. Sampling methods can be applied to the entire study area or to specific sampling locations. Hence, the most appropriate sampling method can be used to analyse the most representative part of a study area. FraNEP calculates the key fracture network statistics, including the length and strike of each fracture, estimates for fracture density, intensity, mean length and length distribution. In addition, information on the number of censored fractures is also provided, which can be used to assess the uncertainty with increasing percentage of censored fractures.

5. Literature

Al Ajmi, H., M. Keller, M. Hinderer, R. Rausch, 2009. New insights into the facies distribution of the Wajid sandstone in its Western outcrop area and implication on reservoir properties: In: Proceedings of the 3rd International Conference on Water Resources and Arid Environments 2008 and the 1st Arab Water Forum, Riyadh, Saudi Arbia, November 2008, 13 pp.

Barthélémy, J.-F., M. L. E. Guiton, J.-M. Daniel, 2009. Estimates of fracture density and uncertainties from well data: International Journal of Rock Mechanics and Mining Sciences, v. 46, p. 590 – 603.

Barton, N., S. Bandis, 1980. Technical Note: Some Effects of Scale on the Shear Strength of Joints: International Journal of Rock Mechanics, Mining Sciences & Geomechancial Abstracts, v. 17, p. 69 – 73.

Barton, N., S. Bandis, K. Bakhtar, 1985. Strength, Deformation and Conductivity Coupling of Rock Joints: International Journal of Rock Mechanics, Mining Sciences & Geomechancial Abstracts, v. 22, p. 121 – 140.

Barton, N., E. F. de Quadros, 1997. Joint aperture and roughness in the prediction of flow and groutability of rock masses: International Journal of Rock Mechanics and Mining Sciences, v. 34, p. 252.e1 – 252.e14.

Becker, M. W., 2006. Potential for satellite remote sensing of ground water: Ground Water, v. 44, p. 306 – 318.

Belayneh, M. W., S. K. Matthäi, M. J. Blunt, S. F. Rogers, 2009. Comparison of deterministic with stochastic fracture models in water-flooding numerical simulations: AAPG Bulletin, v. 93, p. 1633 – 1648.

Berkowitz, B., 2002. Characterizing flow and transport in fractured geological media: A review: Advances in Water Resources, v. 25, p. 861 – 884.

Blöcher, M. G., G. Zimmermann, I. Moeck, W. Brandt, A. Hassanzadegan, F. Magri, 2010. 3D numerical modeling of hydrothermal processes during the lifetime of a deep geothermal reservoir: Geofluids, v. 10, p. 406 – 421.

Blum, P., R. Mackay, M. S. Riley, J. L. Knight, 2005. Performance assessment of a nuclear waste repository: Upscaling coupled hydro-mechanical properties for far-field transport analysis: Journal of Rock Mechanics and Mining Sciences, v. 42, p. 781 – 792.

Blum, P., R. Mackay, M. S. Riley, 2007. Coupled hydro-mechanical modelling of flow in fractured rock: In: Sharp, J. M. & Krasny, J. (Eds.), Groundwater in Fractured Rocks, IAH-Selected Paper Series, v. 9, p. 567 – 574.

Blum, P., R. Mackay, M. S. Riley, J. L. Knight, 2007. Hydraulische Modellierung und die Ermittlung des repräsentativen Elementarvolumens (REV) im Kluftgestein [Hydraulic

modelling and the evaluation of the representative elementary volume (REV) in fractured rock]: Grundwasser, v. 12, p. 48 – 65.

Blum, P., R. Mackay, M. S. Riley, 2009. Stochastic simulations of regional scale advective transport in fractured rock masses using block upscaled hydro-mechanical rock property data: Journal of Hydrology, v. 369, p. 318 – 325.

Bonnet, E., O. Bour, N. E. Odling, P. Davy, I. Main, P. Cowie, B. Berkowitz, 2001. Scaling of fracture systems in geological media: Reviews of Geophysics, v. 39, p. 347 – 383.

Bons, P. D., J. Arnold, M. A. Elburg, J. Kalda, A. Soesoo, B. P. van Milligen, 2004. Melt extraction and accumulation from partially molten rocks: Lithos, v. 78, p. 25 – 42.

Bons, P. D., M. A. Elburg, E. Gomez-Rivas, 2012. A review of the formation of tectonic veins and their microstructures: Journal of Structural Geology, v. 43, p. 33 – 62.

Brace, W., 1960. An extension of the Griffith theory of fracture to rocks: Journal of Geophysical Research, v. 65, p. 3477 – 3480.

Butler, J. J., 2009. Pumping tests for aquifer evaluation: time for a change?: Ground Water, v. 47, p. 615 – 617.

Castaing, C., A. Genter, B. Bourgine, J. P. Chilès, J. Wendling, P. Siegel, 2002. Taking into account the complexity of natural fracture systems in reservoir single-phase flow modeling: Journal of Hydrology, v. 266, p. 83 – 98.

Cox, S. F., 2010. The application of failure mode diagrams for exploring the roles of fluid pressure and stress states in controlling styles of fracture-controlled permeability enhancement in faults and shear zones: Geofluids, v. 10, p. 217 – 233.

Cruden, D. M., 1977. Describing the size of discontinuities: International Journal of Rock Mechanics and Mining Sciences & Geomechanical Abstracts, v. 14, p. 133 – 137.

Darcel, C., O. Bour, P. Davy, 2003. Stereological analysis of fractal fracture networks: Journal of Geophysical Research, v. 108, p. 1 – 14.

Dershowitz, W. S., 1984. Rock Joint Systems: Ph.D. Dissertation, Massachusetts Institute of Technology, Cambridge, Massachusetts.

Dershowitz, B., P. LaPoint, T. Eiben, L. Wei, 2000. Integration of discrete feature network methods with conventional simulator approaches: Society of Petroleum Engineers Reservoir Evaluation and Engineering, v. 3, 165 – 170.

Durham, W. B., B. P. Bonner, 1994. Self-propping and fluid flow in slightly offset joints at high effective pressures: Journal of Geophysical Research, v. 99, p. 9391 – 9399.

Evans, D. S., R. B. Lathon, M. Senalp, T. C. Connally, 1991. Stratigraphy of the Wajid Sandstone of south-western Saudi Arabia: Society of Petroleum Engineers.

Forte, E., M. Pipan, D. Casabianca, R. Di Cuia, A. Riva, 2012. Imaging and characterization of carbonate hydrocarbon reservoir analogue using GPR attributes: Journal of Applied Geophysics, v. 81, p. 76 – 87.

Fouché, O., J. Diebolt, 2004. Describing the geometry of 3D fracture systems by correcting for linear sampling bias: Mathematical Geology, v. 36, p. 33 – 63.

Hatton, C. G., I. G. Main, P. G. Meredith, 1993. A comparison of seismic and structural measurements of fractal dimension during tensile subcritical crack growth: Journal of Structural Geology, v. 15, p. 1485 – 1495.

Hilgers, C., D. L. Kirschner, J.-P. Breton, J. L. Urai, 2006. Fracture sealing and fluid overpressures in limestones of the Jabal Akhdar dome, Oman mountains: Geofluids, v. 6, p. 168 – 184.

Holland, M., J. L. Urai, P. Muchez, E. J. M. Willemse, 2009a. Evolution of fractures in a highly dynamic thermal, hydraulic, and mechanical system - (I) Field observations in Mesozoic Carbonates, Jabal Shams, Oman Mountains: GeoArabia, v. 14, p. 57 – 110.

Holland, M., J. L. Urai, P. Muchez, E. J. M. Willemse, 2009b. Evolution of fractures in a highly dynamic, thermal, hydraulic, and mechanical system - (II) Remote sensing fracture analysis, Jabal Shams, Oman Mountains: GeoArabia, v. 14, p. 163 – 194.

Hornung, J., 1999. Dynamische Stratigraphie, Reservoir- und Aquifer-Sedimentgeologie einer alluvialen Ebene: Der Stubensandstein in Baden-Württemberg (Obere Trias, Mittlerer Keuper) [Dynamic stratigraphy, reservoir- and aquifer-sedimentology of an alluvial plain: the Stubensandstein in Baden-Würtemberg (upper Trias, middle Keuper)]: Tübinger Geowissenschaftliche Arbeiten (TGA), Reihe A, (Nr. 56), Tübingen, Germany, 156 pp.

Hudson, J. A., S. D. Priest, 1983. Discontinuity frequeny in rock masses: International Journal of Rock Mechanics and Mining Sciences & Geomechanical Abstracts, v. 20, p. 73 – 89.

Jackson, C. P., A. R. Hoch, S. Todman, 2000. Self-consistency of a heterogeneous continuum porous medium representation of fractured media: Water Resources Research, v. 36, p. 189 – 202.

Jeanne, P., Y. Guglielmi, F. Cappa, 2012. Multiscale seismic signature of a small fault zone in a carbonate reservoir: Relationships between V_p imaging, fault zone architecture and cohesion: Tectonophysics, v. 554 – 557, p. 185 – 201.

Kellogg, K. S., D. Janjou, L. Minoux, J. Fourniguet, 1986. Explanatory notes to the geologic map of the Wadi Tathlith Quadrangle, sheet 20G: Ministry of Petroleum and Mineral Resources, Kingdom of Saudi Arabia, Riyadh.

Koike, K., S. Nagano, M. Ohmi, 1995. Lineament analysis of satellite images using a segment tracing algorithm (STA): Computers and Geosciences, v. 21, p. 1091 – 1104.

Konert, G., M. A. Abdulkader, A. A. Sa'id, J. D. Henk, 2001. Palaeozoic stratigraphy and hydrocarbon habitat of the Arabian Plate: Geoarabia, v. 6, p. 407 – 442.

Kulatilake, P. H. S. W., T. H. Wu, 1984. The density of discontinuity traces in sampling windows (technical note): International Journal of Rock Mechanics and Mining Sciences & Geomechanical Abstracts, v. 21, p. 345 – 347.

Lacazette, A., 1991. A new stereographic technique for the reduction of scanline survey data of geologic features: Computers and Geosciences, v. 17, p. 445 – 463.

LaPointe, P. R., 2002. Derivation of parent population statistics from trace length measurements of fractal populations: International Journal of Rock Mechanics and Mining Sciences, v. 39, p. 381 – 388.

Laubach, S. E., 2003. Practical approaches to identifying sealed and open fractures: AAPG Bulletin, v. 87, p. 561 – 579.

Laubach, S. E., M. E. Ward, 2006. Diagenesis in porosity evolution of opening-mode fractures, Middle Triassic to Lower Jurassic La Boca Formation, NE Mexico: Tectonophysics, v. 419, p. 75 – 97.

Laubach, S. E., J. E. Olson, M. R. Gross, 2009. Mechanical and fracture stratigraphy: AAPG Bulletin, v. 93, p. 1413 – 1426.

Lee, C.-H, I. Farmer, 1993. Fluid flow in discontinuous rock: London, Chapman & Hall, 169 p.

LeGarzic, E., T. de L'Hamaide, M. Diraison, Y. Géraud, J. Sausse, M. de Urreiztieta, B. Hauville, J.-M. Champanhet, 2011. Scaling and geometric properties of extensional fracture systems in the proterozoic basement of Yemen. Tectonic interpretation and fluid flow implications: Journal of Structural Geology, v. 33, p. 519 – 536.

Louis, C, 1967. Strömungsvorgänge in klüftigen Medien und ihr Wirkung auf die Standsicherheit von Bauwerken und Böschungen im Fels [Flow phenomena in fractured systems and their contribution to structural integrity of buildings and slopes at rock]. PhD Thesis, Technical University Karlsruhe, Germany.

Lyman, G. J., 2003. Rock fracture mean trace length estimation and confidence interval calculation using maximum likelihood methods: International Journal of Rock Mechanics and Mining Sciences, v. 40, p. 825 – 832.

Manda, A. K., S. B. Mabee, 2010. Comparison of three fracture sampling methods for layered rocks: International Journal of Rock Mechanics and Mining Sciences, v. 47, p. 218 – 226.

Manzocchi, T., J. J. Walsh, W. R. Bailey, 2009. Population scaling bias in map samples of power-law fault samples: Journal of Structural Geology, v. 31, p. 1612 – 1626.

Mauldon, M., W. M. Dunne, M. B. Rohrbaugh, Jr., 2001. Circular scanlines and circular windows: new tools for characterizing the geometry of fracture traces: Journal of Structural Geology, v. 23, p. 247 – 258.

Narr, W., 1996. Estimating average fracture spacing in subsurface rock: AAPG Bulletin, v. 80, p. 1565 – 1586.

Neuman, S. P., 2005. Trends, prospects and challenges in quantifying flow and transport through fractured rocks: Hydrogeology Journal, v. 13, p. 124 – 147.

Neuman, S. P., 2008. Multiscale relationship between fracture length, aperture, density and permeability: Geophysical Research Letters, v. 35, p. 1 – 6.

Nirex, 1997a. The lithological and discontinuity characteristics of the Borrowdale Volcanic Group at the outcrop in the Craghouse Park and Latterbarrow areas: Nirex Report SA/97/029, Harwell.

Nirex, 1997b. Evaluation of heterogeneity and scaling of fractures in the Borrowdale Volcanic Group in the Sellafield area: Nirex Report SA/97/028, Harwell.

Odling, N. E., 1997. Scaling and connectivity of joint systems in sandstones from western Norway: Journal of Structural Geology, v. 19, p. 1257 – 1271.

Olson, J. E., 2003. Sublinear scaling of fracture aperture versus length: An exception or the rule?: Journal of Geophysical Research (American Geophysical Union), v. 108, no. B9, 2413.

Olson, J. E., S. E. Laubach, R. H. Lander, 2009. Natural fracture characterization in tight gas sandstones: Integration mechanics and diagenesis: AAPG Bulletin, v. 93, p. 1535 – 1549.

Olson, J. E., R. A. Schultz, 2011. Comment on " A note on the scaling relations for opening mode fractures in rock" by C.H. Schultz: Journal of Structural Geology, v. 33, p. 1523 – 1524.

Ortega, O. J., R. A. Marrett, 2000. Prediction of macrofracture properties using microfracture information, Mesaverde Group sandstones, San Juan basin, New Mexico: Journal of Structural Geology, v. 22, p. 571 – 588.

Ortega, O. J., R. A. Marrett, S. E. Laubach, 2006. A scale-independent approach to fracture intensity and average spacing measurement: AAPG Bulletin, v. 90, p. 193 – 208.

Pahl, P. J., 1981. Estimating the mean length of discontinuity traces: International Journal of Rock Mechanics and Mining Sciences & Geomechanics Abstracts, v. 18, p. 221 – 228.

Pérez-Claros, J. A., P. Palmqvist, F. Olóriz, 2002. First and second orders of suture complexity in ammonites: A new methodological approach using fractal analysis: Mathematical Geology, v. 34, p. 323 – 343.

Philip, Z. G., J. W. Jennings Jr., J. E. Olson, S. E. Laubach, J. Holder, 2005. Modelling coupled fracture-matrix fluid flow in geomechanically simulated fracture networks: Society of Petroleum Engineers.

Phillips, W.J., 1972. Hydraulic fracturing and mineralization: Journal of the Geological Society, London 128, 337 – 359.

Pickering, G., J. M. Bull, D. J. Sanderson, 1995. Sampling power-law distributions: Tectonophysics, v. 248, p. 1 – 20.

Pollard, D. D., P. Segall, 1987. Theoretical displacements and stresses near fractures in rocks: with applications to faults, joints, dikes and solution surfaces: In: Atkinson, B.K. (Ed.), Fracture Mechanics of Rock. Academic Press, London, p. 277 – 348.

Price, N. J., J. W. Cosgrove, 1990. Analysis of Geological Structures: Cambridge University Press, Cambridge.

Priest, S. D., J. A. Hudson, 1981. Estimation of discontinuity spacing and trace length using scanline surveys: International Journal of Rock Mechanics and Mining Sciences & Geomechanics Abstracts, v. 18, p. 183 – 197.

Priest, S. D., 1993. Discontinuity analysis for rock engineering. London, Chapman & Hall, 473 p.

Priest, S. D., 2004. Determination of discontinuity size distributions from scanline data: Rock Mechanics and Rock Engineering, v. 37, p. 347 – 368.

Renshaw, C. E., J. S. Dadakis, S. R. Brown, 2000. Measuring fracture apertures: A comparison of methods: Geophysical Research Letters, v. 27, p. 289 – 292.

Riley, M. S., 2005. Fracture trace length and number distributions from fracture mapping: Journal of Geophysical Research, v. 110.

Rohrbaugh, Jr., M. B., W. M. Dunne, M. Mauldon, 2002. Estimating fracture trace intensity, density and mean length using circular scanlines and windows: AAPG Bulletin, v. 86, p. 2089 – 2104.

Roy, A., E. Perfect, W. M. Dunne, L. D. Mckay, 2007. Fractal characterization of fracture networks: an improved box-counting technique: Journal of Geophysical Research, v. 112, B12201.

Scholz, C. H., 2002. The Mechanics of Earthquakes and Faulting: second ed. Cambridge University Press, Cambridge.

Scholz, C. H., 2010. A note on the scaling relations for opening mode fractures in rock: Journal of Structural Geology, v. 32, p. 1485 – 1487.

Schwarz, J.-O., F. Enzmann, 2013. Simulation of Fluid Flow on Fractures and Implications for Reactive Transport Simulations: Transport in Porous Media, v. 96, p. 501 – 525.

Sibson, R. H., 1998. Brittle failure mode plots for compressional and extensional tectonic regimes: Journal of Structural Geology, v. 20, p. 655 – 660.

Snow, D. T., 1965. A parallel plate model of fractured permeable media. PhD Thesis, University of California, Berkeley, USA.

Steele, A., D. A. Reynolds, B. H. Kueper, D. N. Lerner, 2006. Field determination of mechanical aperture, entry pressure and relative permeability of fractures using NAPL injection: Géotechnique, v. 56, p. 27 – 38.

Sudha, K., B. Tezkan, M. Israil, J. Rai, 2011. Combined electrical and electromagnetic imaging of hot fluids within fractured rock in rugged Himalayan terrain: Journal of Applied Geophysics, v. 74, p. 205 – 214.

Terzaghi, R. D., 1965. Sources of error in joint surveys: Géotechnique, v. 13, p. 287 – 304.

Tóth, T. M., 2010. Determination of geometric parameters of fracture networks using 1D data: Journal of Structural Geology, v. 32, p. 1271 – 1278.

Toublanc, A., S. Renaud, J. E. Sylte, C. K. Clausen, T. Eiben, G. Nadland, 2005. Ekofisk field: fracture permeability evaluation and implementation in the flow model: Petroleum Geoscience, v. 11, p. 321 – 330.

Van der Pluijm, B. A., S. Marshak, 2004. Earth Structure – An Introduction to Structural Geology and Tectontics (Second Edition). W. W. Norton & Company, New York, US.

Weiss, M., 2008. Techniques for estimating fracture size: A comparison of methods: International Journal of Rock Mechanics and Mining Sciences, v. 45, p. 460 – 466.

Wu, H., D. D. Pollard, 1995. An experimental study of the relationship between joint spacing and layer thickness: Journal of Structural Geology, v. 17, p. 887 – 905.

Yeo, I. W., M. H. de Freitas, R. W. Zimmerman, 1998. Effect of shear displacement on the aperture and permeability of a rock fracture: International Journal of Rock Mechanics and Mining Sciences, v. 35, p. 1051 – 1070.

Zeeb, C., D. Göckus, P. Bons, H. Al Ajmi, R. Rausch, P. Blum, 2010. Fracture flow modelling based on satellite images of the Wajid Sandstone, Saudi Arabia: Hydrogeology Journal, v. 18, p. 1699 – 1712.

Zeeb, C., E. Gomez-Rivas, P. D. Bons, P. Blum, 2013a. Evaluation of sampling methods for fracture network characterization using outcrops: AAPG Bulletin, v. 97, p. 1545 – 1566.

Zeeb, C., Gomez-Rivas, P. D. Bons, S. Virgo, P. Blum, 2013b. Fracture Network Evaluation Program (FraNEP): A software for analyzing 2D trace-line maps of fracture networks: Computers & Geosciences, v. 60, p. 11 – 22.

Zhang, L., H. H. Einstein, 1998. Estimating the mean trace length of rock discontinuities: Rock Mechanics and Rock Engineering, v. 31, p. 217 – 235.

Zhang, L., H. H. Einstein, 2000. Estimating the intensity of rock discontinuities: International Journal of Rock Mechanics and Mining Sciences, v. 37, p. 819 – 837.

6. Publications

6.1. Fracture flow modelling based on satellite images of the Wajid sandstone, Saudi Arabia†

Conny Zeeb [a], Daniel Göckus [a], Paul Bons [a], Hussain Al Ajmi [b,c], Randolf Rausch [b], Philipp Blum [a,*]

[a] *University of Tübingen, Institute for Geoscience (IfG), Sigwartstraße 10, 72076 Tübingen, Germany*

[b] *Gesellschaft für Technische Zusammenarbeit International Services (GTZ-IS), Riyadh, Saudi Arabia*

[c] *Ministry of Water and Electricity, Water Resources Development Department, Riyadh, Saudi Arabia*

*Corresponding author
Tel: +49-(0)7071-29 73170
Fax: +49-(0)7071-29 5059
E-mail: philipp.blum@uni-tuebingen.de

Abstract

The focus of the current study is the identification of large scale geological features such as fractures by satellite images and the evaluation of their impact on the regional aquifer system in the Wajid sandstone in Saudi Arabia. The main objective is to evaluate the importance of fractures for the overall flow behaviour in a fractured rock aquifer and the estimation of average in-situ hydraulic apertures. Aquifer fracture flow models for the Wajid sandstone were developed based on satellite images and GPS data obtained in the field. Data on fractures and lineaments were available for three outcrops. By applying a cut-out routine on the fracture endpoint data of these fracture trace windows, three deterministic discrete fracture networks (DFN) with an area of 100 m × 100 m could be generated. These were used to simulate the fracture flow and to determine the hydraulic conductivity tensors. Using additional data on hydraulic pumping tests and matrix conductivities, in-situ hydraulic apertures could be determined. Average in-situ hydraulic apertures range from 1,300 to 1,700 µm. Observations from the field support these results. In addition, a hydraulic conductivity ratio between the matrix and fracture system was used to identify the contribution of the discrete fracture network to the overall fluid transport. A ratio of 10.4 was determined, which indicates that the effective flow behaviour in the Wajid sandstone aquifer is not entirely dominated by the fracture system, though evidently strongly controlled by it.

KEYWORDS: Groundwater management; Remote sensing; Fractured aquifer; Sandstone aquifer; Discrete fracture networks.

Introduction

Increasing population in semi-arid and arid regions results in an increasing stress on the groundwater and surface-water resources in such areas. In particular, the increasing irrigation for agriculture and livestock, which is needed to sustain the demand for food supplies, puts an additional strain on the already scarce water resources. As a result, groundwater levels have continuously declined in many parts of the world over the last decades (e.g. Postel 1999; Shah et al. 2000; Konikow and Kendy 2005). The management and preservation of water resources in semi-arid and arid regions, especially in times of acute climatic changes, is one of the main issues in present hydrogeology research (e.g. Luijendijk and Bruggemann 2008). However, the results of such studies are often constrained by the availability of hydrological and hydrogeological data. Apart from the fact that these sites are often inaccessible due to mountainous geography and/or sand cover, most countries and provinces in semi-arid regions neither have the equipment nor the money for intensive site-specific groundwater investigations. Using remote sensing and GIS methods therefore proved to be a cost effective, non-destructive and non-invasive strategy that can be applied in arid and semi-arid regions (e.g. Hoffmann 2005; Robinson et al. 2007; Hoffmann and Sander 2007).

Over the last decades many studies were undertaken to investigate the feasibility of satellite images for geology and subsurface hydrology (e.g. Becker 2006). The potential of using optical and radar data for geological mapping in arid regions was investigated and discussed by Deroin et al. (1996). They could demonstrate that the quality of the information strongly depends on the quality and the medium of the chosen satellite images as well as on the ability of the interpreter to recognise and identify geological phenomena. Satellite images offer a wide range of spatial, temporal and spectral information, with a ground resolution ranging from km-scale (METEOSAT) down to 1-4 m (OrbView-3) (e.g. Leblanc et al. 2006). The potential of remote sensing for groundwater exploration was investigated, for example, by Becker (2006) and Brunner et al. (2006). Examples for the different methods are the following: for thermal data, METEOSAT and Advanced Very High Resolution Radiometer (AVHRR); for elevation data, the Shuttle Radar Topography Mission (SRTM); for optical data, Moderate Resolution Imaging Spectro-Radiometer (MODIS), Landsat TM and AVHRR; and for vegetation index data, MODIS (Leblanc

et al. 2006). Other remote sensing tools have also been developed in recent years. For example, the Gravity Recovery and Climate Experiment (GRACE) allows estimation on groundwater storage changes as small as 8.7 mm (Rodell and Famiglietti 2002; Yeh et al. 2006).

One main advantage of satellite imagery is the ability to identify structural and tectonic features, which are valuable for the assessment of fractured aquifers (e.g. National Research Council 1996; Castaing et al. 2002). Radar, for example, is able to qualify bedrock nature and in some cases even to determine geological formations beneath layers of sand (Deroin et al. 1996). Prior to the year 2000, analyses relied on Shuttle Imaging Radar (SIR) or low-resolution SIR-C survey images. Studies since 2000 have employed high-resolution, multi-wavelength, multi-polarization Space borne Imaging Radar (SIR-C) or Radarsat-1 data (Robinson et al. 2007). Based on these radar data, many studies were undertaken to identify and characterise rock formations and structures, such as palaeo-drainage networks, in arid areas invisible on Landsat TM images and in the field (Elachi et al. 1986, Davis et al. 1993). Further investigation of areas with faults, fractured rock and fluvial features showed that these patterns are often used by means of groundwater discharge, recharge and flow (e.g. Babiker and Gudmundsson 2004; Galanos and Rokos 2005; Robinson et al. 1999, 2000, 2002, 2007).

The detection and characterisation of lineaments from satellite images could be achieved by an automated Segment Tracing Algorithm (STA) proposed by Koike et al. (1995), which allows the characterization of lineaments in a study area by statistical quantities of orientation, length, distance and density (Koikea et al. 1996). Koike and Ichikawa (2004) analysed lineaments derived from Landsat and SPOT satellite images from the eastern part of the Tohoku district, Japan, to develop a scaling law and to model fracture distribution. Masoud and Koike (2005) used the STA to detect lineaments in the Siwa region, NW Egypt, for a detailed structural analysis and to understand the tectonic evolution of the area. In combination with Digital Elevation Models (DEM), derived from the Shuttle Radar Topographic Mission (SRTM) and Synthetic Aperture Radar (SAR), areas of high groundwater potentials could be identified in the Nubian aquifer in Egypt (Robinson et al. 2006). Using Landsat images, aerial photographs and fractured trace maps, Castaing et al. (1996) studied the scaling relationship in intraplate fracture systems of the Cambrian-Ordovician Saq sandstone formation related to Red Sea rifting in northwestern Saudi-

Arabia. Based on this study, Castaing et al. (2002) conducted some flow simulations of a pumping well, which took into account three different scales of permeability to represent the matrix, joints, and faults. They used the permeability ratio K_f/K_m between the faults (K_f) and the joint rock matrix (K_m) to quantify the influence of the fault system on the overall fluid transport. For example, at a permeability ratio of $K_f/K_m = 100$, groundwater flow starts to be channelled mainly in the fault system.

An alternative method of detecting lineaments is the airborne laser scanning technology that uses the Light Detection And Ranging (LIDAR) laser system (Nyborg et al. 2006). The main drawback of this technology is that it could only be applied on outcrops without cover. An overview of applications and limitations of lineaments in groundwater exploration is given by Sander (2006).

The combination of remote sensing and existing field investigation data through geographic information systems (GIS) has helped to better understand groundwater re- and discharge areas, groundwater and surface-water interactions and palaeohydrological settings, and to identify potential aquifers (Lubczynski 1997, Leblanc et al. 2006, Jha and Chowdary 2006). Sultan et al. (2007) used a combination of satellite images and in-situ data to identify aquifers at the Najd shear system of the Arabian Nubian shield. A different approach was used by Franssen et al. (2007). They generated multiple equally likely recharge realizations for the Chobe region, Botswana, and used hydraulic head data and a DEM to condition their realizations. The evaluation of groundwater potential zones by combining remote sensing and in-situ data have been undertaken for many different regions, for example in Kerala, on the southwest coast of India (Kumar et al. 2007), Rajura Taluka, Chandrapur district, Maharashtra (Rokade et al. 2007), the central highlands of Eritrea (Solomon 2006), Burdur, Turkey (Sener et al. 2005) or for the Nubian Aquifer in southwest Egypt (Robinson 2006). The studies by Castaing et al. (1996, 2002) demonstrated the potential of the application of satellite images on the Arabian Plate. The present study area of the Wajid sandstone formation is southeast of the Saq sandstone formation and therefore constitutes an extension of their work in the southern part of Saudi Arabia.

The main objective of the current study, however, was to develop a method to qualify and quantify fluid flow through deterministic discrete fracture networks (DFN) based mainly on satellite images and to estimate in-situ hydraulic apertures for the upper Wajid sandstone aquifer. In contrast to the flow modelling conducted by

Castaing et al. (2002), which used a channel network to represent the DFN, the DFN in the current study is simulated using a plane parallel plates approach (cubic law). Based on the discrete fracture flow simulations, it was possible to determine hydraulic conductivity tensors of the fracture systems. Furthermore, the importance of the fracture systems relative to the porous matrix could be evaluated and showed the significance of the fracture systems for groundwater recharge and flow in the Wajid sandstone formation.

Study area

The Wajid sandstone outcrop (> 44.000 km^2) is located in the southern part of Saudi Arabia, about 300 km east of the Red Sea and around 100 km north-east of the city of Khamis Mushayt. However, only a small percentage is accessible due to sand cover and rough terrain. Three Wajid sandstone outcrops were studied: (1) Al Jufrah in the southern part, (2) Uruq Khurb in the northern part and (3) Jabal al Bara'im in the far north (Fig. 1). Agricultural areas are located in the desert northeast of the Wajid Sandstone outcrops. Agriculture here completely depends on irrigation, as is the case throughout most parts of Saudi Arabia. The total agricultural area in Saudi Arabia is estimated to be 1.2 million ha, with an estimated groundwater extraction from non renewable resources of 19.8 km^3 for the year 2004. This is in contrast to estimated renewable water resources of 2.4 km^3 (FAO, 2008). Hence, the current use of groundwater in Saudi Arabia is evidently not sustainable.

Geology

The geology of the Arabian Peninsula is dominated by two dissimilar areas: The Arabian Shield in the west and the Arabian Platform in the east. The Arabian Shield consists of crystalline basement of Precambrian continental crust (~ 870Ma – 540Ma), with overlying Cenozoic volcanic rocks from the initial rifting phase of the Red Sea. The Arabian Platform is build up by a succession of Palaeozoic to recent sedimentary rocks that gently dip to the east (Konert et al. 2001). The sediments of the Wajid outcrop belt are of Middle/Late Cambrian to Early Permian age (Evans et al. 1991; Kellogg et al. 1986) and predominantly consist of sandstone with a mostly proximal deposition regime. The Wajid sandstone consists of four stratigraphic

members, separated by unconformities (Kellogg et al. 1986). These members are the Dibsiyah Member (Cambrian or Ordovician) with an approximate thickness of 150 m, the Lower (latest Ordovician to earliest Silurian) and the Upper Sanamah Member (early Silurian) with a thickness of 90 m, the Khusayyayn Member (latest Silurian to earliest Carboniferous) with a thickness of around 180 m and the Juwayl Member (late Carboniferous to early Permian) with a thickness of 130 m. The Khusayyayn Member outcrops in the Al Jufrah and Uruq Khurb study areas, while the Jabal al Bara'im outcrop is situated at the transition from the Khusayyayn to the Juwayl Member. This study, therefore, only deals with the Khusayyayn and Juwayl Members. The Khusayyayn Member consists of very regularly bedded, medium to coarse-grained sandstones that show cross-lamination dipping northwest to north-northwest. The bedding is disturbed by discontinuous intercalations of red and whitish fine-grained micaceous sandstone. The Juwayl Member is separated from the Khusayyayn Member by the Pre-Unayzah unconformity. Above this unconformity, channelled into underlying beds, the Juwayl Member consists of fine to coarse-grained bioturbated sandstone with sandstone and clay fragments. The sandstone shows no clear bedding; joints and local slumping can be found instead. Upwards, the beds change to sandstone with conglomeratic intercalations. Finally, the Upper Juwayl Member consists of sandstone with regular or cross-bedding (Kellogg et al. 1986).

Following the hydrogeological model of the Wajid water resources studies (GTZ-DCO final report, unpublished data, 2007) the Wajid Group is subdivided in three parts. The Lower Wajid Group is composed of the sandstones of the Dibsiyah and the Lower Sanamah Member and forms the lower of the two fractured bedrock aquifers. The second group is the Qalibah formation consisting of the Upper Sanamah Member and acts as an aquitard between the lower and the upper aquifer within the Wajid formation. The Upper Wajid Group, which is referred to as the upper aquifer, consists of the Khusayyayn and the Juwayl Member. Pumping test data are available for both aquifers. However, as only fracture data for the upper aquifer were available from the outcrops at Al Jufrah, Uruq Khurb and Jabal al Bara'im, the pumping test data from the lower aquifer were not considered in this study. The pumping tests were used to estimate the aquifer properties and well characteristics. They were performed at existing wells, which are mainly used for irrigation. In a first approach, methods for the analysis for porous aquifers were used for the

interpretation of the measurements from 33 wells (Butler 2009). The determined transmissivities for the Upper Wajid aquifer are in the range of 7.1×10^{-4} m^2 s^{-1} to 3.3×10^{-2} m^2 s^{-1}. The geometric mean of the transmissivity is 8.7×10^{-3} m^2 s^{-1}. The corresponding effective hydraulic conductivities vary between 1.0×10^{-5} m s^{-1} and 2.3×10^{-4} m s^{-1} with a geometric mean of 8.3×10^{-5} m s^{-1}. The average storage coefficient is 3.8×10^{-4} and the specific yield is estimated to be between 3 % and 10 %.

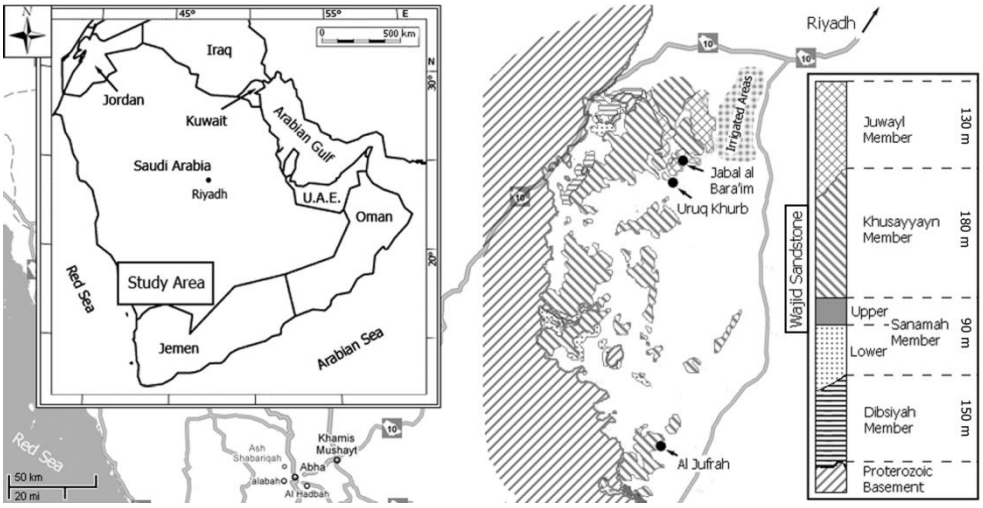

Fig. 1 Location and geology of the study area. Patterns of the schematic stratigraphic column correspond to the patterns of the outcrops of the geological units (stratigraphic column with member thicknesses modified from Kellogg et al. 1986; Evans et al. 1991)

Figure 2 shows the piezometric head distribution and the groundwater flow direction in the Upper Wajid aquifer. Within the study area, the piezometric head of the Upper Wajid aquifer ranges between 500 m above sea level (asl) and 900 m asl. The average hydraulic gradient is 0.2 %. The general groundwater flow is directed from the outcrop area of the Wajid formation towards Wadi Ad Dawasir, which represents the main discharge area for both the Lower Wajid and Upper Wajid aquifers.

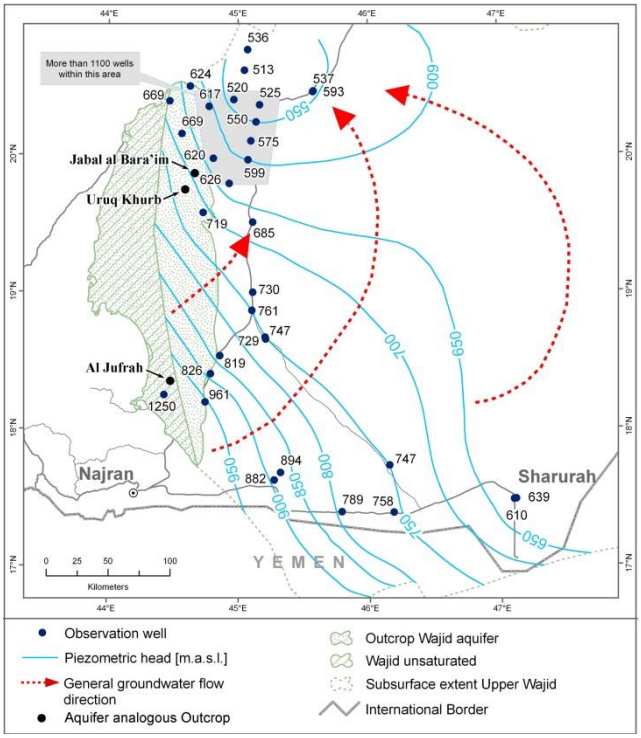

Fig. 2 Piezometric head distribution

Methodology

One objective of this study was the evaluation of two-dimensional (2D) hydraulic conductivity tensors to denote the direction of the maximum flow in the fractured aquifer. The information used for the modelling are based on aquifer analogous outcrops at Al Jufrah, Uruq Khurb and Jabal al Bara'im. The determination of the tensors is based on previous studies by Blum et al. (2005, 2007, 2009) and is illustrated in Fig. 3, which also provides an overview of the applied methodology. In addition, the conductivities modelled for the fractured aquifer were compared with the matrix permeability from laboratory measurements and with conductivities found by in-situ hydraulic pumping tests. This enabled the evaluation of in-situ hydraulic apertures and the estimation of the influence of the DFN on the overall fluid transport in the upper aquifer of the Wajid sandstone formation.

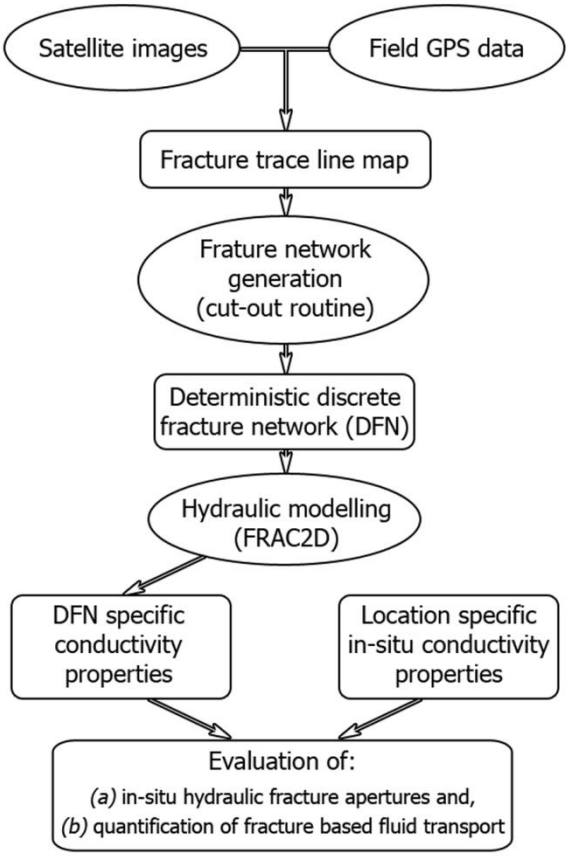

Fig. 3 Schematic diagram showing the applied methodology

Fracture trace maps

The fracture trace maps used are described by the endpoint coordinates, in decimal degrees, of each fracture. The generation of the fracture trace line maps was accomplished by combining Landsat ETM+ data, Saudi Geological Survey aeromagnetic data and field measurements. The fracture endpoints based on the satellite data were created by adding an extra layer to Google Earth™, extracting the fracture traces to that layer and generating the endpoint data using the Garmin Map Source. The remote sensing data were complemented with field GPS measurements, using a handheld GPS device, to enhance fracture data coverage and accuracy. The lower cut-off length for the fracture length sampling in the field was 5 m with an accuracy of ± 2 m. The accuracy of the remote sensing strongly depends on the quality of the satellite images and programs used to evaluate the lineaments and their endpoint coordinates. The satellite images are not to scale (Fig. 4, 5 and 6), as the relation between longitude and latitude depends on the angle of observation.

Fracture network generation

Blum et al. (2005) developed a model (*FracFrac*) to generate random stochastic DFN based on a power-law fracture length distribution using a density constant C and a fractal dimension D_L, which are based on the fracture length distribution. In the current study the density constants and fractal dimensions found for the available fracture length data did not enable the generation of suitable DFN for fracture flow modelling. Instead, the values found indicate that a power-law distribution might not be appropriate. The lack of information due to sand covered areas and non-accessibility in the field in combination with a minimum sampling length of 5 m and an accuracy of ± 2 m for the GPS data results in a high degree of uncertainty in sampling representative statistics of fracture data. Thus, a deterministic approach was used for the generation of the DFN, where actually existing and measured discrete fracture networks were used for the hydraulic modelling.

A program, which is based on Visual Basic for Applications (VBA) in Excel™, was developed to cut-out areas from fracture trace line maps to generate deterministic DFN with an area of 100 m × 100 m (Fig. 4, 5 and 6). The chosen cut-out areas are mainly situated at locations with a good resolution and as much as possible complete data of fracture traces. The size of the area mainly derives from the resolution of the identified fracture traces. Since all fractures are described by their endpoints in decimal degrees, the necessary calculations in the program are based on trigonometry. In a first step the endpoint coordinates in decimal degrees are changed to coordinates within an assumed rectangular grid with the south western corner of the cut-out area as point of origin. This is done by subtracting the longitude and latitude coordinate of that corner from the longitude and latitude of the endpoints of each fracture. The updated coordinates are used to calculate the angle of each fracture. Afterwards, based on the angle and the relative position of the endpoints of a fracture to the corners of the cut-out area, all fractures which do not intersect with a boundary or are beyond a boundary are excluded from further calculations. Finally, the program evaluates the endpoints of the fractures within the cut-out area and the points of intersection with the four boundaries. The points of intersection with the boundaries are evaluated depending on the position of the fracture endpoint relative to the cut-out area and the angle of the fracture. The x- or y-coordinates of the new fracture endpoint at an intersection are known. The unknown coordinate is calculated using the difference between the boundary and the

original fracture endpoint coordinate and the tangents of the fracture angle. Whether this value is added to the original coordinate or subtracted from it depends on the position of the original endpoint and the angle of the fracture. The final result of these calculations is the coordinates of the fracture endpoints within the cut-out area.

Fractures connecting the boundaries which are therefore significant to fluid transport were visualised using a VBA code in Excel™ (Blum et al. 2007). The code deletes all fractures that are not accessible to the fluid flow (i.e. dead end fractures), providing a good first visual impression whether a DFN percolates or not. The code scans each fracture for intersection nodes with other fractures. All fractures or parts of fractures, which do not connect two nodes, and are thus dead end fractures, are deleted. Afterwards an updated fracture network is generated using the calculated intersection nodes and the connecting fractures and fracture parts resulting in the so-called backbone of the DFN (Berkowitz 1995). If the boundaries of the DFN are not connected by this fracture network, the flow simulations did not percolate. The deterministic fracture networks were then used in the hydraulic modelling calculations.

Hydraulic modelling

The fracture flow code FRAC2D was used for the hydraulic modelling of fracture-based fluid flow (Blum et al. 2005). FRAC2D uses the endpoints of the fractures within a DFN to calculate the flow across its boundaries using the cubic law of Snow (1965) and Louis (1967):

$$Q = \frac{\rho g}{12\mu} {a_h}^3 \nabla h \qquad (1)$$

where Q is the flow through a single fracture ($m^2\ s^{-1}$), ρ is the density of the fluid ($kg\ m^{-3}$), g is the gravitational acceleration ($m\ s^{-2}$), μ is the dynamic viscosity of the fluid ($kg\ m^{-2}\ s^{-1}$), a_h is the hydraulic aperture and ∇h is the hydraulic gradient (-). A hydraulic gradient of -1 is applied to the DFN and is rotated in six steps of 30° from 0° to 150°, with the first gradient oriented in the east-west direction. For each orientation, FRAC2D calculates the flow across the four boundaries, which was used to evaluate the flow in x- and y-direction. As field measurements of hydraulic apertures were lacking, apertures between 50 µm and 200 µm were used as first estimates. These values are well within the range normally found in fractured rocks (Steele et al. 2006, Hitchmough et al. 2007). In addition to the flow balance calculations from FRAC2D, the modelled conductivities for the different hydraulic

apertures were used in an analytical scaling approach (Eq. 2) to verify the results. By comparing the modelled with the scaled values, which are based on the modelled value for a hydraulic aperture of 200 µm, the results were found to be consistent. This scaling factor was also used to evaluate the hydraulic conductivities for hydraulic apertures above the simulated value of 200 µm. The applied scaling factor is based on the cubic law and is given by Blum et al. (2007):

$$f = \left(\frac{a_{h(new)}}{a_{h(old}}\right)^3 \tag{2}$$

where f is the scaling factor (-), $a_{h(new)}$ is the new hydraulic aperture in µm and $a_{h(old)}$ is the old hydraulic aperture in µm of the previously simulated hydraulic conductivity.

To calculate the orientation of maximum flow, a method was used that is based on Jackson et al. (2000) and modified by Blum et al. (2005). To evaluate the components of the conductivity tensors, Darcian flow across the domain is assumed (Blum et al. 2005):

$$\begin{bmatrix} q_x \\ q_y \end{bmatrix} = \begin{bmatrix} k_{xx} & k_{xy} \\ k_{yx} & k_{yy} \end{bmatrix} \begin{bmatrix} \frac{\partial h}{\partial x} \\ \frac{\partial h}{\partial y} \end{bmatrix} \tag{3}$$

where q_x is the flow x-direction ($m^3\ s^{-1}$), q_y is the flow in y-direction ($m^3\ s^{-1}$), k_{xx} is the component of the hydraulic conductivity tensor in x-direction ($m\ s^{-1}$), k_{xy} is the component of the hydraulic conductivity tensor in xy-direction ($m\ s^{-1}$), k_{yy} is the component of the hydraulic conductivity tensor in y-direction ($m\ s^{-1}$) and h is the gradient with $\nabla h = 1$ ($m\ m^{-1}$). The flows q_x and q_y are derived from the boundary flows calculated by FRAC2D. However, as six different directions were used for the gradient in FRAC2D, the hydraulic gradient in Eq. 3 is denoted by (Blum et al. 2005):

$$\frac{\partial h}{\partial x} = \cos\theta \tag{4}$$

$$\frac{\partial h}{\partial y} = \sin\theta \tag{5}$$

where θ (°) is the angle of the gradient, counter clockwise from the x-axis. The hydraulic conductivity components are transformed into the principal hydraulic conductivities and the principal direction of the maximum conductivity by the following equations (Blum et al. 2005):

$$k_{max} = \frac{k_{xx} + k_{yy} + \sqrt{\left(k_{xx} + k_{yy}\right)^2 - 4\left(k_{xx}k_{yy} - {k_{xy}}^2\right)}}{2} \tag{6}$$

$$k_{min} = \frac{k_{xx} + k_{yy} - \sqrt{\left(k_{xx} + k_{yy}\right)^2 - 4\left(k_{xx}k_{yy} - {k_{xy}}^2\right)}}{2} \quad (7)$$

$$\theta_{max} = \tan^{-1}\left(\frac{k_{max} - k_{xx}}{k_{xy}}\right) \quad (8)$$

where k_{max} is the maximum principal hydraulic conductivity component (m s^{-1}), k_{min} is the minimum principal conductivity component (m s^{-1}) and θ_{max} is the principal direction of the maximum hydraulic conductivity, the angle between k_{max} and the x-axis (counter clockwise). The main fluid flow direction in the fractured aquifer can be obtained from the conductivity ellipsoid or tensor, which can be derived from the principal hydraulic conductivities and their orientations, using Eq. (6-8). For further calculations k_{max} was used for the fracture hydraulic conductivity k_f. The latter were compared with the permeability measurements from plug samples, which were taken from the outcrops of the different stratigraphic members, and also with the hydraulic conductivities based on local pumping tests. For all four members of the Wajid sandstone formation, the matrix porosity and matrix permeability were measured using the method after Hornung (1999). However, permeabilities > 1 Darcy can not be accurately determined with this method. Dirner (University of Tübingen, unpublished data, 2007) determined the matrix porosity and matrix permeability for the Khusayyayn and the Juwayl member, and Filomena (University of Tübingen, unpublished data, 2007) for the Dibsiyah and the Sanamah member. The measured matrix permeabilities are transformed into hydraulic conductivities using the following equation:

$$k = \frac{K\gamma}{\mu} \quad (9)$$

where k is the hydraulic conductivity (m s^{-1}), K is the permeability (m^2), γ is the specific weight of water, which was assumed to be 1000 N m^{-2} and μ is the viscosity of water, which was assumed to be 0.001 Pa s. The determined matrix porosities, matrix permeabilities and corresponding matrix hydraulic conductivities for the four members of the Wajid sandstone formation are summarised in Table 1. In this study the Khusayyayn and the Juwayl member were considered. In particular, the Khusayyayn member shows high porosity values ranging between 19 % and 29 %, and high permeabilities above 1000 mD. Although the Juwayl member has similar high porosities, permeabilities are locally lower due to extensive clay cementation (Dirner, University of Tübingen, unpublished data, 2007).

Furthermore, the effective in-situ hydraulic fracture conductivity and hydraulic aperture of the DFN are estimated. For a system of parallel and continuous fractures assuming laminar flow, the equivalent hydraulic conductivity of the medium can be determined using the following equation by de Marsily (1981):

$$k_{eff} = k_m + \frac{a}{b} k_f \quad (10)$$

where *a* is the aperture of the fractures, *b* is the mean distance between the fractures, k_{eff} is the bulk effective hydraulic conductivity (m s^{-1}) of the fractured porous sandstone, which in the present study was obtained by local hydraulic pumping tests, and k_m and k_f are the hydraulic conductivities of the matrix and fracture, respectively. However, since FRAC2D calculates the flow over the boundaries of a DFN, the evaluated hydraulic conductivities for the fracture network are of equivalent character for the area of the respective DFN. Hence, parameters *a* and *b* in Eq. (10) can be neglected and therefore the following equation can be used in the present study (Toublanc et al. 2005):

$$k_{eff} = k_m + k_f \quad (11)$$

Knowing the hydraulic conductivity of the matrix from laboratory measurements (Dirner, University of Tübingen, unpublished data, 2007, Filomena, University of Tübingen, unpublished data, 2007) and the bulk effective hydraulic conductivity from pumping tests, it was possible to evaluate in-situ hydraulic apertures for the studied discrete fracture networks. By solving Eq. (10) for k_f it was possible to assign a hydraulic conductivity $k_{f(eva)}$ to the DFN of each specific outcrop. This new hydraulic fracture conductivity $k_{f(eva)}$ allowed the correlation of the hydraulic conductivity and the hydraulic aperture using Eq. (2).

The in-situ hydraulic aperture of the fractures in the subsurface was calculated by solving Eq. (2) for $a_{h(new)}$. The scaling factor equals the evaluated hydraulic fracture conductivity divided by the modelled hydraulic fracture conductivity for an hydraulic aperture of 200 µm ($f = k_{f(eva)}/k_f$) and $a_{h(old)}$ being 200 µm. A similar approach was used by Toublanc et al. (2005), who determined total permeability maps for the Ekofisk Field in the North Sea, which is a large, naturally fractured limestone field. The total permeabilities were obtained by adding the matrix and the calculated fracture permeabilities. The latter were estimated using correlations between the fault and fracture intensity and the fracture distribution from cores and logs, and the fracture component of the well test permeability. This way, Toublanc et al. (2005) could validate their permeability predictions from fault intensity mapping

with results from DFN modelling. To quantify the impact of the fracture based fluid transport on the overall flow, an approach from Castaing et al. (2002) was used. Castaing et al. (2002) showed that the dominance of either the fault permeability K_f (m^2) or the matrix permeability K_m (m^2) in controlling the fluid flow can be correlated to the ratio K_f/K_m. However, instead of using the permeability ratio of K_f/K_m, the conductivity ratio k_f/k_m is used in the current study to evaluate the dominant fluid transport medium. According to Castaing et al. (2002), the influence of a fault system begins to be visible at a ratio of 100, and the hydraulic fluid transport is totally dominated by the fault system at a ratio of 10,000.

Table 1 Matrix porosities and permeabilities after Hornung (1999), and hydraulic conductivities based on plug samples taken from the four members of the Wajid Sandstone (Dirner, University of Tübingen, unpublished data, 2007, Filomena, University of Tübingen, unpublished data, 2007). The integrated hydraulic conductivities were used in the present study

Porosity [%]	Permeability [mD] xy/z	Integrated permeability [mD]	Integrated hydraulic conductivity [m s^{-1}]
Khusayyayn member			
19.1	320/1177	748	7.5×10^{-6}
27.1	-	>1000	$>1.0 \times 10^{-5}$
26.4	527/>1000	>1000	$>1.0 \times 10^{-5}$
29.1	138/280	209	2.1×10^{-6}
26.3	-	>1000	$>1.0 \times 10^{-5}$
Juwayl member			
22.5	891/348	620	6.2×10^{-6}
29.5	1072/1136	1104	1.1×10^{-5}
31.6	-	>1000	$>1.0 \times 10^{-5}$
28.4	298/941	620	6.2×10^{-6}
12.2	0/26	13	1.3×10^{-7}
Dibsiyah member			
25.3	205/340	273	2.7×10^{-6}
27.8	264/>1000	632	6.3×10^{-6}
25.8	175/111	143	1.4×10^{-6}
24.1	394/376	385	3.9×10^{-6}
29.4	497/>1000	749	7.5×10^{-6}
28.3	242/277	260	2.6×10^{-6}
26.8	244/151	198	2.0×10^{-6}
24.8	116/202	159	1.6×10^{-6}
24.3	62/292	177	1.8×10^{-6}
26.7	200/246	223	2.2×10^{-6}
24.1	177/108	143	1.4×10^{-6}
24.9	>1000/>1000	>1000	$>1.0 \times 10^{-5}$
28.1	202/1000	601	6.0×10^{-6}
22.3	>1000/>1000	>1000	$>1.0 \times 10^{-5}$
25.9	>1000/>1000	>1000	$>1.0 \times 10^{-5}$
Sanamah member			
23.3	24/16	20	2.0×10^{-7}
28.4	408/244	326	3.3×10^{-6}

Results and discussion

Due to sampling bias, which was mainly caused by sand cover and the resolution of the satellite images, it was impossible to create a deterministic DFN for the outcrop at Al Jufrah (Fig. 4). Hence, no fracture flow model could be performed for this location in the south of the irrigated areas (Fig. 1). The backbone of the DFN for the investigated area illustrates the incomplete fracture data and the missing connectivity between the boundaries, which also demonstrates the limitations of the present approach.

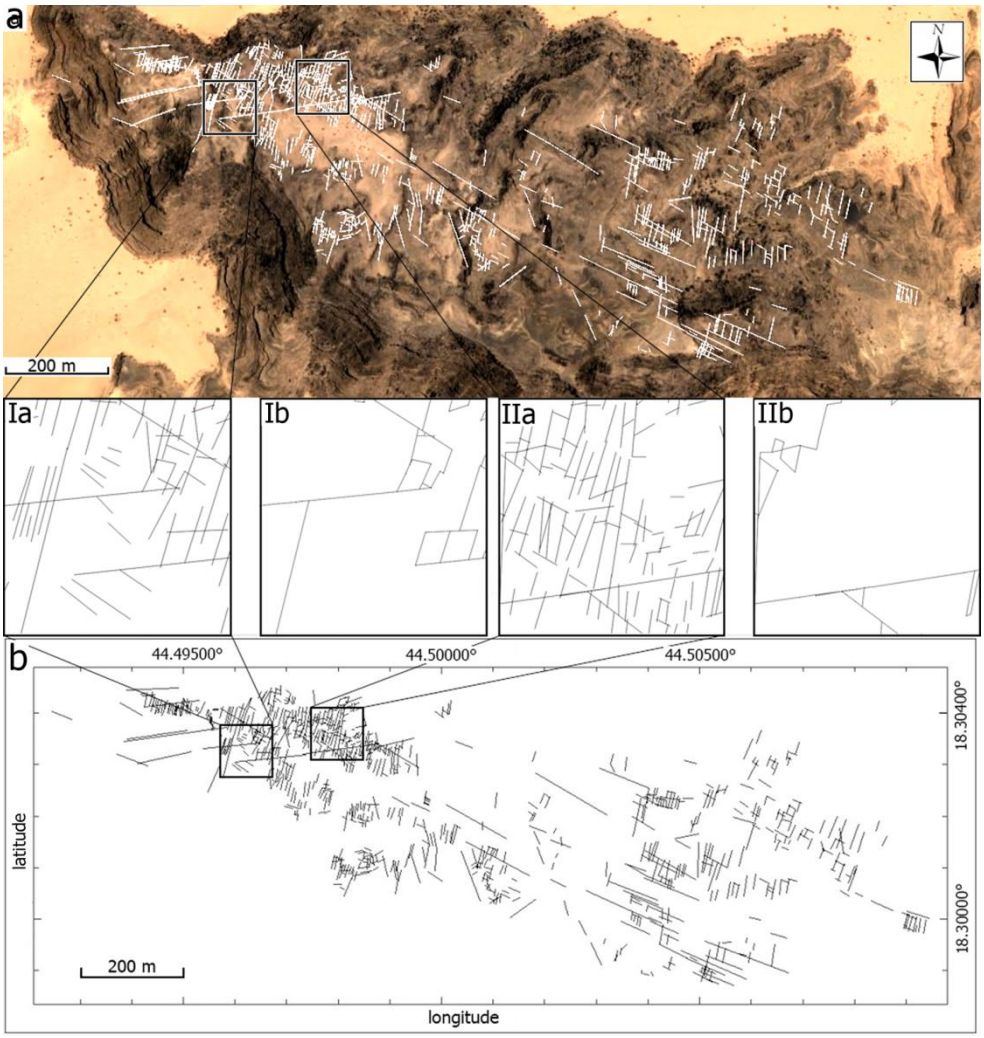

Fig. 4 (a) Satellite image taken from Google Earth™. (b) Fracture trace line map from combined remote sensing and field data for the outcrop at Al Jufrah. (a) White and (b) black lines indicate the identified fracture traces and black squares indicate the chosen *cut-out* areas with an extent of 100 m × 100 m. Ia and IIa show the chosen DFN in more detail, Ib and IIb the backbone of the DFN (black lines indicate fracture traces)

The monitored fractures at the Uruq Khurb outcrop are intersected by several sand covered areas or overlaying members, causing difficulties in finding a useful and complete DFN (Fig. 5). Thus, only one complete DFN with an area of 100 m × 100 m could be identified for the hydraulic modelling (Fig. 5, IIb). The backbone of this DFN shows a very good connection between all boundaries. In all other areas, however, the backbone of the DFN shows gaps and missing connectivity (Fig. 5, Ib).

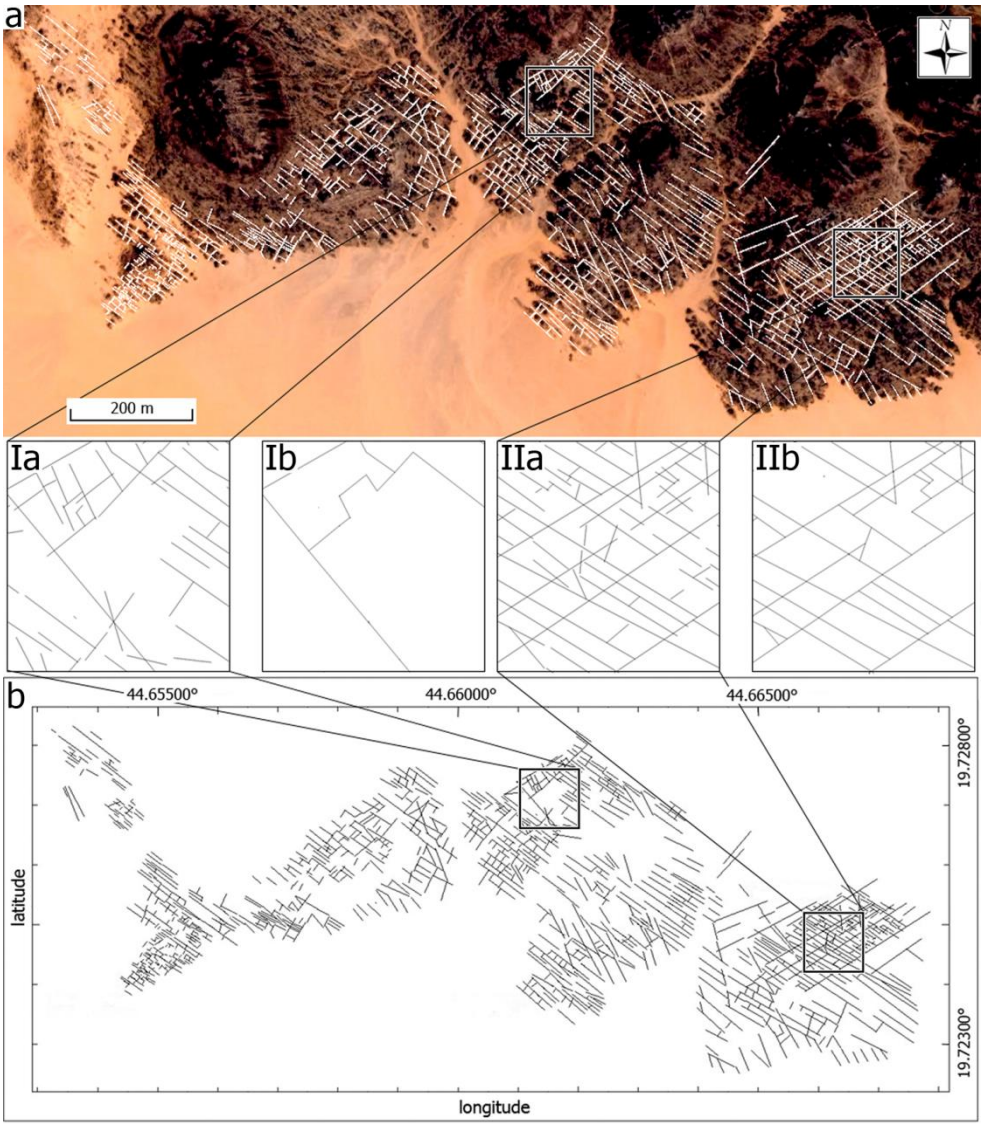

Fig. 5 (a) Satellite image taken from Google Earth™. (b) Fracture trace line map from combined remote sensing and field data for the outcrop at Uruq Khurb. (a) White and (b) black lines indicate the identified fracture traces and black squares indicate the chosen *cut-out* areas with an extent of 100 m × 100 m. Ia and IIa show the chosen DFN in more detail, Ib and IIb the backbone of the DFN (black lines indicate fracture traces)

The trace map from the Jabal al Bara'im outcrop site shows a good connectivity between the different fracture sets, and two DFNs were thus available for hydraulic modelling (Fig. 6). The backbone of the DFN proves this connectivity between the boundaries (Fig. 6: I b, II b).

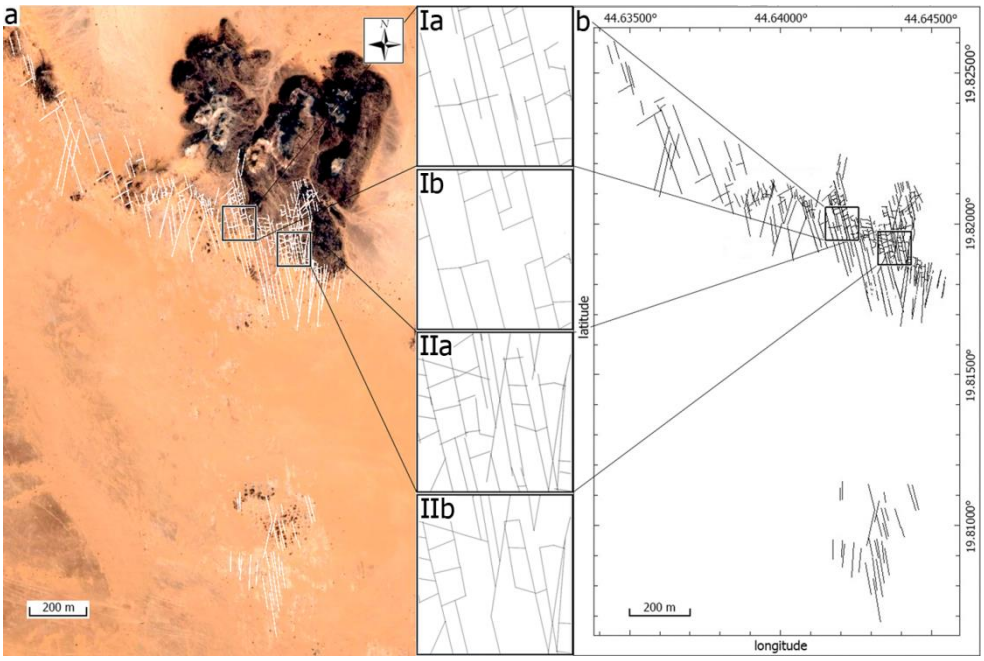

Fig. 6 (a) Satellite image taken from Google Earth™. (b) Fracture trace line map from combined remote sensing and field data for the outcrop at Jabal al Bara'im. (a) White and (b) black lines indicate the identified fracture traces and black squares indicate the chosen *cut-out* areas with an extent of 100 m × 100 m. Ia and IIa show the chosen DFN in more detail, Ib and IIb the backbone of the DFN (black lines indicate fracture traces)

Unfortunately, no hydraulic fracture aperture values or any other information on the hydraulic behaviour were available for the hydraulic modelling. Hence, all DFN were initially modelled assuming a constant hydraulic aperture between 50 µm and up to 200 µm. Hydraulic conductivities for larger hydraulic apertures are evaluated using the scaling law from Eq. (2). The hydraulic modelling of the DFN for Uruq Khurb, with an assumed fracture aperture of 200 µm, resulted in a maximum hydraulic conductivity (k_{max}) of 1.8×10^{-7} m s^{-1} with an evaluated principal flow direction of 147°. For Jabal al Bara'im the hydraulic conductivity of 1.6×10^{-7} m s^{-1} was determined for the first *cut-out* area with an evaluated principal flow direction of approximately 152°, and 2.9×10^{-7} m s^{-1} for the second *cut-out* area with an evaluated principal flow direction of 158° (Fig. 7). The results show that the flow along the fractures is strongly controlled by the orientation of the main NW – SE

fracture set (Figs. 4-6). If the representative elementary volume (REV) is achieved at the scale of observation (100 m × 100 m), which would still need to be comprehensively tested (Blum et al. 2005), these evaluated hydraulic conductivity tensors could be applied to large-scale (kilometre-scale) upscaled continuum models using an equivalent porous media (EPM) approach (e.g. Blum et al. 2009).

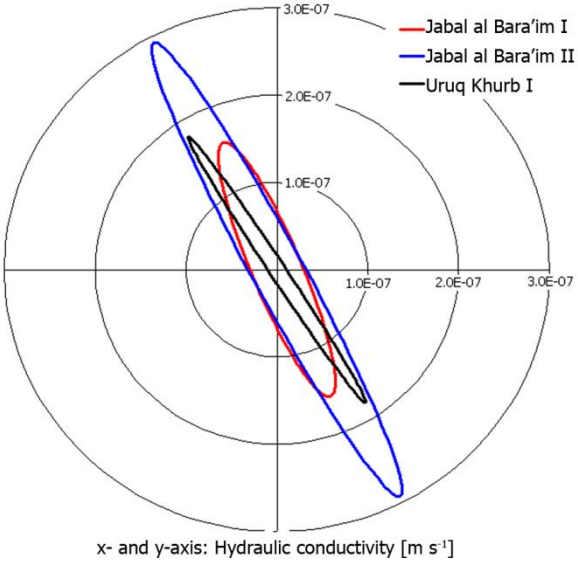

Fig. 7 Hydraulic conductivity tensors for the studied discrete fracture networks using a constant hydraulic aperture of 200 µm at Uruq Khurb I (black) and at Jabal al Bara'im I (red) and II (blue)

For each outcrop the main and subordinate fracture sets and their orientation using fracture length versus orientation diagrams were identified. Comparing the orientation of the fluid flow with the orientation of the main fractures sets indicates that the flow mainly follows the main fractures. Figure (7) shows the principal conductivity ellipsoids for the fracture based fluid transport derived from Eqs. (6), (7) and (8). At Uruq Khurb the direction of principal flow is 147° and varies by ~ 27° from the orientation of the main fracture set at 120°. For the first DFN at Jabal al Bara'im the principal flow direction is 158° and differs only by ~ 12° from the main fracture set orientation at 170°. The orientation of the principal flow for the second DFN is 152° and thus differs from the main fracture set by only ~ 18°. The difference is most likely caused by minor fluid flow along the subordinate fracture sets connecting these fractures with the main fracture set.

Al Ajmi et al. (2009) investigated the facies distribution of the Wajid sandstone and the implication on the hydraulic aquifer properties. The subsurface consists of

two individual fractured bedrock aquifers separated by an aquitard. For the lower aquifer, represented by the Dibsiyah Member and the lower Sanamah Member, hydraulic pumping tests resulted in a geometric mean hydraulic conductivity of 2.2×10^{-5} m s^{-1} with values ranging between 4.1×10^{-6} m s^{-1} and 5.7×10^{-5} m s^{-1}. The upper aquifer is separated from the lower one by siltstones and shales of the upper Sanamah Member and consists of the Khusayyayn Member and the Juwayl Member. For these two members the geometric mean of the hydraulic conductivity based on pumping tests is 8.3×10^{-5} m s^{-1} with values ranging from 1.0×10^{-5} m s^{-1} to 2.3×10^{-4} m s^{-1} (Fig. 8).

For all studied DFNs, assuming a constant hydraulic aperture of 200 µm, the determined hydraulic conductivities for the fractured aquifer are lower than those measured for the sandstone matrix (Fig. 8). Nevertheless, for the estimation of in-situ hydraulic apertures Eq. (10) was applied. In addition the conductivity ratios k_f/k_m are used to determine the impact of the flow transport through the DFN on the overall flow system. In all further calculations the geometric means for the bulk effective and the matrix conductivities of the upper aquifer were used, as the outcrop sites of the studied areas consist of the Juwayl and Khusayyayn Members (Fig. 1). Thus, for the upper aquifer $k_{eff} = 8.3 \times 10^{-5}$ m s^{-1} and $k_m = 7.3 \times 10^{-6}$ m s^{-1} were used. Based on Eq. (10), the average hydraulic conductivity of the fracture system k_f is therefore 7.6×10^{-5} m s^{-1} with a hydraulic conductivity ratio k_f/k_m of 10.4. This indicates that the overall flow is influenced by the fracture network, but only to a minor degree (Castaing et al. 2002). The intersection points between the calculated fracture conductivity and the simulated hydraulic conductivities of the deterministic DFN allow a first approximation of the in-situ hydraulic fracture apertures (Fig. 8).

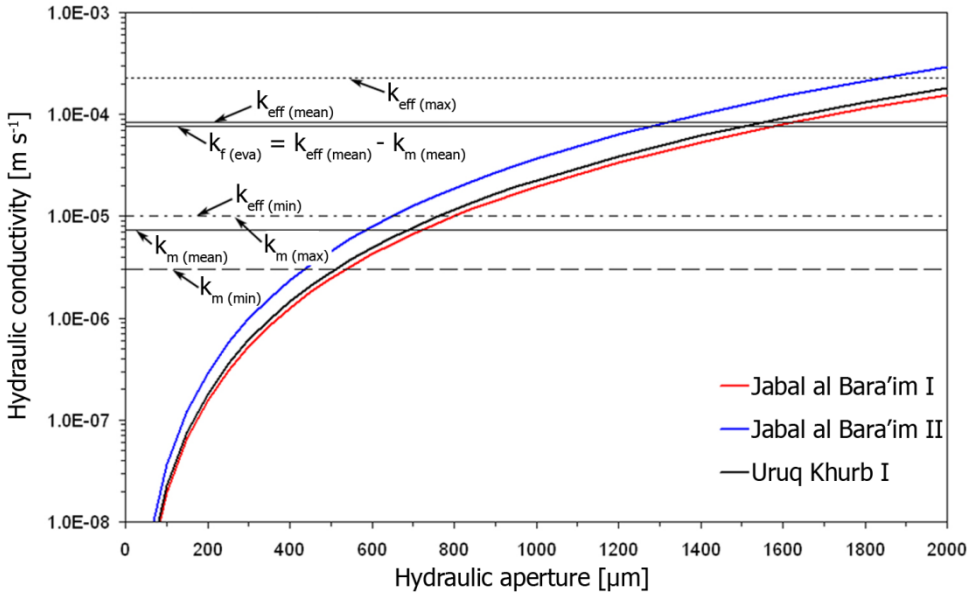

Fig. 8 Hydraulic conductivities determined for the three studied DFNs (Jabal al Bara'im I (red) and II (blue) Uruq Khurb I (black)). The matrix conductivity is denoted as k_m, with the mean, the maximum and the minimum values $k_{m\ (mean)}$, $k_{m\ (max)}$ and $k_{m\ (min)}$. The bulk effective hydraulic conductivity based on pumping test data is denoted as k_{eff}, with the mean, the maximum and the minimum values $k_{eff\ (mean)}$, $k_{eff\ (max)}$ and $k_{eff\ (min)}$. The evaluated fracture hydraulic conductivity is shown as $k_{f\ (eva)}$

At Uruq Khurb the interpolation of the in-situ hydraulic fracture aperture using Eq. (2) gives a value of ~ 1,500 µm. For Jabal al Bara'im the hydraulic fracture aperture would be ~ 1,300 µm for the first DFN and ~ 1,700 µm for the second DFN. Although laboratory (Yeo et al. 1998) and other field-scale studies (Steele et al. 2006) show smaller fracture apertures (< 1,000 µm) for sandstones, field observations at the Wajid sandstone outcrops indicate even larger open fracture apertures (>> 1 mm, Fig. 9). However, extrapolating surface observations to the subsurface still poses a challenging task. Case studies at Sellafield in the UK (Nirex 1997) and at the Forsmark site in Sweden (SKB 2006), however, indicate that fracture properties from the surface and subsurface are comparable, especially for fracture orientation and in particular for fracture dips > 30°-40°, which is true for the current work. However, these near-surface observations would need to be confirmed by borehole logs such as Caliper Logging or Borehole Televiewer to identify fracture zones. Additional information can be obtained by in-situ hydraulic tests such as dilution experiments (e.g. Novakowski et al. 2006). If the DFN significantly contributes to the overall fluid transport, which according to Castaing et al. (2002) would be at a permeability ratio of 100, the hydraulic apertures would be even larger. At Uruq

Khurb such an assumption would result in even larger hydraulic fracture apertures of ~ 3,200 µm. For Jabal al Bara'im the apertures would be ~ 2,700 µm and ~ 3,300 µm, respectively. Both results clearly demonstrate the minor impact of the dissimilar fracture geometries on the estimate of the in-situ hydraulic apertures at both studied outcrops.

Fig. 9 Typical fracture in the sandstones of the Upper Wajid at Al Jufrah

Several uncertainties in evaluating the importance of the DFN to the overall flow behaviour of the studied Wajid sandstone formation and estimation of in-situ representative hydraulic apertures still remain. For example, the maximum size of the current DFN models did not exceed 100 m × 100 m, although the studied outcrop areas covered at least 1 km^2. Hence, the impact of the fracture systems on the large-scale (> 1 km^2) flow transport is still uncertain. Furthermore, the applied method for the determination of the matrix permeabilities by Hornung (1999) is not able to determine permeabilities > 1 Darcy. It is therefore possible that the actual hydraulic matrix conductivities are too low, which would result in an overestimation of the determined fracture hydraulic conductivity and hydraulic aperture, respectively. The assumption that all hydraulic fracture apertures are constant also needs further

testing, as only constant representative in-situ hydraulic apertures could be estimated with the proposed method.

Conclusion

The presented method is able to generate deterministic discrete fracture networks (DFN) based on fracture trace maps, which were generated by a combination of satellite images and field measurements. A simple routine was developed to cut-out specific DFNs from these trace map data. These DFNs were used for fracture flow modelling using constant hydraulic fracture apertures. The outcome for the determined hydraulic conductivities of the DFNs was compared with actual pumping tests and matrix hydraulic conductivity data. Using these hydraulic data it was possible to estimate in-situ hydraulic apertures for the upper Wajid sandstone aquifer resulting in an average in-situ hydraulic fracture aperture of ~ 1,500 µm. Although the latter appears to be high in comparison with previous observations in other sandstones, field observations at the studied outcrops show even larger open fracture apertures (>> 1 mm). The fluid transport in the aquifer is not entirely dominated by the fracture systems. However, a conductivity ratio k_f/k_m of 10.4 evidently indicates a strong control. Hence, the fracture systems should be considered for the determination of the groundwater recharge and for the study of the flow behaviour of the Wajid sandstone aquifer.

Acknowledgements

We would like to thank the Ministry of Water and Electricity of the Kingdom of Saudi Arabia for their help and guidance regarding the field investigations. Special thanks to our colleagues Sebastian Dirner, Claudio Filomena and Thomas Aigner from the University of Tübingen, Institute for Geoscience for providing the matrix porosity and permeability data. Furthermore, we would like to acknowledge the manifold support of Martin Keller, Helmut Bock and Johannes Döhler from GTZ and Dornier Consulting in Riyadh, Saudi Arabia.

References

Al Ajmi H, Keller M, Hinderer M, Rausch R (2009) New Insights into the Facies Distribution of the Wajid Sandstone in its Western Outcrop Area and Implication on Reservoir Properties. Proceedings of the 3rd International Conference on Water Resources and Arid Environments 2008 and the 1st Arab Water Forum, 13 p. (in print)

Babiker M, Gudmundsson A (2004) The effects of dykes and faults on groundwater flow in arid land: the Red Sea Hills, Sudan. J Hydrol 297(1-4):256–273

Becker MW (2006) Potential for Satellite Remote Sensing of Ground Water. Ground Water 44:306–318

Berkowitz B (1995) Analysis of fracture network connectivity using percolation theory. Mathe Geol 27(4):467-483

Blum P, Mackay R, Riley MS (2009) Stochastic simulations of regional scale advective transport in fractured rock masses using block upscaled hydro-mechanical rock property data. J Hydrol 369: 318–325

Blum P, Mackay R, Riley MS, Knight JL (2007) Hydraulische Modellierung und die Ermittlung des representativen Elementarvolumens (REV) im Kluftgestein (Hydraulic modelling and the determination of the representative elementary volume (REV) in fractured rock). Grundwasser 12: 48–65

Blum P, Mackay R, Riley MS, Knight JL (2005) Performance assessment of a nuclear waste repository: upscaling coupled hydro-mechanical properties for far-field transport analysis. Inter J Rock Mech Min Sci 42(5-6):781–792

Brunner P, Franssen H-JH, Kgotlhang L-, Bauer-Gottwein P, Kinzelbach W (2006) How can remote sensing contribute in groundwater modelling? Hydrogeol J 15:5–18

Butler JJ (2009) Pumping Tests for Aquifer Evaluation—Time for a Change? Ground Water 47(5): 615-617

Castaing C, Genter A, Bourgine B, Chilès JP, Wendling J, Siegel P (2002) Taking into account the complexity of natural fracture systems in reservoir single-phase flow modelling. J Hydrol 266:83–98

Castaing C, Halawani MA, Gervais F, Chilès JP, Genter A, Bourgine B, Ouillion G, Brosse JM, Martin P, Genna A, Janjou D (1996) Scaling relationships in intraplate fracture systems related to the Red Sea drifting. Tectonophysics 261:291–314

Davis PA, Breed CS, McCauley JF, Schaber GG (1993) Surficial geology of the Safsaf region, south-central Egypt, derived from remote-sensing and field data. Remote Sens Environ 46(2):183–203

Deroin J-P, Motti E, Simonin A (1996) A comparison of the potential for using optical and SAR data for geological mapping in an arid region: the Atar site, Western Sahara, Mauritania. Inter J Remote Sens 19(6):1115–1132

de Marsily G (1981) Quantitative Hydrogeology. Masson, Paris

Elachi C, Cimino J, Settle M (1986) Overview of the Shuttle Imaging Radar-B Preliminary Scientific Results. Science 232(4757):1511–1516

Evans DS, Lathon RB, Senalp M, Connally TC (1991) Stratigraphy of the Wajid Sandstone of South-western Saudi Arabia. Society of Petroleum Engineers

Food and Agriculture Organization (2008). Review of World Water Resources by Country. Rome, Italy, Food and Agriculture Organization of the United Nations.

Franssen H-JH, Brunner P, Makobo P, Kinzelbach W (2007) Equally likely inverse solutions to a groundwater flow problem including pattern information from remote sensing images. Water Resour Res 44: W01419

Galanos I, Rokos D (2005) A statistical approach in investigating the hydrogeological significance of remotely sensed lineaments in the crystalline mountainous terrain of the island of Naxos, Greece. Metsovion Interdisciplinary Research Center, National Technical University of Athens

Hitchmough AM, Riley MS, Herbert AW, Tellam JH (2007) Estimating the hydraulic properties of the fracture network in a sandstone aquifer. J Contam Hydrol 93:38–57

Hoffmann J, Sander P (2007) Remote sensing and GIS in hydrogeology. Hydrogeol J 15:1–3

Hoffmann J (2005) The future of satellite remote sensing in hydrogeology. Hydrogeol J 13:247–250

Hornung J (1999) Dynamische Stratigraphie, Reservoir- und Aquifer-Sedimentgeologie einer alluvialen Ebene: Der Stubensandstein in Baden-Württemberg (Obere Trias, Mittlerer Keuper) (Dynamic stratigraphy, reservoir- and aquifer-sedimentology of an alluvial plain: The Stubensandstein in Baden-Würtemberg (upper Trias, middle Keuper). Tübinger Geowissenschaftliche Arbeiten (TGA) Reihe A (Nr. 56): 156pp

Jackson CP, Hoch AR, Todman S (2000) Self-consistency of a heterogeneous continuum porous medium representation of fractured media. Water Resour Res 36(1):189–202

Jha MK, Chowdary VM (2006) Challenges of using remote sensing and GIS in developing nations. Hydrogeol J 15:197–200

Kellogg KS, Janjou D, Minoux L, Fourniguet J (1986). Explanatory notes to the Geologic Map of the Wadi Tathlith Quadrangle, sheet 20G, Kingdom of Saudi Arabia. Ministry of Petroleum and Mineral Resources

Koike K, Ichikawa Y (2004) Spatial correlation structures of fracture systems for deriving a scaling law and modelling fracture distribution. Comp Geosci 32:1079–1095

Koike K, Nagano S, Kawaba K (1996) Construction and analysis of interpreted fracture planes through combination of satellite-image derived lineaments and digital elevation model data. Comp Geosci 24:573–583

Koike K, Nagano S, Ohmi M (1995) Lineament analysis of satellite images using a Segment Tracing Algorithm (STA). Comp Geosci 21(9):1091–1104

Konert G, Abdulkader M A, Sa'id A A, Henk J D (2001) Palaeozoic Stratigraphy and Hydrocarbon Habitat of the Arabian Plate. Geoarabia 6(3):407–442

Konikow LF, Kendy E (2005) Groundwater depletion: A global problem. Hydrogeol J 13(1):317–320

Kumar PKD (2007) Application of remote sensing and GIS for the demarcation of groundwater potential zones of a river basin in Kerala, southwest coast of India. Inter J Remote Sens 28:5583–5601

Leblanc M, Favreau G, Tweed S, Leduc C, Razack M, Mofor L (2006) Remote sensing for groundwater modelling in large semiarid areas: Lake Chad Basin, Africa. Hydrogeol J 15:97–100

Louis C (1967) Strömungsvorgänge in klüftigen Medien und ihr Wirkung auf die Standsicherheit von Bauwerken und Böschungen im Fels (Flow phenomena in fractured systems and their contribution to structural integrity of buildings and slopes at rock). Ph.D. Thesis, Technical University Karlsruhe

Lubczynski M (1997). Application of numerical flow modelling combined with remote sensing and GIS techniques for the quantification of regional groundwater resources in hard rock terrain. International Symposium on Hard Rock Hydrosystems, Rabat, Morocco, IAHS Publication.

Luijendijk E, Bruggeman A (2008) Groundwater resources in the Jabal Al Hass region, northwest Syria: an assessment of past use and future potential. Hydrogeol J 16:511–530

Masoud A, Koike K (2005) Tectonical architecture through Landsat-7 ETM+/SRTM DEM-derived lineaments and relationship to the hydrogeological setting in Siwa region, NW Egypt. J African Earth Sci 45(4-5):467–477

Nirex (1997) Evaluation of heterogeneity and scaling of fractures in the Borrowdale Volcanic Group in the Sellafield Area. Nirex Report SA/97/028.

Novakowski K, Bickerton G, Lapcevic P, Voralek J, Ross N (2006) Measurements of groundwater velocity in discrete rock fractures. J Cont Hydrogeol 82(1-2):44–60

Nyborg M, Berglund J, Triumf C-A (2006) Detection of lineaments using airborne laser scanning technology: Laxemar-Simpevarp, Sweden. Hydrogeol J 15:29–32

Postel S (1999) Pillar of Sand: Can the Irrigation Miracle last? Norton: New York

Robinson CA, El-Baz F, Kusky TM, Mainguet M, Dumay F, Suleimani ZA, Marjeby AA (2007) Role of fluvial and structural processes in the formation of the Wahiba Sands, Oman: A remote sensing perspective. J Arid Environ 69:679–694

Robinson CA, Werner A, El-Baz F, El-Shazly M, Fritch T, Kusky T (2006) The Nubian Aquifer in Southwest Egypt. Hydrogeol J 15:33–45

Robinson CA (2002) Application of satellite radar data suggest that the Kharga Depression in south-western Egypt is a fractured rock aquifer. Inter J Remote Sens 23(19):4101–4113

Robinson CA, El-Baz F, Ozdogan M, Ledwith M, Blanco D, Oakley S, Inzana J (2000) Use of radar data to delineate palaeodrainage flow directions in the Selima Sand Sheet, Eastern Sahara. Photogrammetric Eng Remote Sens 66:745–753

Robinson CA, El-Baz F, Singhroy V (1999) Subsurface imaging by Radarsat: comparison with Landsat TM data and implications to ground water in the Selima area, north-western Sudan. Canadian J Remote Sens 25:268–277

Rodell M, Famiglietti JS (2002) The potential of satellite-based monitoring of groundwater storage changes using GRACE: the High Plains aquifer, Central US. Journal of Hydrology 623(1-4):245–256

Rokade VM, Kundal P (2007) Groundwater potential modelling through remote sensing and GIS: A cas study from Rajura Taluka, Chandrapur district, Maharashtra. J Geol Soc India 69(5):943–948

Sander P (2006) Lineaments in groundwater exploration: a review of applications and limitations. Hydrogeol J 15:71–74

Sener E, Davraz A, Ozcelik M (2005) An integration of GIS and remote sensing in groundwater investigations: A case study in Burdur, Turkey. Hydrogeol J 13(5-6):826–834

Shah T, Molden D, Sakthivadivel R, Seckler D (2000) The global groundwater situation:overview of opportunities and challenges. International Water Management Institute

SKB (2006) Discrete fracture network for the Forsmark site. SKB Report R/06/79

Snow DT (1965) A parallel plate model of fractured permeable media. Ph.D. Thesis, University of California, Berkeley

Solomon S (2006) Groundwater study using remote sensing and geographic information systems (GIS) in the central highlands of Eritrea. Hydrogeol J 14(5):729–741

Steele A, Reynolds DA, Kueper BH, Lerner DN (2006) Field determination of mechanical aperture, entry pressure and relative permeability of fractures using NAPL injection. Geotechn 56(1):27–38

Sultan M, Wagdy A, Manocha N, Sauck W, Gelil KA, Youssef AF, Becker R, Milewski A, Alfy ZE, Jones C (2007) An integrated approach for identifying aquifers in transcurrent fault systems: The Najd shear system of the Arabian Mubian shield. J Hydrol 349:475–488

Toublanc A, Renaud S, Sylte JE, Clausen CK, Eiben T, Nadland G (2005) Ekofisk Field: fracture permeability evaluation and implementation in the flow model. Petrol Geosci 11(4):321–330

Yeh PJ-F, Swenson SC, Famiglietti JS, Rodell M (2006) Remote sensing of groundwater storage changes in Illinois using the Gravity Recovery and Climate Experiment (GRACE). Water Resour Res 42: W12203

Yeo IW, Freitas MH de, Zimmerman RW (1998) Effect of shear displacement on the aperture and permeability of a rock fracture. Int J Rock Mech Min Sci 35(8):1051-1070

6.2. Evaluation of sampling methods for fracture network characterization using outcrops[†]

Conny Zeeb* (1), Enrique Gomez-Rivas (2), Paul D. Bons (2), Philipp Blum (1)

(1) *Karlsruhe Institute of Technology (KIT), Institute for Applied Geosciences (AGW), Kaiserstrasse 12, 76131 Karlsruhe, Germany*

(2) *University of Tübingen, Department of Geosciences, Wilhelmstrasse 56, 72074 Tübingen, Germany*

* Corresponding author. Tel.: +49-721-608 47609, Fax: + 49-606-279; E-mail: conny.zeeb@kit.edu

ACKNOWLEDGEMENTS

This study was carried out within the framework of DGMK (German Society for Petroleum and Coal Science and Technology) research project 718 "Mineral Vein Dynamics Modelling", which is funded by the companies ExxonMobil Production Deutschland GmbH, GDF SUEZ E&P Deutschland GmbH, RWE Dea AG and Wintershall Holding GmbH, within the basic research program of the WEG Wirtschaftsverband Erdöl- und Erdgasgewinnung e.V. We thank the companies for their financial support, their permission to publish these results and funding of PhD grant to CZ and postdoctoral grant to EGR. We are grateful to Janos Urai and Marc Holland from the RWTH Aachen for the permission to use their remote sensing data from the Oman Mountains, Oman. We are especially grateful for the revisions of Tricia F. Allwardt, Alfred Lacazette and an anonymous reviewer.

ABSTRACT

Outcrops provide valuable information for the characterization of fracture networks. Sampling methods such as scanline sampling, window sampling, and circular scanline and window methods are available to measure fracture network characteristics in outcrops and/or from well cores. These methods vary in their application, the parameters they provide, and therefore have advantages and limitations. We provide a critical review on the application of these sampling methods and apply them to evaluate two typical natural examples: (a) a large-scale satellite image from the Oman Mountains, Oman (120,000 m^2), and (b) a small-scale outcrop at Craghouse Park, UK (19 m^2). The differences in the results emphasize the importance to (1) systematically investigate the required minimum number of measurements for each sampling method, and (2) to quantify the influence of censored fractures on the estimation of fracture network parameters. Hence, a program was developed to analyze 1300 sampling areas from nine artificial fracture networks with power-law length distributions. For the given settings, the lowest minimum number of measurements to adequately capture the statistical properties of fracture networks was found to be ~110 for the window sampling method, followed by the scanline sampling method with ~225. These numbers may serve as a guideline for analyses of fracture populations with similar distributions. Furthermore, the window sampling method proved to be the method that is least sensitive to censoring bias. Reevaluating our natural examples with the window sampling method showed that the existing percentage of censored fractures significantly influences the accuracy of inferred fracture network parameters.

INTRODUCTION

Fractures and other mechanical discontinuities act as preferential fluid pathways in the subsurface, thus strongly controlling fluid flow in hydrocarbon reservoirs. An essential step for reservoir characterization is the acquisition of fracture-network data and the subsequent upscaling of their statistical properties (Long et al., 1982; Jackson et al., 2000; Blum et al., 2009). Since terminology for mechanical defects in rocks is diverse and often has genetic connotations, we also include joints and veins when using the term “fractures”. A common method to evaluate the degree of fracturing in the subsurface is the characterization of fracture networks from outcropping subsurface analogues, well cores or image logs (Dershowitz and Einstein, 1988; Priest, 1993; National Research Council, 1996; Mauldon et al., 2001; Bour et al., 2002; Laubach, 2003; Blum et al., 2007; Jing and Stephansson, 2007; Guerriero et al., 2011). This process includes the acquisition of geometric data from fractures and its subsequent analysis to find statistical distributions and relationships between parameters (Einstein and Baecher, 1983; Priest 1993; Blum et al., 2005; Barthélémy et al., 2009; Tóth, 2010; Tóth and Vass, 2011). The most widely used acquisition methods for fracture network statistical parameters are (Figure 1): (1) scanline sampling (Priest and Hudson, 1981; LaPointe and Hudson, 1985; Priest 1993), (2) window sampling (Pahl, 1981; Priest 1993), and (3) circular scanline and window (or "circular estimator") methods (Mauldon et al., 2001; Rohrbaugh et al., 2002).

In the subsurface, fracture sampling is constrained to boreholes, which basically corresponds to scanline sampling. Well cores and image logs provide valuable in-situ information on, for example, fracture spacing, orientation, aperture and cementation (e.g. Olson et al., 2009). However, fracture sampling strongly depends on borehole inclination. Fracture intersection frequency is highest for a borehole perpendicular to the fractures of a set, whereas if the borehole is parallel to the fracture set, sampling is very limited and no or only few data can be acquired. Some parameters, such as average fracture spacing (Narr, 1996), can be estimated irrespectively of borehole inclination. Ortega and Marrett (2000) showed that an extrapolation of fracture frequencies from the microscopic scale to the macroscopic scale is possible up to the scale of mechanical layering. However, it is impossible to directly measure fracture lengths in the subsurface, which is crucial for fluid flow

modeling and the evaluation of an equivalent permeability in subsurface reservoirs (e.g. Philip et al., 2005). Although scaling relationships between the apertures and lengths for opening-mode fractures have been reported (e.g. Scholz, 2010), the exact nature of these relationships is still under debate (e.g. Olsen & Schultz, 2011). Furthermore, to our knowledge, scaling relationships for fractures in layered rocks have not been systematically investigated yet. Thus, the analysis of outcropping subsurface analogues can provide valuable additional information, especially on fracture length distributions for the simulation of fluid flow in subsurface reservoirs (e.g. Belayneh et al., 2009).

Each of the three sampling methods mentioned above has advantages and limitations when applied to an outcrop. Previous studies by Rohrbaugh et al. (2002), Weiss (2008), Belayneh et al. (2009) and Manda and Mabee (2010) provide information concerning the application of the scanline sampling, window sampling and circular estimator methods for specific case studies. However, a comprehensive analysis including (a) the application of all three sampling methods to the same case, (b) their verification using artificial fracture networks (AFNs) with known input parameters, and (c) the use of a power-law to describe the distribution of fracture lengths, which is often reported for natural fracture networks (e.g. Pickering et al., 1995; Odling 1997; Bonnet et al., 2001; Blum et al., 2005; Tóth, 2010; LeGarzic et al., 2011) is still lacking. A main issue here is the lack of a general consensus regarding the minimum number of length measurements required to adequately determine the length distribution of a fracture network. According to Priest (1993) the sampling area should contain between 150 and 300 fractures, of which about 50% should have at least on end visible. Furthermore, Bonnet et al (2001) suggested the sampling of a minimum of 200 fractures to adequately define exponents of power-law length distributions. However, these numbers only apply to specific case studies. Accordingly, the minimum number of fractures a sampling area should contain in order to apply the scanline sampling, window sampling or circular estimator methods are not unequivocally defined yet. A systematic study evaluating this issue is therefore needed.

A topic concerning the measurement of fracture networks in outcrops is the actual influence of censored fractures on network parameter estimates. Correcting censoring bias is a challenging task and relies on certain assumptions of fracture shape (e.g. disc, ellipsoid or rectangle) and fracture-size distributions (Priest, 2004),

as well as their spatial distribution (Riley, 2005). However, the use of such assumptions may also influence the results. Thus, it is important to systematically quantify the influence of censored fractures to assess the uncertainty of the measured fracture network parameters.

The required number of length measurements and the influence of censored fractures are evaluated in this paper by applying the three sampling methods to artificially generated fracture networks with known input parameters. Fracture lengths of natural fracture networks have been reported to follow power-law (e.g. Bonnet et al., 2001), log-normal (Priest and Hudson, 1981), gamma (Davy, 1993) and exponential distributions (Cruden, 1977). However, power-law relationships are the most commonly used to describe the distribution of fracture lengths (e.g. Pickering et al., 1995; Odling 1997; Blum et al., 2005; Tóth, 2010; LeGarzic et al., 2011). The arguments in favor of power-laws are comprehensively discussed by Bonnet et al. (2001). A point in favor of using power-law distributions is the absence of a characteristic length scale in the fracture growth process. On the other hand, all power-law distributions in nature are bound by a lower and upper cut-off. The size of a fracture can be restricted, for example, by lithological layering. The presence of such a characteristic length scale can give rise to log-normal distributions (Odling et al., 1999; Bonnet et al., 2001), even though the underlying fracturing is a power-law process. Considering the above, we chose to use a power-law to describe the distribution of fracture lengths in this study.

The objective of the present study is to further investigate the use and applicability of different sampling methods for the characterization of fracture networks at outcrops. We specifically provide a critical review of the application and limitations for the scanline sampling, window sampling and circular estimator methods and describe their typical application using two natural fracture networks: (1) lineaments from a satellite image of the Oman Mountains, Oman (Holland et al., 2009a) and (2) fractures from an outcrop at the Craghouse Park, UK (Nirex, 1997a). In the second part of this study AFNs are used to evaluate (1) the required minimum number of measurements and (2) the uncertainty of the results for increasing percentages of censored fractures. The results of these analyses are then used to re-evaluate the natural examples, to determine which sampling method is best-suited and to provide the uncertainty due to censoring bias. For the evaluation of the

fracture networks a novel software, called FraNEP (Fracture Network Evaluation Program), was developed.

FRACTURE SAMPLING AT OUTCROPS

This section provides an overview of (a) typical fracture and fracture network parameters (Table 2), (b) biases related to fracture sampling and (c) the application of three typical sampling methods used for outcrop analysis. The methods presented are the scanline sampling, window sampling and circular estimator methods (Figure 1). In addition, we summarize typical techniques to correct the sampling biases associated to these methods. Finally, previous comparisons of sampling methods are presented.

Fracture and fracture network parameters

Based on geometric data, statistical distributions and relationships between fracture network parameters, AFNs can be generated stochastically in order to predict the fluid flow behavior in fractured reservoirs under different scenarios (Berkowitz, 2002; Castaing et al. 2002; Neuman, 2005; Toublanc et al., 2005; Blum et al., 2009). Typical parameters for AFN characterization are fracture density, intensity, spacing, mean length or length distribution, and orientation of fractures (Priest, 1993; Narr, 1996; Mauldon et al., 2001; Castaing et al., 2002; Ortega et al., 2006; Blum et al. 2007; Neuman, 2008).

Fracture length and length distribution are important parameters for flow simulations. However, the definition of fracture lengths at outcrops is a challenging task. For example, fractures identified as single strands at one scale of observation (e.g. satellite image), may be seen as linked segments when changing the scale of observation (e.g. at ground level). Moreover, the intersection of different fractures (e.g. Ortega and Marrett, 2000) and fracture cementation (e.g. Olson et al., 2009; Bons et al., 2012) add significant complexity to the identification of individual fractures. Simulating fluid transport in an AFN generated from well characterized but irrelevant fractures will provide irrelevant results. Hence, it is important to link the observations in the subsurface with those obtained at outcrops. This can be

accomplished by comparison of scanline measurements (e.g. fracture apertures) from well cores or image logs with those from a outcropping subsurface analogues.

Mean fracture length is another commonly used parameter. Here we want to briefly address the issue of evaluating a mean length for a power-law distribution of fracture lengths. Considering the absence of a characteristic scale of power-laws and the limited information on lower and upper cut-off lengths for natural systems, a mean value is only valid for the sampled fracture length population. Using such a parameter, for example for fluid flow upscaling is therefore meaningless.

Additional information is necessary in order to quantify fluid flow through fracture networks, including fracture filling, displacement, wall rock rheology and mechanic or hydraulic fracture aperture (e.g. Lee and Farmer, 1993; Barton and Quadros, 1997; Odling et al., 1999; Renshaw et al., 2000; Laubach, 2003; Laubach and Ward, 2006; Llewellin, 2010). For a better prediction of fractures in diagenetically and structurally complex settings, evidence of the host rock's loading and mechanical property history, as well as current mechanical states are also required (Laubach et al., 2009). A summary of fracture (Table 1) and fracture network parameters (Table 2) is provided below.

Table 1. Additional important fracture parameters, necessary to adequately simulate fluid flow through fractured rocks. Furthermore, definitions of fracture size are also presented.

Parameter		Definition
Filling		The filling of the fracture void defines, if a fracture acts as conduit or prevents fluid flow.
Displacement		The displacement of fracture walls against each other.
Wall rock rheology		The uniaxial compressive strength (UCS) and the joint roughness coefficient (JRC) influence fracture closure under increased loading. Furthermore, JRC also controls hydraulic fracture aperture.
Aperture	Mechanical (*m*)	Real distance between the two walls of a fracture.
	Hydraulic (*a*)	Effective hydraulic fracture aperture according to the cubic law.
Size	Length	The length of the fracture trace on a sampling plane [m]
	Area	The area of the fracture plane [m^2]
	Volume	The volume of the fracture void [m^3]

Table 2. Definition of fracture density (p), intensity (I), spacing (S) and mean length (l_m) (Dershowitz, 1984) and governing equations to calculate these parameters using the scanline sampling, window sampling and circular estimator methods. The latter is based on Rohrbaugh et al. (2002). The definitions of fracture length distributions and orientations evaluated by the scanline sampling and window methods are also included.

Parameter		Definition	Scanline sampling	Window sampling	Circular estimator
Density (p)	Areal (P20)	Number of fractures per unit area [m^{-2}]	-	$p_{WS} = \frac{N}{A}$	$p_{CE} = \frac{m}{2\pi r^2}$
	Volumetric (P30)	Number of fractures per unit volume [m^{-3}]	-	-	-
Intensity (I)	Linear (P10)	Number of fractures per unit length [m^{-1}]	$I_{SLS} = \frac{N}{L}$	-	-
	Areal (P21)	Fracture length per unit area [m m^{-2}]	-	$I_{WS} = \frac{\sum l}{A}$	$I_{CE} = \frac{n}{4r}$
	Volumetric (P32)	Fracture area per unit volume [m^2 m^{-3}]	-	-	-
Spacing (S)	Linear	Spacing between fractures [m]	$S = 1/I_{SLS}$	-	-
Mean length (l_m)	Linear	Mean fracture length [m]	$l_{m;\,SLS} = \frac{\sum l}{N}$	$l_{m;\,WS} = \frac{\sum l}{N}$	$l_{m;\,CE} = \frac{\pi r}{2}\frac{n}{m}$
Length distribution	1D	Fractures intersecting with a scanline	yes	-	-
	2D	Fractures intersecting with a sampling area	-	yes	-
Orientation	2D	Orientation of a fracture on a sampling plane	yes	yes	-
	3D	Orientation of a fracture in a sampling volume	(yes)[a, b]	(yes)[b]	-

N is the total number of sampled fractures, *L* is the scanline length, *A* is the sampling area, *r* is the radius of the circular scanline, *l* is the fracture length, *n* and *m* are the number of intersections with a circular scanline and the number of endpoints in a circular window enclosed by the circular scanline. The subscripts *WS* (window sampling), *SLS* (scanline sampling) and *CE* (circular estimator) of the parameters indicate the corresponding sampling method.

[a] Borehole: possible for oriented well cores and image logs.

[b] Outcrop: possible for 3D outcrop settings.

Sampling biases and correction techniques

Orientation, truncation, censoring and size bias, amongst others, can cause significant under- or over-estimation of statistical parameters, and can thus potentially prejudice the characterization of fracture networks (Zhang and Einstein, 1998).

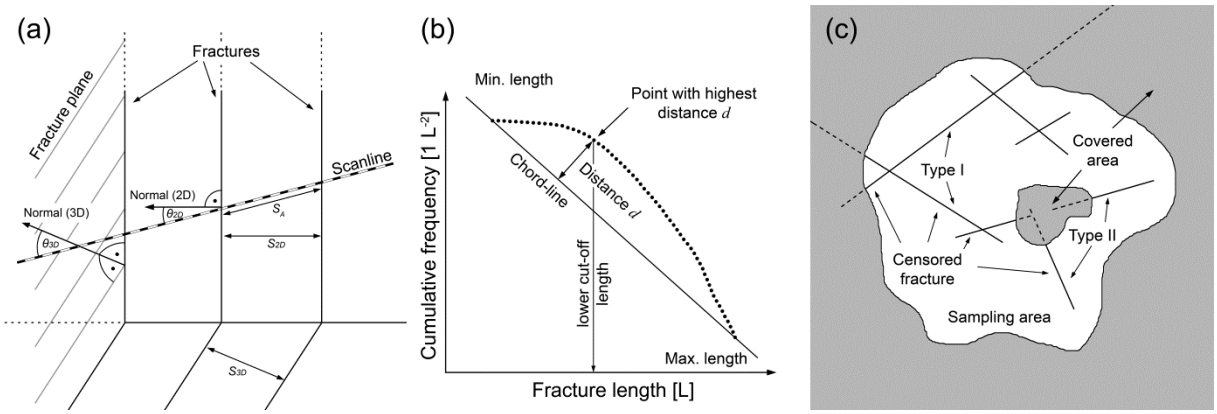

Figure 1. (a) Sketch illustrating orientation bias and the Terzaghi correction. S_A is the apparent spacing measured along a scanline, S_{2D} is the true spacing between two fracture traces and S_{3D} is the true spacing between two fracture planes. θ_{2D} and θ_{3D} are the angles between the normal to a fracture trace, or a fracture plane respectively, and a scanline. (b) Illustration of the Chord method (Pérez-Claros et al., 2002; Roy et al., 2007). In a log-log plot of fracture length against cumulative frequency, the line through the data point with the shortest length and the data point with the longest length is calculated. The fracture length from the data point with the highest distance *d* to this line is used as lower cut-off for the truncation bias. (c) Censoring bias caused by the boundaries of a sampling area (Type I) and covered parts in an outcrop (Type II).

Orientation bias is caused by fractures that intersect the outcrop surface or scanline at oblique angles. Thus, an apparent distance, or spacing, is measured between two adjacent fractures, which cause an underestimation of fracture frequency (Figure 1a). A typical correction method for orientation bias is the Terzaghi correction (Terzaghi, 1965; Priest, 1993), where the apparent distance (S_A) is corrected by the cosine of the acute angle θ of the fracture normal and the scanline or scan surface to obtain the true spacing (S):

$$S = S_A \times \cos\theta. \quad (1)$$

Fracture frequency is equal to 1/S. In three dimensions cos θ is given by (Hudson and Priest, 1983):

$$\cos\theta_i = \cos(\alpha - \alpha_i)\cos\beta\cos\beta_i + \sin\beta\sin\beta_i \quad (2)$$

where α and β are the dip direction and dip of the scanline, and α_i and β_i the dip direction and dip of the *i*-th fracture set normal. The problem with this correction method is that fractures have to be grouped into fracture sets. An alternative technique is presented by Lacazette (1991), which corrects orientation bias for each individual fracture:

$$Occurence = 1/(L \times \cos\theta) \quad (3)$$

where *Occurence* may be thought of as the frequency of a individual fracture, *L* is the length of a scanline and α is the angle between the pole to the fracture and the scanline. The fracture frequency of a set is the sum of the *Occurence* parameters calculated for the individual fractures in this set. A method presented by Narr (1996) allows estimating average fracture spacing in the subsurface. The method uses the spacing and height of fractures, and the borehole diameter to predict fracture intersection frequencies for all possible well deviations.

Truncation bias is caused by unavoidable resolution limitations, which depend on the used detection device (e.g. satellite image, human eye or microscope) and the contrast between the host rock and fractures. Parameters such as fracture size (length or width) are not detectable below a certain scale. Moreover, as fracture size approaches the detection limit, the actual number of recognized fractures significantly decreases. Thus, defining a lower cut-off of fracture size based on data resolution is needed to correct truncation bias (Nirex, 1997b). The truncation bias of sampled fracture lengths can be corrected by applying the Chord method (Figure 1b) (Pérez-Claros et al., 2002; Roy et al., 2007). Bonnet et al. (2001) plotted lower cut-off lengths against sampling areas reported in literature and could show that the cut-off lengths are typically in the range of 0.5 to 25% of the square root of the sampling area, with an average around 5%.

Censoring bias is typically related to limited outcrop size (Type I: Fractures with one or both ends outside the sampling area), uneven outcrops (e.g. erosion features) and/or coverage by overlaying rock layers or vegetation (Type II: Fractures with both ends inside the sampling area, but partly hidden from observation) (Figure 1c) (Priest, 1993; Pickering et al., 1995; Zhang and Einstein, 2000; Bonnet et al., 2001; Rohrbaugh et al., 2002; Fouché and Diebolt, 2004). The focus of the current study is on Type I. A typical effect of this censoring bias is an overestimation of fracture density (Kulatilake and Wu, 1984; Mauldon et al., 2001). For this type of

censored fractures it is impossible to know the relative lengths of the visible and censored part. Therefore, it is also impossible to tell whether the fracture center is inside the sampling area or not. However, it can be assumed that half of these fracture centers should be inside and the other half outside the sampled area. Thus, half of the censored fractures can be neglected for the calculation of fracture density (Mauldon, 1998; Mauldon et al., 2001; Rohrbaugh et al., 2002). For Type II censored fractures we know that the center is inside the sampling area. Unfortunately, if a fracture transects a covered part of the outcrop, it is impossible to tell whether we look at one transecting fracture or two fractures with obscured ends. To make a prediction whether we look at a transecting fracture or not, the true fracture length distribution needs to be known. However, correcting censoring bias for fracture-length distributions is complex and a complete review is beyond the scope of this study. Detailed descriptions on this topic are provided by, for example, Priest (2004) and Riley (2005).

Size bias is associated with the scanline sampling method (Bonnet et al., 2001; Manzocchi et al., 2009). Since the probability of a fracture to intersect a scanline is proportional to its length, shorter fractures are underrepresented in the measurements gathered along scanlines (Figure 2a) (Priest, 1993; LaPointe, 2002). Possible correction techniques are provided below, along with the description of the scanline sampling method.

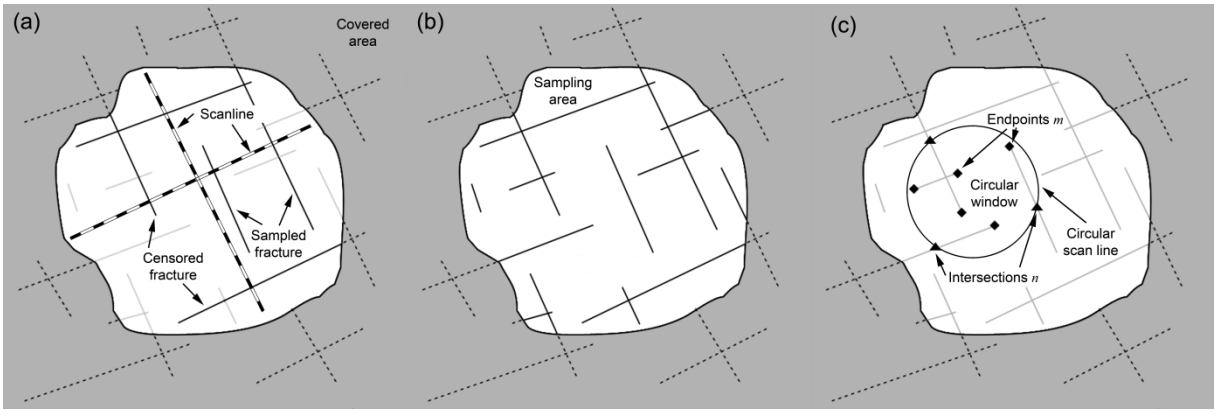

Figure 2. (a) Window sampling, (b) scanline sampling, and (c) circular estimator method. Solid black lines indicate sampled fractures, light gray lines indicate non-sampled fractures and dashed lines non-observable (censored) parts of fractures (modified from Rohrbaugh et al., 2002).

Scanline sampling

The scanline sampling method (Figure 2a; Table 2) is based on data collection from all fractures that intersect a scanline (Priest and Hudson, 1981; Priest, 1993; Bons et al., 2004). The method allows quick measurement of fracture characteristics in the field and is the main method used for the analysis of borehole image logs and cores. Its application provides 1-dimensional information on fracture networks (Table 2). The method is affected by: (a) orientation bias, (b) truncation bias, (c) censoring bias and (d) size bias. Orientation bias can be reduced or even avoided by placing a scanline perpendicular to a fracture set. If necessary, several scanlines can be used in outcrops to capture different fracture sets. However, well logs and drill cores constitute only one single scanline.

Several additional equations and assumptions are necessary to: (a) correct size bias, (b) compare linear with areal fracture intensity (Table 2) and (c) evaluate fracture density. The assumptions and equations provided here are only valid for power-law distributions of fracture lengths and need to be modified for other distributions. If we assume uniformly distributed, disc-shaped fractures with a power-law distribution of disc diameters in 3D, the fracture lengths measured in a plane also follow a power-law. The relationship between 3D-, 2D- and 1D-exponents of a power-law length distribution follows (Darcel et al., 2003):

$$E_{3D} = E_{2D} + 1 = E_{1D} + 2 \quad (4)$$

where E_{3D} is the exponent for a 3D rock mass volume, E_{2D} the exponent for a 2D sampling area and E_{1D} the exponent for a 1D scanline. However, fractures in stratified rocks are probably not disc-shaped. Moreover, equation (4) is only valid for well-sampled, representative populations of uniformly distributed fractures. For fractures with strong spatial correlation, clustering, or directional anisotropy, Hatton et al. (1993) provide a more appropriate relationship between 3D- and 2D-exponents:

$$E_{3D} = A \times E_{2D} + B \quad (5)$$

where A = 1.28 and B = -0.23. Since it is impossible to evaluate 2D-exponents from scanline measurements using equation (5), we use equation (4).

Size bias causes an overestimation of mean fracture length. For a given minimum fracture length l_0, a mean length l_m can be calculated as follows (LaPointe, 2002):

$$l_m = \frac{E_{2D} l_0}{E_{2D} - 1} = \frac{(E_{1D} + 1) l_0}{E_{1D}} \quad (6)$$

The scanline sampling method estimates linear fracture intensity *P*10 (Table 2), which is often also referred to as frequency. A relationship between linear (*P*10) and volumetric (*P*32) fracture intensities (Table 2) is provided by Barthélémy et al. (2009):

$$P10 = P32 \times e[\cos(\theta)] \quad (7)$$

where *e*[*cos(θ)*] is the expected mean of the cosines of angles *θ* for the fractures of one set. For a scanline parallel to the normal of a fracture set *e*[*cos(θ)*] equals 1, thus the relationship between linear (*P*10), areal (*P*21) and volumetric (*P*32) fracture intensities (Table 2) is given by:

$$P10 = P21 = P32 \quad (8)$$

Fracture intensity *I* is defined as the product of density *p* and mean length l_m:

$$I = p \times l_m \quad (9)$$

Combination and rearrangement of equations (4), (8) and (9) allows estimating areal fracture density based on measurements obtained by the scanline sampling method:

$$p = \frac{P10}{l_m} = \frac{P10 \times E_{1D}}{(E_{1D} + 1) \times l_0} \quad (10)$$

Window sampling

The window sampling method (Figure 2b; Table 2) estimates the statistical properties of fracture networks by measuring parameters from all fractures present within the selected sampling area (Pahl, 1981; Wu and Pollard, 1995). Typical applications of this method are the analysis of outcropping subsurface analogues (Belayneh et al., 2009) or the characterization of fracture networks using remote sensing data from satellite images or aerial photographs (Koike et al., 1995; Becker, 2006; Holland et al., 2009a; Zeeb et al., 2010). In general, three types of sampling bias affect the window sampling method: (1) orientation, (2) truncation and (3) censoring biases.

Circular estimator

The circular estimator method uses a combination of circular scanlines and windows (Mauldon et al., 2001; Figure 2c). It is in fact a maximum likelihood estimator (Lyman, 2003). This means that instead of directly sampling individual fractures and measuring their characteristics, for example orientation or length, parameters are estimated using statistical models that are described in detail by Mauldon et al. (2001). Based on the number of intersections (*n*) between a circular scanline and fractures and the number of fracture endpoints (*m*) in a circular window formed by this scanline, fracture density, intensity and mean length are calculated (Table 2). To assure an accuracy of the results of 15% or higher, ten circular scanlines with a diameter exceeding the mean fracture block size, or fracture spacing, but significantly smaller than the minimum dimension of the sample region, are randomly placed in the sampling area (Rohrbaugh et al., 2002). In addition, *m*-counts should be higher than 30 (Rohrbaugh et al., 2002). The circular estimator is a time-efficient method to evaluate fracture network characteristics. Being a maximum likelihood estimator, the method is not subject to sampling bias. However, this method does not provide information on important parameters such as fracture orientation, length distribution or width. Hence, it should in principle be combined with other sampling methods.

Comparison of different sampling methods in the literature

Several studies compared the effectiveness of the different sampling methods for specific case studies. For example, Belayneh et al. (2009) conducted water-flooding numerical simulations on deterministic and stochastic discrete fracture networks and matrix models. To generate these networks, outcropping subsurface analogues of Jurassic carbonate platforms on the southern margin of the Bristol Channel Basin were studied using the window sampling and scanline sampling methods. The measured parameters included fracture orientation, length, spacing and aperture. Numerical simulations on deterministic models (window sampling) showed that flow is fracture dominated. Simulating flow through fracture network models (scanline sampling) varied from fracture to matrix dominated. They concluded that this uncertainty may be caused by undersampling of fractures along scanlines.

Manda and Mabee (2010) studied the effectiveness of the single scanline, the multiple scanline and the window sampling methods using them to acquire the properties of fractures from layered dolomites in a quarry in Wisconsin. They used overall volumetric intensity and permeability of fracture network models to assess the accuracy of these methods, and recommended the use of the window sampling method. Weiss (2008) utilized the scanline sampling, window sampling and circular estimator methods to characterize fracture networks from chalk in the Northern Negev in Israel. He concluded that the circular estimator method is a useful tool to assess mean fracture size without the need of accounting for sampling bias. However, the sampling areas were very limited in size. Hence, large fractures controlling the fluid transport in the aquifer were not adequately defined by the relatively small circular and/or rectangular sampling windows. Weiss (2008) suggested a combination of the scanline and window sampling methods to calculate the distribution of fracture length. Rohrbaugh et al. (2002) used AFNs with scale dependent length distributions to investigate the accuracy of the results from the scanline sampling, window sampling and circular estimator methods in estimating fracture density, intensity and mean length. Based on their results Rohrbaugh et al. (2002) presented a guideline for the application of the circular estimator method and followed this guideline to characterize eight natural fracture networks.

STUDY OF NATURAL FRACTURE NETWORKS

In this section we show a typical application of the scanline sampling, window sampling and circular estimator methods. The fracture network parameters of two natural examples are evaluated: (1) lineaments measured from a satellite image of the Oman Mountains, Oman (Figure 3; from Holland et al., 2009a), and (2) fractures from an outcrop located at Craghouse Park, UK (Figure 4; Nirex 1997a, b). The three sampling methods are used to estimate fracture density, intensity, mean length and length distribution.

The first natural fracture network (Figure 3) is an analysis of lineament data (fractures, faults, joints, veins, etc.) extracted from a Quickbird satellite image from the southern flank of the Jabal Akhdar dome in the Oman Mountains, Oman (Hilgers et al., 2006; Holland et al., 2009a,b). The sampling area has an extent of 120,000 m^2,

in which 650 lineaments with lengths ranging between 3 and 179 m could be identified by optical picking. Applying the chord method (Pérez-Claros et al., 2002; Roy et al., 2007), the cut-off length for truncation bias is 23.3 m. For interpretation the panchromatic band, which offers a spatial resolution of 0.7 m, was used. Based on the number of fractures extending beyond the boundaries of the sampling area, approximately 5% of the sampled fractures appear to be censored.

The second natural fracture network is an outcrop located at Craghouse Park, UK (Figure 4; Nirex, 1997a). This sampling area has a size of 19 m^2, containing a total of 288 visible fractures with lengths ranging between 0.05 and 4.0 m. The application of the chord method (Pérez-Claros et al., 2002; Roy et al., 2007) provided a cut-off length for truncation bias of 0.8 m. The limited outcrop size, which is typical for a humid climate, causes 30% of the fractures to be censored.

Table 3 summarizes the fracture network parameters obtained from the two natural examples. The deviation between the results for length distribution exponents evaluated by scanline and window sampling for the Oman example might be due to difficulties when interpreting fracture lengths in the satellite image. Erosion features (Figure 3a) cause Type II censoring bias (Figure 1c). Thus, the interpretation of two short fractures is actually one long fracture. Moreover, what looks like one long fracture in the satellite image might be a series of fracture segments when studied at the ground level.

When analyzing the second example from the UK a power-law length distribution was assumed. Such an assumption is valid (and necessary), if an upscaling of the results is intended. If the length distribution at the scale of observation is evaluated, then a log-normal distribution is probably a better choice. However, the length measurements should not be corrected for truncation bias, since the procedure removes the short fracture lengths, which are essential for a log-normal distribution.

For the analysis of both natural examples it was impossible to sample 30 fracture endpoints with a radius of the circular scanlines equal to 1/10 of sampling area extend. Therefore, the radii were increased (Table 3) to satisfy the 30 endpoint criteria defined by Rohrbaugh et al. (2002).

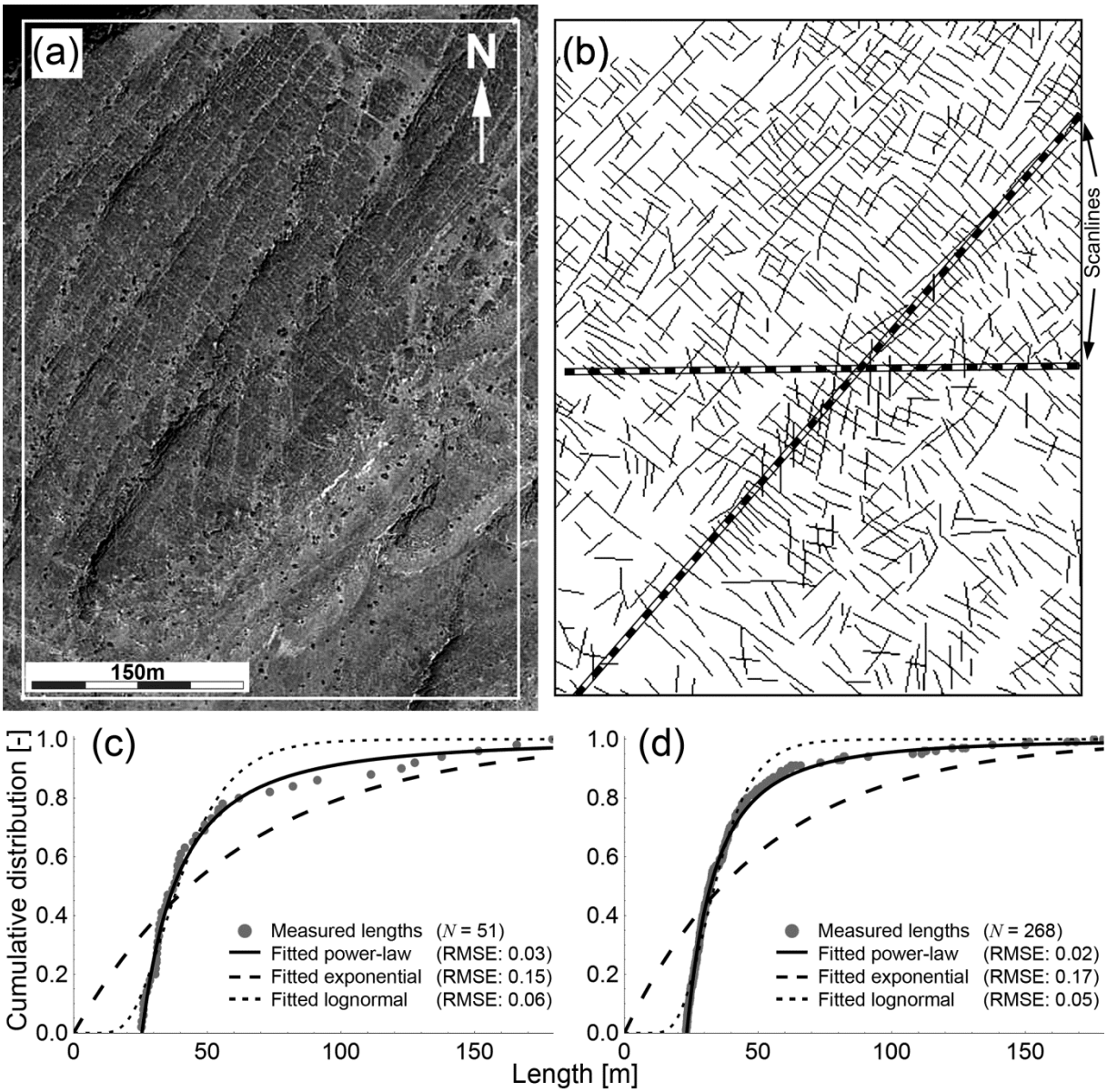

Figure 3. (a) Quickbird satellite image from the southern flank of the Jabal Akhdar dome in the Oman Mountains, Oman. (b) Interpretation of the fractures in the white rectangle in (a) after correction of truncation bias (modified after Holland et al., 2009a). UMT coordinates of the lower left and upper right corners are 40N 525496 2562373 and 40N 525799 2562760. Please note that the satellite image and the trace line map are not to scale due to the slope of the flank. (c) and (d) show a plot of fracture lengths (gray dots) against the cumulative distribution measured by (c) two scanlines and (d) one window sampling of the whole study area (a). The solid, dashed and dotted black lines indicate power-law, exponential and lognormal fits. The fitting accuracy is given by root mean squared errors (RMSE).

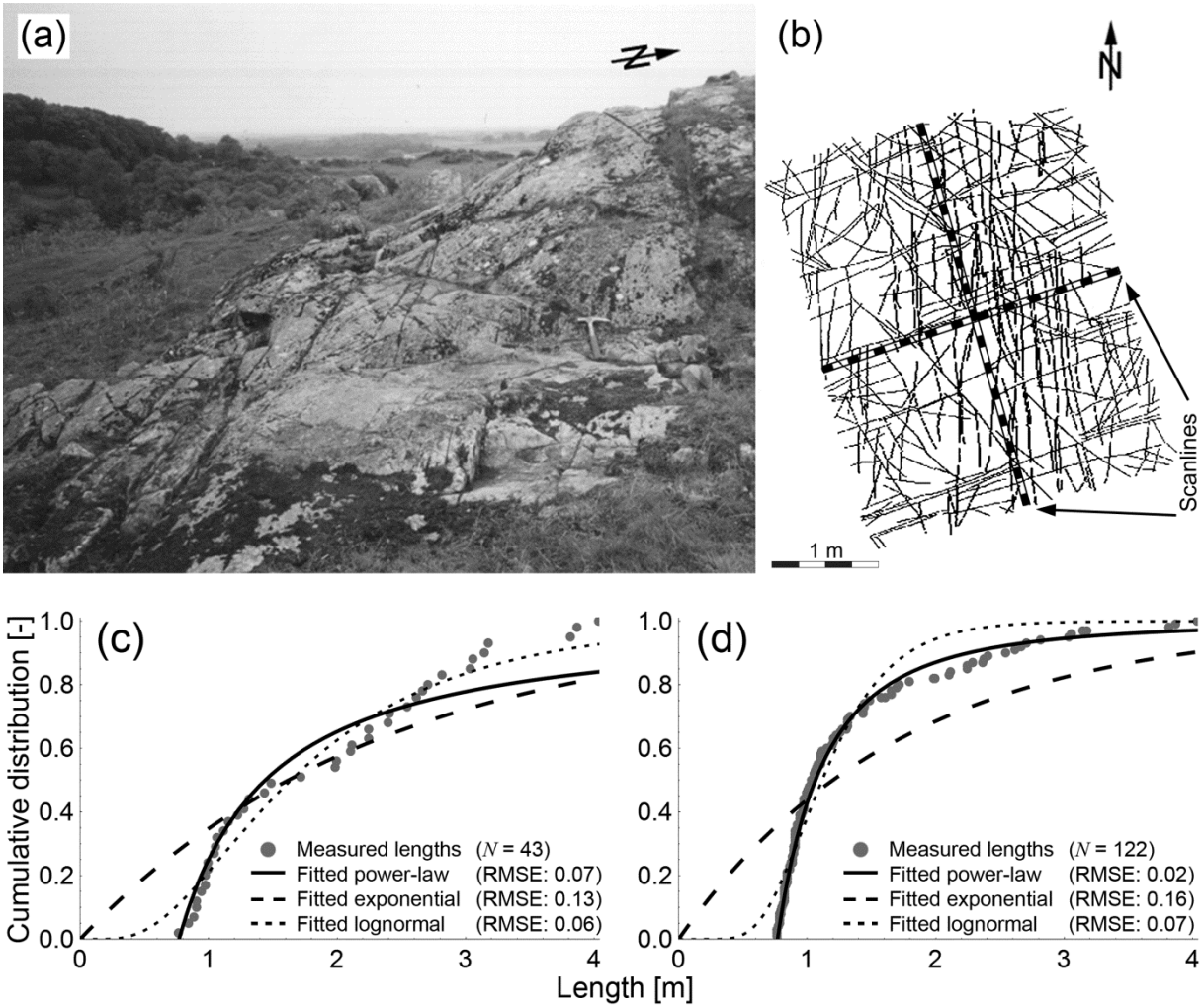

Figure 4. (a) Photo of the investigated outcrop at Craghouse Park, UK (geologic hammer for scale). (b) Trace line map of the cleaned outcrop. (c) and (d) show a plot of fracture lengths (gray dots) against the cumulative distribution measured by (c) two scanlines and (d) one window sampling of the whole study area (a). The solid, dashed and dotted black lines indicate power-law, exponential and lognormal fits. The fitting accuracy is given by the root mean squared error (RMSE).

Table 3. The fracture network parameters estimated for the two natural fracture networks. The results are corrected for orientation, truncation and size bias. The fracture density is estimated by the window sampling method, and half of the Type I censored fractures (Figure 1) are neglected.

Location	*Oman Mountains (Oman)*			*Craghouse Park (UK)*		
Parameter	Scanline sampling	Window sampling	Circular estimator	Scanline sampling	Window sampling	Circular estimator
Number of measurements [-]	51	268	-	43	122	-
Length range [m]	25.6-179	23.3 - 179	-	0.8 - 4.0	0.8 - 4.0	-
Radius [m]	-	-	100	-	-	1.6
Censored fractures [%]	0	5	-	11	30	-
Density p [m^{-2}]	0.002	0.002	0.002	3.5	5.4	2.8
Intensity I [m m^{-2}]	0.07	0.09	0.10	5.1	7.4	3.6
Mean length l_m [m]	39.7	41.6	53.9	1.5	1.4	1.3
Exponent E_{2D} [-]	2.8	2.2	-	2.1	2.2	-

ARTIFICIAL FRACTURE NETWORKS (AFN)

In this section we apply the scanline sampling, window sampling and circular estimator methods to AFN with known input values and compare them with the calculated fracture network parameters. With this systematic approach we evaluate, for each sampling method, (1) the minimum number of required measurements and (2) the influence of censored fractures on estimates of fracture network parameters.

Fracture network generation

The fracture network generator FracFrac (Blum et al., 2005), a program based on Visual Basic for Applications (VBA) in Microsoft® Excel, was used to generate nine 2D AFNs (Figure 5). The networks are defined by fracture density and length distribution. For the density three values with p = 0.5 m^{-2}, p = 1.0 m^{-2} and p =1.5 m^{-2} were assumed. Power-law exponents reported for natural fracture systems typically range between 0.8 and 3.5, with the majority in the range between 1.7 and 2.8, and most of which are actually around 2 (Bonnet et al., 2001). For the generation

of the AFN we used exponents of E = 1.5, E = 2.0 and E = 2.5. In the current study a truncated power-law is used to describe the cumulative distribution of fracture lengths (Blum et al., 2005; Riley, 2005):

$$f(l) = 1 - \left(\frac{l}{l_0}\right)^{-E} \quad (10)$$

We define a lower cut-off length l_0 of one meter. Although, Odling et al. (1999) observed a similar cut-off for joints in sandstones of western Norway, this value is probably only valid for this specific case study. The lower cut-off is necessary to constrain the range of fracture lengths in the AFNs and is an arbitrary value.

Table 4 provides a summary of true fracture density, intensity, mean length, and power-law exponent for each of the nine AFNs (Figure 5a). Orientation bias is avoided by using two sets of perfectly parallel fractures with orientations of 90° and 180°. Furthermore, the input fracture density is equally distributed between the two fracture sets.

Table 4. Summary of the true fracture network parameters for the nine generated AFNs. Values for fracture intensity and mean length are calculated from the fracture density and power-law exponent used as input by applying equations (4) and (7).

Parameter	AFN								
	1	2	3	4	5	6	7	8	9
Density p [m^{-2}]	0.5	1.0	1.5	0.5	1.0	1.5	0.5	1.0	1.5
Intensity I [m m^{-2}]	1.5	3.0	4.5	1.0	2.0	3.0	0.8	1.7	2.5
Mean length l_m [m]	3.0	3.0	3.0	2.0	2.0	2.0	1.7	1.7	1.7
Exponent E_{2D} [-]	1.5	1.5	1.5	2.0	2.0	2.0	2.5	2.5	2.5

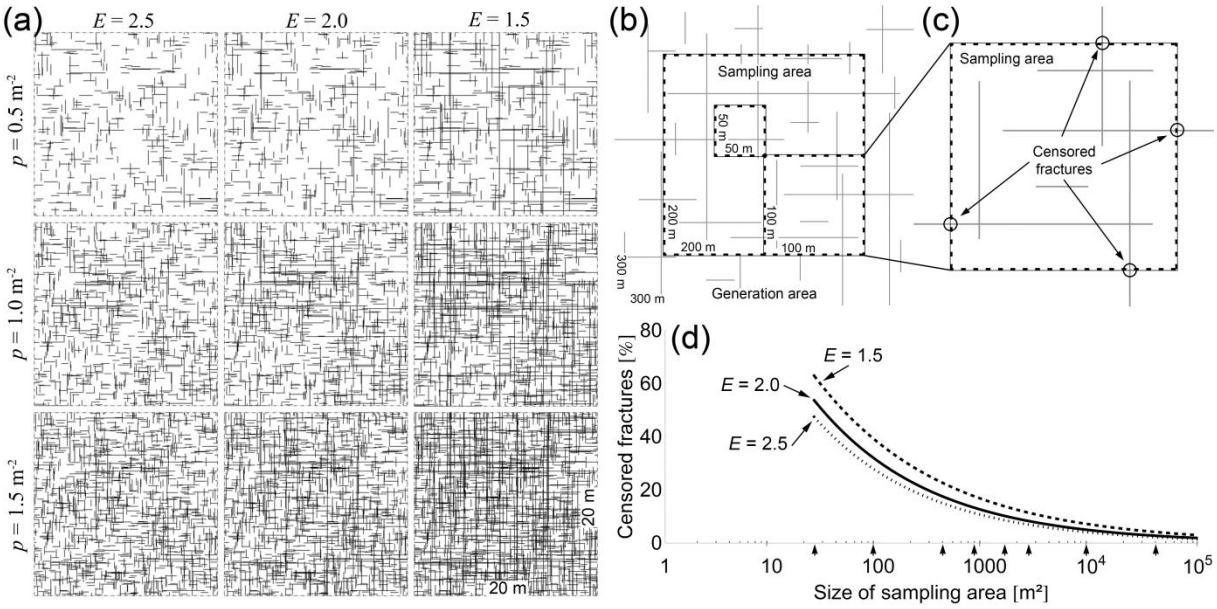

Figure 5. (a) Examples for a 20 m × 20 m sampling area from each of the nine 2D AFNs, with input values for fracture density in m^{-2} (*p*) and exponent (*E*) of the power-law length distribution. (b) Sketch illustrating the generation area and the definition of sampling areas. (c) Definition of the censored fractures in a sampling area. (d) The relationship between the size of the sampling area and the average percentage of censored fractures for the three power-law length distributions. The black arrows on the x-axis indicate the size of the sampling areas analyzed in this study.

The generation area of each AFN is 300 m × 300 m. In this whole area, a total of 146 squared sampling areas are defined (one area with an edge length of 200 m, four with 100 m, 16 with 50 m and 25 sampling areas with edge lengths of 40 m, 30 m, 20 m, 10 m and 5 m), providing a total of 1314 sampling areas for all nine AFNs (Figure 5b). Fractures are treated as censored, if one or both ends intersect with a boundary of the sampling area (Figure 5c). The percentage of censored fractures is calculated from the total number of fractures in a sampling area and the number of fractures that are censored. Figure 5d presents the percentages of censored fractures averaged for the different sized sampling areas. The highest percentages are found for small sampling areas and high power-law exponents (Figure 5a: *E* = 1.5).

Each sampling area is analyzed using FraNEP (Fracture Network Evaluation Program). FraNEP is a novel software, which characterizes fracture networks applying either the scanline sampling, window sampling or the circular estimator methods. For the scanline sampling method one scanline is placed perpendicular to each of the two fracture sets. The window sampling method is applied on the entire

sampling area. For the application of the circular estimator method we follow the guideline of Rohrbaugh et al. (2002). Ten circular scanlines are randomly placed inside the sampling area, with the radius equal to 1/10 of the edge length. Values for fracture density, intensity, mean length and length distribution are calculated and compared with the true values. For the calculation of the fracture density, half of the censored fractures are neglected. For the other three parameters all sampled fractures are used. The distribution of fracture lengths is evaluated by fitting power-law, log-normal and exponential cumulative distribution functions to the sampled fracture lengths. The root mean square error approach is used to compare the quality of a best fit, which is calculated from the sum of squared errors, the number of measurements and the mean value of the measured parameter (Loague and Green, 1991).

Table 5 provides an example for three sizes of sampling areas from AFN-5. Shown are the ranges of values (lowest to highest) of calculated fracture network parameters for all sampling areas of the same size. Table 5 illustrates well how the spread of values, and thus the uncertainty, increases for smaller sampling areas. For fractures sampled by scanline sampling in the 10 m × 10 m sampling area, fracture lengths follow a log-normal distribution. We conclude that scanline sampling does not suffice to characterize these sampling areas. Figure 6 shows fracture lengths and fitted distributions for one exemplary sampling area from each size presented in Table 5. The fitting accuracy of the power-law distribution decreases for smaller sampling areas.

Table 5. Examples of fracture network parameters evaluated for AFN-5. Shown are the lowest and highest value found by the three sampling methods in all sampling areas of the presented sizes. The numbers in brackets are the input values.

Edge length [m]	Sampling method	Value range			
		Density [1 m^{-1}] (p = 1.0)	Intensity [m m^{-2}] (I = 2.0)	Mean length [m] (l_m = 2.0)	Exponent [-] (E_{2D} = 2.0)
100	SLS	0.96 - 1.08	1.87 - 2.16	1.92 - 2.05	1.95 - 2.09 (4/4)[a]
	WS	0.99 - 1.00	1.96 - 2.01	1.93 - 1.98	1.97 - 2.02 (4/4)[a]
	CE	0.94 - 1.00	1.82 - 2.20	1.93 - 2.21	- (4/4)[b]
40	SLS	0.74 - 1.21	1.50 - 2.40	1.77 - 2.19	1.84 - 2.27 (25/25)[a]
	WS	0.96 - 1.04	1.87 - 2.08	1.80 - 1.97	1.90 - 2.11 (25/25)[a]
	CE	0.90 - 1.07	1.88 - 2.63	2.03 - 2.58	- (25/25)[b]
10	SLS	0.35 - 1.30	1.00 - 2.80	1.49 - 4.27	1.99 - 3.03 (2/25)[a]
	WS	0.83 - 1.16	1.45 - 2.64	1.35 - 1.97	1.54 - 2.62 (25/25)[a]
	CE	-	-	-	- (0/25)[b]

[a] (Number of sampling areas with power-law distribution of fracture lengths / sampling areas)

[b] (Number of sampling areas with m-counts > 30 / sampling areas)

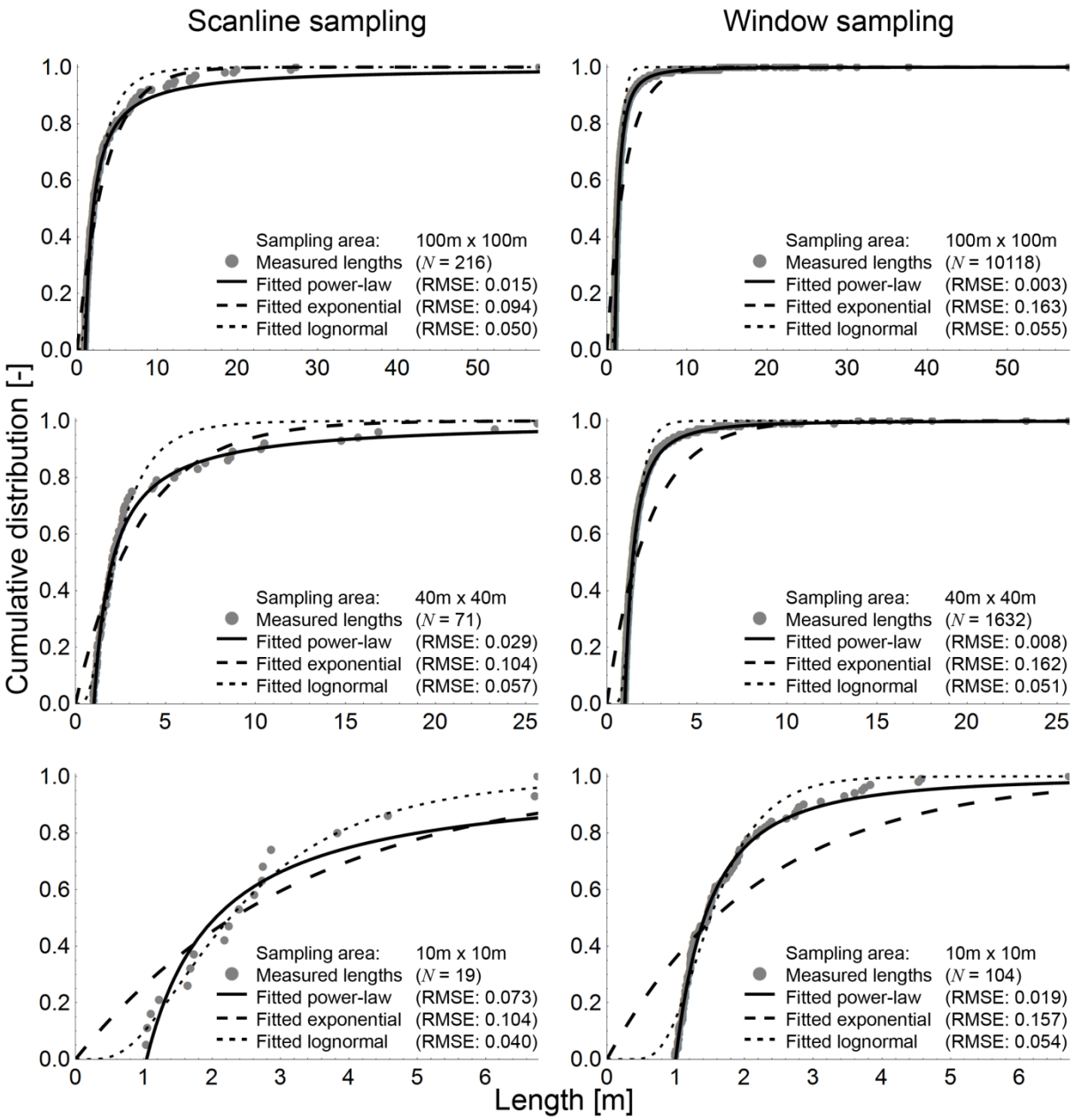

Figure 6. Plot of measured fracture lengths (grey dots) against their cumulative distribution. The black lines indicate the best fitting power-law (solid), exponential (dashed) and lognormal (dotted) distributions. The RMSE in the brackets indicates the accuracy of the fits.

Required minimum number of measurements

There is a lack of well-established criteria to define the required minimum number of measurements to sufficiently capture the statistical properties of fracture networks for specific sampling methods. For each sampling method a criterion is defined in such a way that it sufficiently captures the statistical properties. For the scanline and window sampling methods we defined the criterion as the number of

measurements, above which a power-law always provides the best fit to the fracture length measurements (Figure 6). The criterion of the circular estimator method is defined as the number of fractures in a sampling area, above a circular window always contains 30 or more fracture endpoints (Rohrbaugh et al., 2002). These criteria are applied to the data obtained by the three sampling methods for each of the 146 sampling areas defined within each of the nine AFNs. Furthermore, two numbers are evaluated for each sampling method: (1) the highest number of measurements that does not satisfy the criterion in any of the 146 sampling areas (Table 6: *not satisfied*), and (2) the lowest number of measurements above which the criterion is always satisfied in any of the 146 sampling areas (Table 6: *satisfied*). This is repeated for all nine AFNs. However, these numbers are fracture network specific and depend on the properties of the network. Thus, for the determination of the minimum number, which is universally applicable to all nine studied AFNs, we need to compare these results. The lowest number of (2), which is also higher than all numbers of (1), is the required minimum number of measurements of the sampling method (Table 6).

At least 112 fractures should be measured for the window sampling method, 225 for the scanline sampling method and 860 for the circular estimator method. Since only the fractures intersecting with a line are considered for the scanline sampling method, significantly more fractures have to be present in a sampling area to measure 225 fractures. For sampling areas with a simple geometry and fracture network pattern, for example similar to the AFNs, approximately 4000 fractures should be present. A more complex sampling area and/or fracture network may imply that even more fractures have to be present. Note that the required minimum corresponds to the number of measurements after accounting for truncation bias. Despite the efforts to universally find a minimum number of measurements to properly capture the properties of fracture networks, each case study may require a different minimum number of measurements depending on the network itself.

Table 6. The required minimum number of measurements for each sampling method (value is underlined). The numbers for the nine AFNs in the columns *not satisfied* are the highest number of measurements for which the criteria [(1)] and [(2)] were not satisfied. The numbers in the columns *satisfied* are the lowest number of measurements above which the criteria [(1)] and [(2)] were always satisfied.

Sampling method		Number of measurements					
		Window sampling [(1)]		Scanline sampling [(1)]		Circular estimator [(2)]	
AFN (Table 4)	1	78	83	88	123	846	849
	2	46	106	152	165	478	908
	3	64	65	224	<u>225</u>	710	1364
	4	78	79	48	49	858	<u>860</u>
	5	38	39	106	107	466	919
	6	53	58	58	61	684	686
	7	78	80	46	47	821	823
	8	110	<u>112</u>	91	97	460	875
	9	53	54	48	50	675	1315
Criterion		*not satisfied*	*satisfied*	*not satisfied*	*satisfied*	*not satisfied*	*satisfied*

[(1)] Criterion: power-law fits best the fracture length distribution

[(2)] Criterion: circular window contains more than 30 fracture endpoints.

Uncertainty analysis

The effects responsible for censoring bias are well known. However, to our knowledge, the actual influence of censored fractures on estimates of fracture network parameters has not been comprehensively investigated. The influence is assessed here for four typical fracture network parameters: (1) fracture density, (2) intensity, (3) mean length, and (4) length distribution. For each sampling area, which contains the necessary minimum number of fractures to apply the respective sampling method, the difference between estimated and input value is calculated. The percentage of censored fractures in this sampling area is plotted against the difference in percent for each parameter and sampling method. The plots illustrate the maximum difference observed for increasing percentages of censored fractures (Figure 7). In the present study the range of potential differences between those

maximum differences is referred to as the uncertainty. Figure 7 shows an example for the uncertainty in estimating fracture density using the window sampling method.

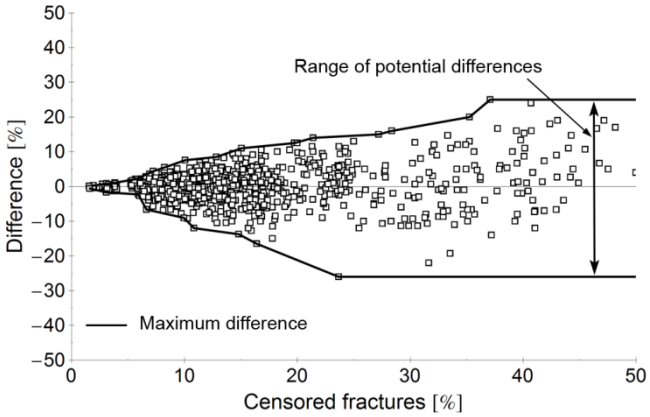

Figure 7. Plot of censored fractures (in percent) against the difference (in percent) between estimated and input fracture density for window sampling. Each point represents a sampling area from the nine AFNs. The maximum difference is highlighted by the two solid black lines. The range of potential differences between those two lines represents the uncertainty of a result for a specific sampling area with the percentage of censored fractures.

Figure 8 summarizes the uncertainty of the four parameters estimated by the three sampling methods. For all sampling methods and parameters the uncertainty of the measured values clearly increases with the percentage of censored fractures. In general, the results based on the window sampling method indicate the lowest uncertainty, especially for the evaluation of fracture density, mean length and length distribution. An interesting result is the high uncertainty of all three sampling methods in estimating fracture intensity. Even though the circular estimator highly overestimates fracture intensity, the method exhibits the lowest uncertainty. All results obtained by the scanline sampling method are within an 80% confidence interval. However, estimates of fracture density and mean length depend on the correct estimate of a power-law length distribution and thus only data sets equal to or above the required minimum number of 225 measurements can be used for the calculations, and thus can be carried out for the cases of 0 - 5% censored fractures only.

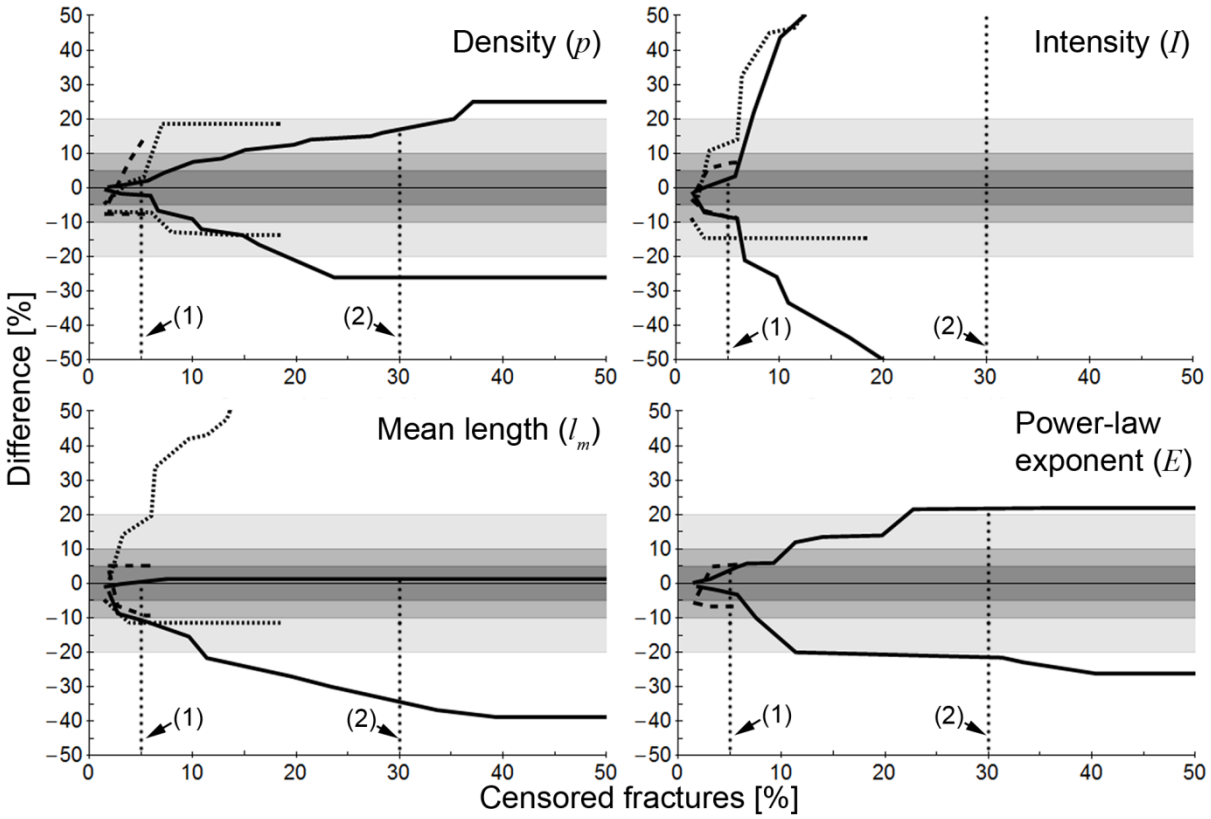

Figure 8. Summary of potential differences evaluated for scanline sampling (dashed), window sampling (solid) and circular estimator (dotted) methods, illustrated as lines of maximum difference (Figure 7). The areas highlighted in dark grey, grey and light grey represent the 95%, 90% and 80% confidence intervals of the true value. The vertical dotted lines indicate the percentage of censored fractures for the studied natural fracture networks: (1) the Oman Mountains, and (2) Craghouse Park. CI denotes the confidence intervals.

DISCUSSION

Characterizing fracture networks in the subsurface is a challenging task due the limitations of borehole/log/core analysis. Studying outcrops analogue to the subsurface provides valuable data, especially on fracture lengths (mean length and length distribution). Additional information on fracture density and intensity can improve our understanding of the subsurface even more. However, the characterization of fracture networks using outcrops is also challenging. The interpretation of a single fracture can change with the scale of observation. For example, a fracture interpreted as a single entity in an aerial photograph can prove to be a segmented fracture at ground level. Moreover, fractures are altered by weathering when exposed, they normally crosscut each other and can be filled, partly

or completely, by mineral precipitates or debris. Defining the length, or the endpoints, of a fracture can be difficult under such circumstances. In addition, fracture networks are three-dimensional, whereas the analysis of boreholes and outcrops are often constrained to one- or two-dimensions, respectively. Therefore, models of subsurface fracture networks can be significantly improved if cross-correlated data from borehole and outcrop analysis is considered.

The main advantage of the scanline sampling and window sampling methods is the comprehensive information on fracture parameters they provide, especially measurements of fracture length, aperture and orientation. However, the two methods are subjected to sampling bias and in such cases it is essential to perform corrections for orientation, truncation, censoring and size biases. As a maximum likelihood estimator the circular estimator method eliminates these sampling biases, but only provides information on fracture density, intensity and mean length, and not on other parameters (e.g. orientation, aperture or length of individual fractures). The analysis of the two natural fracture networks using these three sampling methods resulted in different fracture characteristics (Table 3), which emphasizes the necessity of a review concerning (1) the minimum required number of measurements and (2) the influence of censored fractures on the estimates of fracture network parameters.

Bonnet et al. (2001) provided a minimum number of measurements required to evaluate the exponent of a power-law fracture length distribution. Similarly, Priest (1993) suggested a minimum number of fractures a sampling area should contain in order to properly characterize fracture network parameters. Despite these studies provide some basic guidelines, a universally applicable minimum number is probably impossible to obtain since the required number of samples depends on the studied fracture network itself. In the current study we provide a required minimum number for simple fracture networks with power-law length distributions. The power-law exponents used to generate the AFNs represent those commonly reported. For other length distributions, complex fracture networks and/or complex sampling area geometries more fracture lengths should be measured. Though the numbers presented below are not universally applicable, they allow a better estimate on the number of measurements necessary to adequately capture fracture statistics. Our results indicate that the required minimum number of length measurements to define a power-law distribution is ~225 for scanline sampling and ~110 for window sampling.

Note that the size of a sampling area, and therefore the fracture density, does not directly influence the definition of a length distribution. However, a small sampling area may cause more fractures to be censored, which would lead to a more complex fracture network. For the application of the circular estimator method we found that ~ 860 fractures should be present in a sampling area to always sample a minimum of 30 fracture endpoints. This minimum number depends on the radius of the circular scanline and decreases for larger radii.

For all three sampling methods the uncertainty increases with the percentage of censored fractures. The AFNs used in the current study are simple and natural examples, like the ones used here, are often much more complex. Hence, it is likely that more fractures are censored. However, since we use percentages of censored fractures, the approach to evaluate the uncertainty is also applicable to natural fracture networks.

The window sampling method provides results with the lowest uncertainty for all network parameters, except for fracture intensity. The reason for this high uncertainty can be explained by the definition of fracture intensity (Table 2) and the approach we used to elaborate the uncertainty due to censoring bias (Figure 7). Note that fracture intensity can be described as the product of fracture density and mean length (Eq. 9). If in a sampling area both fracture density and mean length are overestimated, then fracture intensity is even more so.

Both, the required minimum number of measurements and the uncertainty due to censoring bias indicate that the window sampling method is the most suitable for the evaluation of the studied natural fracture networks. Table 6 summarizes the measured fracture network parameters and their uncertainty, based on the evaluation in Figure 8.

Table 7. Fracture network parameters evaluated for the two natural fracture networks. The values in brackets indicate the range of possible true values due to the uncertainty.

Parameter	*Oman Mountains (Oman)*		*Craghouse Park* (*UK*)	
Number of fractures [-]	268		122	
Length range [m]	23.3 - 179		0.76 - 4.04	
Censored fractures [%]	5		30	
Density p [m^{-2}]	0.002	(insignificant)	5.44	(4.52 - 6.80)
Intensity I [m m^{-2}]	0.09	(0.09 - 0.10)	7.40	(<< 3.70 >> 11.1)
Mean length l_m [m]	41.6	(41.6 - 46.2)	1.36	(1.33 - 1.84)
Exponent E_{2D} [-]	2.15	(2.06 - 2.21)	2.17	(1.69 - 2.65)

The uncertainty due to censoring bias is rather low for the analysis of the lineaments from the satellite image of the Jabal Akhdar dome (Figure 3; Holland et al., 2009a). However, it is also important to consider the resolution limitations of satellite images, which causes a significant truncation bias. For example, LeGarzic et al. (2011) investigated extensional fracture systems in the Proterozoic basement of Yemen at different scales from multi-kilometric satellite imagery to ten meter field observations, with length data ranging over three orders of magnitude. The combined multi-scale analysis of several thousands of fracture lengths follows a power-law distribution with an exponent of E = 1.8. However, fracture lengths investigated at individual scales were found to follow varying distributions. Truncation bias might be an explanation for the deviation of the length distributions from a power-law at individual resolution scales. Hence, correcting the fracture length data for this sampling bias could result in the attainment of distributions closer to the real one.

The results evaluated for the second natural fracture network (Craghouse Park, UK; Figure 4; Nirex, 1997a) illustrate the high uncertainty of fracture characteristics calculated for such a small outcrop (Table 6). For the power-law exponent we obtained a value of E = 2.17. However, since 30% of the fractures are censored the potential true value ranges between 1.69 and 2.65, which covers approximately 70% of the values reported by Bonnet et al. (2001). Limitations in the number of measured fractures, the extent of the sampling area and a high percentage of censored fractures are typical for such small outcrops. However, such outcrops are often the only option for the characterization of subsurface fracture networks. For example, Manda and Mabee (2010) sampled between 5 and 76

fractures for two different sets, with 69% or more censored fractures for one of the sets. Although, Weiss (2008) considered every outcrop in his study area, he also encountered the problem of having a low number of measurements with a high percentage of censored fractures. A cross-correlation with borehole data could improve the characterization of the subsurface fracture network.

CONCLUSIONS

The characterization of fracture networks at outcrops can provide essential information for subsurface reservoir models. We present a review on the application of the scanline sampling, window sampling and circular estimator methods, their governing equations and a summary of several techniques to correct for sampling bias. In addition, a set of equations and assumptions allow to compare the results of these sampling methods and to extrapolate these parameters for 3D fracture networks.

Furthermore, the required minimum number of measurements was evaluated. For the scanline sampling method ~225 measurements are required to define the power-law length distribution, whereas the window sampling requires ~110 measurements. These numbers apply for fracture networks that are similar to the AFNs used here. Additional measurements should be considered for the characterization of more complicated fracture network settings. For the application of the circular estimator method, with a radius equal to 1/10 of sampling area extend and assuring a minimum of 30 sampled endpoints, at least 860 fractures should be present in the sampling area. The required minimum number for this method can be reduced by applying a larger radius. If (or how) different radii affect the accuracy of the results should be a topic of future studies.

Uncertainty caused by censored fractures can have large implications for simulations designed to understand the flow behavior of fractured reservoirs. By evaluating the influence of censored fractures on estimates of fracture network parameters, we found that an increasing percentage of censored fractures obviously cause an increase in the difference between measured and true values. Here, the window sampling method provides results with the lowest uncertainty, except for

estimates of fracture intensity. To determine intensity, the circular estimator method appears the least sensitive method.

By analyzing the results from a window sampling applied to an outcrop at Craghouse Park (UK) we found that already 30% censored fractures cause a significant uncertainty. However, such small outcrops are often all we have to factor into subsurface fracture networks. Therefore, a cross-correlation of data from the analysis of boreholes and outcrops may significantly improve our understanding of the subsurface. Finally, if possible, more than one outcrop or borehole should be analyzed.

REFERENCES CITED

Barthélémy, J.-F., M. L. E. Guiton, J.-M. Daniel, 2009, Estimates of fracture density and uncertainties from well data: International Journal of Rock Mechanics and Mining Sciences, v. 46, p. 590-603. doi:10.1016/j.ijrmms.2008.08.003

Barton, N., E. F. de Quadros, 1997, Joint aperture and roughness in the prediction of flow and groutability of rock masses: International Journal of Rock Mechanics and Mining Sciences, v. 34. doi:10.1016/S1365-1609(97)00081-6

Becker, M. W., 2006, Potential for satellite remote sensing of ground water: Ground Water, v. 44, p. 306-318. doi:10.1111/j.1745-6584.2005.00123.x

Belayneh, M. W., S. K. Matthäi, M. J. Blunt, S. F. Rogers, 2009, Comparison of deterministic with stochastic fracture models in water-flooding numerical simulations: AAPG Bulletin, v. 93, p. 1633-1648. doi:10.1306/07220909031

Berkowitz, B., 2002, Characterizing flow and transport in fractured geological media: A review: Advances in Water Resources, v. 25, p. 861-884. doi:10.1016/S0309-1708(02)00042-8

Blum, P., R. Mackay, M. S. Riley, J. L. Knight, 2005, Performance assessment of a nuclear waste repository: Upscaling coupled hydro-mechanical properties for far-field transport analysis: Journal of Rock Mechanics and Mining Sciences, v. 42, p. 781-792. doi:10.1016/j.ijrmms.2005.03.015

Blum, P., Mackay, R., Riley, M. S., 2007, Coupled hydro-mechanical modelling of flow in fractured rock. In: Sharp, J. M. & Krasny, J. (Eds.), Groundwater in Fractured Rocks, IAH-Selected Paper Series, v. 9, p. 567-574.

Blum, P., R. Mackay, M. S. Riley, 2009, Stochastic simulations of regional scale advective transport in fractured rock masses using block upscaled hydro-mechanical rock property data: Journal of Hydrology, v. 369, p. 318–325. doi:10.1016/j.jhydrol.2009.02.009

Bonnet, E., O. Bour, N. E. Odling, P. Davy, I. Main, P. Cowie, B. Berkowitz, 2001, Scaling of fracture systems in geological media: Reviews of Geophysics, v. 39, p. 347-383. doi:10.1029/1999RG000074

Bons, P.D., J. Arnold, M.A. Elburg, J. Kalda, A. Soesoo, B.P. van Milligen, 2004, Melt extraction and accumulation from partially molten rocks: Lithos, v. 78, p. 25-42. doi:10.1016/j.lithos.2004.04.041

Bons, P.D., M.A. Elburg, E. Gomez-Rivas, 2012 A review of the formation of tectonic veins and their microstructures: Journal of Structural Geology, v. 43, p- 33-62. doi:10.1016/j.jsg.2012.07.005

Bour, O., P. Davy, C. Darcy, N. Odling, 2002, A statistical model for fracture network geometry, with validation on a multiscale mapping of joint network (Hornelen Basin, Norway): Journal of Geophysical Research, v. 107, p. ETG4-1-ETG4-12. doi:10.1029/2001JB000176

Castaing, C., A. Genter, B. Bourgine, J. P. Chilès, J. Wendling, P. Siegel, 2002, Taking into account the complexity of natural fracture systems in reservoir single-phase flow modelling: Journal of Hydrology, v. 266, p. 83-98. doi:10.1016/S0022-1694(02)00114-2

Cruden, D. M., 1977, Describing the size of discontinuities: International Journal of Rock Mechanics and Mining Sciences Geomechanical Abstracts, v. 14, p. 133-137.

Darcel, C., O. Bour, P.Davy, 2003, Stereological analysis of fractal fracture networks: Journal of Geophysical Research, v. 108, p. 1-14. doi:10.1029/2002JB00209

Davy, P., 1993, On the frequency-length distribution of the San Andreas fault system: Journal of Geophysical Research, v. 98, p. 12141-12151. doi:10.1029/93JB00372

Dershowitz, W.S., 1984, Rock Joint Systems: Ph.D. Dissertation, Massachusetts Institute of Technology, Cambridge, Massachusetts.

Dershowitz, W. S., H. H. Einstein, 1988, Characterizing rock joint geometry with joint system models: Rock Mechanics and Rock Engineering, v. 21, p. 21-51. doi: 10.1007/BF01019674

Einstein, H. H., G. B. Baecher, 1983, Probalistic and statistical methods in engineering geology: Rock Mechanics and Rock Engineering, v. 16, p. 39-72. doi:10.1007/BF01030217

Fouché, O., J. Diebolt, 2004, Describing the geometry of 3D fracture systems by correcting for linear sampling bias: Mathematical Geology, v. 36, p. 33-63. doi:10.1023/B:MATG.0000016229.37309.fd

Guerriero, V., S. Vitale, S. Ciarcia, S. Mazzoli, 2011, Improved statistical multi-scale analysis of fractured reservoir analogues: Tectonophysics, v. 504, p. 14-24. doi:10.1016/j.tecto.2011.01.003

Hatton, C. G., I. G. Main, P. G. Meredith, 1993, A comparison of seismic and structural measurements of fractal dimension during tensile subcritical crack growth: Journal of Structural Geology, v. 15, p. 1485-1495. doi:10.1016/0191-8141(93)90008-X

Hilgers, C., D. L. Kirschner, J.-P. Breton, J. L. Urai, 2006, Fracture sealing and fluid overpressures in limestones of the Jabal Akhdar dome, Oman mountains: Geofluids, v. 6, p 168-184. doi:10.1111/j.1468-8123.2006.00141.x

Holland, M., N. Saxena, J. L. Urai, 2009a, Evolution of fractures in a highly dynamic thermal hydraulic, and mechanical system - (II) Remote sensing fracture analysis, Jabal Shams, Oman Mountains: GeoArabia, v. 14, p. 163-194.

Holland, M., J. L. Urai, P. Muchez, E. J. M. Willemse, 2009b, Evolution of fractures in a highly dynamic, thermal, hydraulic, and mechanical system - (I) Field observations in Mesozoic Carbonates, Jabal Shams, Oman Mountains: GeoArabia, v. 14, p. 57-110.

Hudson, J. A., S. D. Priest, 1983, Discontinuity frequeny in rock masses: International Journal of Rock Mechanics and Mining Sciences and Geomechanical Abstracts, v. 20, p. 73-89. doi: 10.1016/0148-9062(83)90329-7

Jackson, C. P., A. R. Hoch, S. Todman, 2000, Self-consistency of heterogeneous continuum porous medium representation of fractured medium: Water Resources Research, v. 36, p. 189-202. doi:10.1029/1999WR900249

Jing, L. O. Stephansson, 2007, The basics of fracture system characterization - field mapping and stochastic simulations: Developments in Geotechnical Engineering, v. 85, p. 147-177. doi:10.1016/S0165-1250(07)85005-X

Koike, K., S. Nagano, M. Ohmi, 1995, Lineament analysis of satellite images using a segment tracing algorithm (STA): Computers and Geosciences, v. 21, p. 1091-1104. doi:10.1016/0098-3004(95)00042-7

Kulatilake, P. H. S. W., T. H. Wu, 1984, The density of discontinuity traces in sampling windows (technical note): International Journal of Rock Mechanics and Mining Sciences and Geomechanical Abstracts, v. 21, p. 345-347.

Lacazette, A., 1991, A new stereographic technique for the reduction of scanline survey data of geologic features: Computers and Geosciences, v. 17, p. 445-463. doi:10.1016/0098-3004(91)90051-E

LaPointe, P. R., J. A. Hudson, 1985, Characterization and interpretation of rock mass joint patterns: Special Paper Geological Society of America, v. 199, p. 37 pp.

LaPointe, P. R., 2002, Derivation of parent population statistics from trace length measurements of fractal populations: International Journal of Rock Mechanics and Mining Sciences, v. 39, p. 381-388. doi:10.1016/S1365-1609(02)00021-7

Laubach, S. E., 2003, Practical approaches to identifying sealed and open fractures: AAPG Bulletin, v. 87, no. 4, p. 561–579. doi:10.1306/11060201106

Laubach, S. E., M. E. Ward, 2006, Diagenesis in porosity evolution of opening-mode fractures, Middle Triassic to Lower Jurassic La Boca Formation, NE Mexico: Tectonophysics, v. 419, p. 75-97. doi:10.1016/j.tecto.2006.03.020

Laubach, S. E., J. E. Olson, M. R. Gross, 2009, Mechanical and fracture stratigraphy: AAPG Bulletin, v. 93, p. 1413-1426. doi:10.1306/07270909094

Lee, C.-H-, I. Farmer, 1993, Fluid flow in discontinuous rock: London, Chapman & Hall, 169 p.

LeGarzic, E., T. de L'Hamaide, M. Diraison, Y. Géraud, J. Sausse, M. de Urreiztieta, B. Hauville, J.-M. Champanhet, 2011, Scaling and geometric properties of extensional fracture systems in the proterozoic basement of Yemen. Tectonic interpretation and fluid flow implications: Journal of Structural Geology, v. 33, p. 519-536. doi:10.1016/j.jsg.2011.01.012

Llewellin, E. W., 2010, LBflow: An extensible lattice Boltzmann framework for the simulation of geophysical flows. Part I: theory and implementation: Computers & Geosciences, v. 36, p. 115-122. doi:10.1016/j.cageo.2009.08.004

Loague, K., R. E. Green, 1991, Statistical and graphical methods for evaluating solute transport models: Overview and application: Journal of Contaminant Hydrology, v. 7, p. 51-73. doi:10.1016/0169-7722(91)90038-3

Long, J. C. S., J. S. Remer, C. R. Wilson, P. A. Witherspoon, 1982, Porous media equivalents for networks of discontinuous fractures: Water Resources Research, v. 18, p. 645-658. doi:10.1029/WR018i003p00645

Lyman, G. J., 2003, Rock fracture mean trace length estimation and confidence interval calculation using maximum likelihood methods: International Journal of Rock Mechanics and Mining Sciences, v. 40, p. 825-832. doi:10.1016/S1365-1609(03)00043-1

Manda, A. K., S. B. Mabee, 2010, Comparison of three fracture sampling methods for layered rocks: International Journal of Rock Mechanics and Mining Sciences, v. 47, p. 218-226. doi:10.1016/j.ijrmms.2009.12.004

Manzocchi, T., J. J. Walsh, W. R. Bailey, 2009, Population scaling bias in map samples of power-law fault samples: Journal of Structural Geology, v. 31, p. 1612-1626. doi:10.1016/j.jsg.2009.06.004

Mauldon, M., 1998, Estimating mean fracture trace length and density from observations in convex windows: Rock Mechanics and Rock Engineering, v. 31, p. 201-216. doi:10.1007/s006030050021

Mauldon, M., W. M. Dunne, M. B. Rohrbaugh, Jr., 2001, Circular scanlines and circular windows: new tools for characterizing the geometry of fracture traces: Journal of Structural Geology, v. 23, p. 247-258. doi:10.1016/S0191-8141(00)00094-8

National Research Council, 1996, Rock Fractures and Fluid Flow: Contemporary Understanding and Applications: Washington, DC: The National Academies Press, 551p.

Narr, W., 1996, Estimating average fracture spacing in subsurface rock: AAPG Bulletin, v. 80, p. 1565-1586.

Neuman, S. P., 2005, Trends, prospects and challenges in quantifying flow and transport through fractured rocks: Hydrogeology Journal, v. 13, p. 124-147. doi:10.1007/s10040-004-0397-2

Neuman, S. P., 2008, Multiscale relationship between fracture length, aperture, density and permeability: Geophysical Research Letters, v. 35, p. 1-6. doi:10.1029/2008GL035622

Nirex, 1997a, The lithological and discontinuity characteristics of the Borrowdale Volcanic Group at the outcrop in the Craghouse Park and Latterbarrow areas: Nirex Report SA/97/029, Harwell.

Nirex, 1997b, Evaluation of heterogeneity and scaling of fractures in the Borrowdale Volcanic Group in the Sellafield area: Nirex Report SA/97/028, Harwell.

Odling, N. E., 1997, Scaling and connectivity of joint systems in sandstones from western Norway: Journal of Structural Geology, v. 19, p. 1257-1271. doi:10.1016/S0191-8141(97)00041-2

Odling, N. E., P. Gillespie, B. Bourgine, C. Castaing, J.-P. Chilés, N. P. Christensen, E. Fillion, A. Genter, C. Olsen, L. Thrane, R. Trice, E. Aarseth, J. J. Walsh, J. Watterson, 1999, Variations in fracture system geometry and their implications for fluid flow in fractured hydrocarbon reservoirs: Petroleum Geoscience, v. 5, p. 373-384. doi:10.1144/petgeo.5.4.373

Olson, J. E., S. E. Laubach, R. H. Lander, 2009, Natural fracture characterization in tight gas sandstones: Integration mechanics and diagenesis: AAPG Bulletin, v. 93, p. 1535-1549. doi:10.1306/08110909100

Olson, J. E., R. A. Schultz, 2011, Comment on " A note on the scaling relations for opening mode fractures in rock" by C.H. Schultz: Journal of Structural Geology, v. 33, p. 1523-1524. doi:10.1016/j.jsg.2011.07.004

Ortega, O. J., R. A. Marrett, 2000, Prediction of macrofracture properties using microfracture information, Mesaverde Group sandstones, San Juan basin, New Mexico: Journal of Structural Geology, v. 22, p. 571-588. doi:10.1016/S0191-8141(99)00186-8

Ortega, O. J., R. A. Marrett, S. E. Laubach, 2006, A scale-independent approach to fracture intensity and average spacing measurement: AAPG Bulletin, v. 90, p. 193-208. doi:10.1306/08250505059

Pahl, P. J., 1981, Estimating the mean length of discontinuity traces: International Journal of Rock Mechanics and Mining Sciences & Geomechanics Abstracts, v. 18, p. 221-228. doi:10.1016/0148-9062(81)90976-1

Pérez-Claros, J. A., P. Palmqvist, F. Olóriz, 2002, First and second orders of suture complexity in ammonites: A new methodological approach using fractal analysis: Mathematical Geology, v. 34, p. 323-343. doi:10.1023/A:1014847007351

Philip, Z. G., J. W. Jennings Jr., J. E. Olson, S. E. Laubach, J. Holder, 2005, Modelling coupled fracture-matrix fluid flow in geomechanically simulated fracture networks: Society of Petroleum Engineers. doi:10.2118/77340-MS

Pickering, G., J. M. Bull, D. J. Sanderson, 1995, Sampling power-law distributions: Tectonophysics, v. 248, p. 1-20. doi:10.1016/0040-1951(95)00030-Q

Priest, S. D., J. A. Hudson, 1981, Estimation of discontinuity spacing and trace length using scanline surveys: International Journal of Rock Mechanics and Mining Sciences & Geomechanics Abstracts, v. 18, p. 183-197. doi:10.1016/0148-9062(81)90973-6

Priest, S. D., 1993, Discontinuity analysis for rock engineering: London, Chapman & Hall, 473 p. doi:10.1016/0926-9851(93)90044-Y

Priest, S. D., 2004, Determination of discontinuity size distributions from scanline data: Rock Mechanics and Rock Engineering, v. 37, p. 347-368. doi:10.1007/s00603-004-0035-2

Renshaw, C. E., J. S. Dadakis, S. R. Brown, 2000, Measuring fracture apertures: A comparison of methods: Geophysical Research Letters, v. 27, p. 289-292. doi:10.1029/1999GL008384

Riley, M. S., 2005, Fracture trace length and number distributions from fracture mapping: Journal of Geophysical Research, v. 110. doi:10.1029/2004JB003164

Rohrbaugh, Jr., M. B., W. M. Dunne, M. Mauldon, 2002, Estimating fracture trace intensity, density and mean length using circular scanlines and windows: AAPG Bulletin, v. 86, p. 2089-2104. doi:10.1306/61EEDE0E-173E-11D7-8645000102C1865D

Roy, A., E. Perfect, W. M. Dunne, L. D. Mckay, 2007, Fractal characterization of fracture networks: an improved box-counting technique: Journal of Geophysical Research, v. 112, B12201. doi:10.1029/2006JB004582

Scholz, C. H., 2010, A note on the scaling relations for opening mode fractures in rock: Journal of Structural Geology, v. 32, p. 1485-1487. doi:10.1016/j.jsg.2010.09.007

Terzaghi, R. D., 1965, Sources of error in joint surveys: Géotechnique, v. 13, p. 287-304. doi:10.1680/geot.1965.15.3.287

Tóth, T. M., 2010, Determination of geometric parameters of fracture networks using 1D data: Journal of Structural Geology, v. 32, p. 1271-1278. doi:10.1016/j.jsg.2009.04.006

Tóth, T. M., I. Vass, 2011, Relationship between the geometric parameters of rock fractures, the size of percolation clusters and REV: Mathematical Geosciences, v. 43, p. 75-97. doi:10.1007/s11004-010-9315-4

Toublanc, A., S. Renaud, J. E. Sylte, C. K. Clausen, T. Eiben, G. Nadland, 2005, Ekofisk Field: fracture permeability evaluation and implementation in the flow model: Petroleum Geoscience, v. 11, p. 321-330. doi:10.1144/1354-079304-622

Weiss, M., 2008, Techniques for estimating fracture size: A comparison of methods: International Journal of Rock Mechanics and Mining Sciences, v. 45, p. 460-466. doi:10.1016/j.ijrmms.2007.07.010

Wu, H., D. D. Pollard, 1995, An experimental study of the relationship between joint spacing and layer thickness: Journal of Structural Geology, v. 17, p. 887-905. doi:10.1016/0191-8141(94)00099-L

Zeeb, C., D. Göckus, P. Bons, H. AlAjmi, R. Rausch, P. Blum, 2010, Fracture flow modelling based on satellite images of the Wajid sandstone, Saudi Arabia: Hydrogeology Journal, v. 18, p. 1699-1712. doi:10.1007/s10040-010-0609-x

Zhang, L., H. H. Einstein, 1998, Estimating the mean trace length of rock discontinuities: Rock Mechanics and Rock Engineering, 31 (4), 217-235. doi:10.1007/s006030050022

Zhang, L., H. H. Einstein, 2000, Estimating the intensity of rock discontinuities: International Journal of Rock Mechanics and Mining Sciences, v. 37, p. 819-837. doi:10.1016/S1365-1609(00)00022-8

6.3. Fracture Network Evaluation Program (FraNEP): A software for analyzing 2D trace-line maps of fracture networks

Conny Zeeb* (1,4), Enrique Gomez-Rivas (2), Paul D. Bons (2), Simon Virgo (3), Philipp Blum (1)

(1) *Karlsruhe Institute of Technology (KIT), Institute for Applied Geosciences (AGW), Kaiserstraße 12, 76131 Karlsruhe, Germany*

(2) *University of Tübingen, Department of Geosciences, Wilhelmstraße 56, 72074 Tübingen, Germany*

(3) *RWTH Aachen University, Structural Geology Tectonics Geomechanics, Lochnerstrasse 4-20, 52056 Aachen, Germany*

(4) Now at: Geotechnical Institute, TU Bergakademie Freiberg, Gustav-Zeuner-Str. 1, 09596 Freiberg, Germany

*Corresponding author. Tel.: +49-3731-39-2484, Fax: +49-3731-39-3638; E-mail: conny.zeeb@ifgt.tu-freiberg.de

Abstract

Fractures, such as joints, faults and veins, strongly influence the transport of fluids through rocks by either enhancing or inhibiting flow. Techniques used for the automatic detection of lineaments from satellite images and aerial photographs, LIDAR technologies and borehole televiewers significantly enhanced data acquisition. The analysis of such data is often performed manually or with different analysis software. Here we present a novel program for the analysis of 2D fracture networks called FraNEP (Fracture Network Evaluation Program). The program was developed using Visual Basic for Applications in Microsoft Excel™ and combines features from different existing software and characterization techniques. The main novelty of FraNEP is the possibility to analyse trace-line maps of fracture networks applying the (1) scanline sampling, (2) window sampling or (3) circular scanline and window method, without the need of switching programs. Additionally, binning problems are avoided by using cumulative distributions, rather than probability density functions. FraNEP is a time-efficient tool for the characterisation of fracture network parameters, such as density, intensity and mean length. Furthermore, fracture strikes can be visualized using rose diagrams and a fitting routine evaluates the distribution of fracture lengths. As an example of its application, we use FraNEP to analyse a case study of lineament data from a satellite image of the Oman Mountains.

Keywords: fracture network analysis; fracture sampling; sampling methods; fracture density;

1. Introduction

Mechanical discontinuities have a significant influence on the transport of fluids in the subsurface, for example in fractured oil and gas reservoirs or aquifers. Since the terminology for mechanical defects in rocks is diverse and often has genetic connotations, we will refer to the term "fractures" to include linear structures such as fractures, joints or veins. Fluid flow and transport through a fractured medium can be simulated by discrete fracture network (DFN) modelling (e.g. Blum et al., 2009). The DFN concept is commonly used to translate deterministic and/or statistical information on the geometry of fracture networks into equivalent fluid flow properties (i.e. permeability, hydraulic conductivity or hydraulic fracture aperture) along them. A detailed review of these concepts as well as the characterization of flow and transport behaviour in fractured media is provided, for example, by Neuman (2005).

In DFN models each fracture is individually represented with all its geometric parameters (i.e. fracture length and aperture). Typical geometric parameters used to describe fracture networks are fracture density, intensity, orientation, mean length or length distribution (Priest, 1993). The hydraulic properties influencing the fluid transport through a DFN include mechanical or hydraulic fracture aperture, displacement along fractures, mineral precipitates on fracture walls and mechanical properties of the host rock (Lee and Farmer, 1993). The most widely used methods to acquire these geometric parameters from outcrops or well cores are: (1) scanline sampling (e.g. Priest and Hudson, 1981), (2) window sampling (e.g. Pahl, 1981), and (3) circular scanline and window sampling (e.g. Mauldon et al., 2001). From now we will refer to the latter as the circular estimator method.

DFN models are typically treated in a stochastic framework (Berkowitz, 2002). Based on the aforementioned parameters, multiple realizations of fracture networks are often studied using Monte Carlo analysis (e.g. Blum et al., 2005; 2009). Several open access and commercial programs are available for the generation of artificial DFNs and subsequent analysis of their fluid flow behaviour using numerical simulations. The outcome of these simulations is normally a 2D or 3D permeability tensor, which can be used for the subsequent upscaling of the fracture network hydraulic properties in an equivalent porous media (EPM) (e.g. Bernard et al., 2002; Blum et al., 2005; Bodin et al., 2007; FracMan7, 2012). A typical way to acquire the

data required for the generation of artificial DFN involves time-consuming and tedious manual measurements from outcrops or well cores. Recent developments in the automatic detection of lineaments from aerial photographs and satellite images (e.g. Masoud and Koike, 2011), the LIDAR technology (e.g. Wilson et al., 2011) and televiewer imaging of boreholes (e.g. Spillmann et al., 2007) provide time-efficient methods to acquire large quantities of fracture data. However, the information obtained by these methods should be cross-checked by local manual measurements and/or ground truthing to distinguish between true and false discontinuities (e.g. goat tracks), which could be interpreted as a lineament on a satellite image or aerial photograph.

Some of the programs that are used to process the information acquired by LIDAR and borehole televiewer measurements also provide basic tools for the analysis of fracture lengths and strike (e.g. Masoud and Koike, 2011; FracMan7, 2012). Programs specifically designed for the analysis of fracture data are often better suited. The open-access codes LINDENS (Casas et al., 2000) and SAL (Ekneligoda and Henkel, 2010) use the coordinates of fracture endpoints, for example from GIS analysis (e.g. Holland et al., 2009a), as inputs. Both programs analyze fracture length and orientation using frequency histograms and rose diagrams. The first one provides information on fracture density, whereas the second one focuses on additional spatial properties such as fracture spacing and unidirectional frequency. Markovaara-Koivisto and Laine (2012) provide a MATLAB script for the analysis and visualization of scanline data. The software package FracSim3D (Xu and Dowd, 2010) is in fact a fracture network generator, but also incorporates scanline, window and planar methods to sample fracture network characteristics from the generated networks. FracSim3D also offers statistical tools including histogram analysis, probability plots, rose diagrams and hemispherical projections (Xu and Dowd, 2010). Since statistical analysis by histograms and probability plots strongly depend on the binning of the data (e.g. Bonnet et al., 2001), the cumulative distribution function (cdf) is used in FraNEP to analyze fracture lengths. Though numerous other programs are available for the evaluation of fracture data, a complete review of them is beyond the scope of the current work. Nevertheless, the given examples illustrate well that such programs are often developed for a specific study. Moreover, to our knowledge, no open-access software

provides a comprehensive and complete analysis, which includes all three typical sampling methods for the analysis of fracture networks.

The objective of the current study is therefore to provide such a program. FraNEP (Fracture Network Evaluation Program) was developed to quickly evaluate large amounts of fracture data, thus closing the gap between the automatic detection of lineaments and DFN modelling. For input the fractures have to be defined by their endpoint coordinates. Complementary information about the dimension of the study area and fracture sets support fracture network analysis. The statistical characteristics of a fracture network can be evaluated by applying the scanline sampling, the window sampling or the circular estimator method. The results of the analysis provide information on: (a) single fracture characteristics, such as fracture length and strike, (b) fracture network characteristics, like fracture density, intensity, mean length and length distribution, and (c) censoring bias. FraNEP was specifically developed in Visual Basic for Applications for Microsoft Excel™, which makes the program easy-to-use and enables a post-processing of the results without the need to export them to other software.

In the following sections we provide information and references for the theory behind sampling methods, correction techniques and data analysis in FraNEP. The data required for input, the definitions of the sampling process and the options that allow adopting the program to personal preferences are described in detail. Finally, a study area from the Oman Mountains is used to illustrate the application of FraNEP.

2. Background

2.1 Sampling methods

The following chapter briefly describes the three main sampling methods (scanline, window sampling and circular estimator) and the main biases typically related to the sampling process. A summary of governing equations used to calculate fracture density, intensity and mean length are presented in Table 1.

Table 1. Definitions and governing equations of fracture density (*p*), intensity (*I*) and mean length (l_m) for the scanline sampling, window sampling and circular estimator methods. The latter is based on Rohrbaugh et al. (2002).

Parameter		Definition	Scanline sampling	Window sampling	Circular estimator
Density (p)	Areal	Number of fractures per unit area [L^{-2}]	-	$p = \frac{N}{A}$	$p = \frac{m}{2\pi r^2}$
Intensity (I)	Linear [a]	Number of fractures per unit length [L^{-1}]	$I = \frac{N}{L}$	-	-
	Areal	Fracture length per unit area [L L^{-2}]	-	$I = \frac{\sum l}{A}$	$I = \frac{n}{4r}$
Mean length (l_m)		Mean fracture length [L]	$l_m = \frac{\sum l}{N}$	$l_m = \frac{\sum l}{N}$	$l_m = \frac{\pi r}{2}\frac{n}{m}$

L is an arbitrary unit of length, *N* is the total number of sampled fractures, *SL* is the scanline length, *A* is the sampling area, *r* is the radius of the circular scanline, *l* is the fracture length, *n* and *m* are the number of intersections with a circular scanline and the number of endpoints in a circular window enclosed by the circular scanline. [a] Also often referred to as fracture frequency.

The scanline sampling method evaluates the characteristics of the fracture network based on the collection of data using all fractures intersecting with a sampling line (e.g. Priest and Hudson, 1981). This method allows a quick analysis of fracture network characteristics on outcrops and is the most widely used method for subsurface analysis (e.g. borehole image-logs and cores). A scanline survey can be used to measure parameters of individual fractures (e.g. orientation, length and aperture) and to calculate 1-dimensional information of fracture networks, such as linear fracture intensity (Table 1). Scanline measurements can be affected by (a) orientation bias (e.g. Terzaghi, 1965; Lacazette 1991; Priest, 1993), (b) size bias (e.g. Priest, 1993; Bonnet et al., 2001; La Pointe, 2002; Manzocchi et al., 2009), (c) truncation bias (e.g. Bonnet et al., 2001; Pérez-Claros et al., 2002; Roy et al., 2007) and (d) censoring bias (e.g. Priest, 1993; Pickering et al., 1995; Priest, 2004; Riley, 2005). There are several techniques available to correct these biases (section 2.2).

The window sampling method evaluates the characteristics by considering all fractures present within a selected sampling area (e.g. Pahl, 1981). The method is typically used for the analysis of outcropping subsurface analogues (e.g. Belayneh et al., 2009). It can be applied either directly on the ground or to aerial photographs and satellite images (e.g. Becker, 2006; Zeeb et al., 2010). Similar to the scanline method, the window sampling method can be used to measure parameters of individual fractures. However, window sampling provides 2-dimensional information of fracture networks such as fracture density (Table 1). Measurements can be affected by (a) orientation bias, (b) truncation bias and (c) censoring bias.

The circular estimator method uses a combination of circular scanlines and windows. The method is a maximum likelihood estimator (Lyman, 2003) and therefore it is not subject to sampling biases (Mauldon et al., 2001). Instead of directly sampling individual fractures, network parameters are estimated using statistical models (e.g. Mauldon et al., 2001). The method provides estimates of fracture density, intensity and mean length by counting the number of intersections (*n*) between fractures and a circular scanline, as well as the number of fracture endpoints (*m*) located within the area defined by this scanline (Table 1). According to Rohrbaugh et al. (2002) a minimum of ten circular scanlines should be placed in a sampling area with a radius exceeding the fracture spacing/block size, but considerable smaller than the extension of the area. In addition, more than 30 endpoints should be sampled (Rohrbaugh et al., 2002).

2.2 Correction techniques

In this section the correction techniques for sampling biases are described. The orientation bias of scanline surveys is automatically corrected by applying the Terzaghi correction (Terzaghi, 1965; Priest, 1993):

$$S = S_A \times \cos\theta \quad (1)$$

where S is the true mean spacing of fractures in a set, S_A is the apparent mean spacing of fractures in a set and θ is the acute angle between the scanline and the normal to fractures of a set. Linear fracture intensity (Table 1) is equal to 1/*S*. Orientation bias can be minimized by placing a scanline parallel to the normal of a fracture set, such that θ is close to 0°. Additional scanlines should be used to acquire the fracture network data, if one scanline is not enough to capture all fracture sets (Priest, 1993).

Size bias is related to scanline sampling. The probability of a fracture intersecting with a scanline is proportional to the fracture length. Therefore, short fractures are underrepresented in the fracture length measurements acquired by scanline sampling, which causes an overestimation of fracture mean length and wrong estimates of fracture length distributions. Possible correction techniques for size bias are described by, for example, Bonnet et al. (2001), LaPointe (2002) and Zeeb et al. (in press).

Truncation bias is caused by the resolution limitations of an observation device (e.g. satellite image, human eye, hand lenses or microscope). Fractures with a size (length or width) below a certain value, which depends on the used observation device, are not detectable. Moreover, as fracture size approaches this detection limit, fewer fractures are recognized. In a log-log plot of fracture size versus cumulative number, this effect causes a flattening of the plotted data curve towards small fracture sizes. A possible correction technique is the application of the chord method (Pérez-Claros et al., 2002; Roy et al., 2007; Zeeb et al., in press).

Censoring bias is typically related to the presence of eroded or altered parts of the sampling area, the vegetation coverage or the presence of overlaying rock layers (e.g. Priest, 1993; Pickering et al., 1995). Censoring bias often causes an overestimation of fracture density (e.g. Kulatilake and Wu, 1984; Mauldon et al., 2001). Only fractures with their centre inside a sampling area should be included when calculating fracture density. In order to know the relative lengths of censored fractures and to correct for censoring bias, the exact fracture length distribution needs to be known (e.g. Priest, 2004; Riley, 2005). Since the underlying distribution of fracture lengths is generally unknown, it is difficult to ascertain whether a fracture center is inside the sampling area or not (Mauldon, 1998). This author uses the principle of associated endpoints to calculate an unbiased fracture density, which is also implemented in the circular estimator method (Mauldon et al., 2001). For window sampling an optional correction technique ("*Fracture density*") is available to reduce the overestimation of fracture density. The technique is based on the assumption that 50% of the censored fractures have more than half of their length, and thus also their centre, outside the selected sampling area. Applying this simple rule significantly reduces the typical overestimate and provides results closer to the true fracture density (Zeeb et al., in press). Note that this technique does not correct censoring bias per se, but instead reduces the trend in overestimating fracture density with increasing censoring bias.

An additional bias induced by the application of the window sampling method (section 3.2) is the artificial censoring bias. Fractures intersecting the boundaries of a sampling area become artificially censored. This can result in extremely short fracture lengths (Fig. 1a), which strongly influence the resulting length distribution. Although the impact on the best-fit distribution is relatively small or even negligible for lognormal or exponential distributions, it has a significant influence if the distribution

is power-law (Eq. 2). An optional correction technique ("*Lower uncensored cut-off length*") can be applied to neglect all fractures with lengths below the shortest uncensored fracture. The fracture lengths measured by the application of the window sampling to the field example are used to illustrate the effect of the correction technique on a truncated power-law fit. The fitting accuracy increases significantly, when all lengths below the lower uncensored cut-off length are neglected for the evaluation of the length distribution (Fig. 1b).

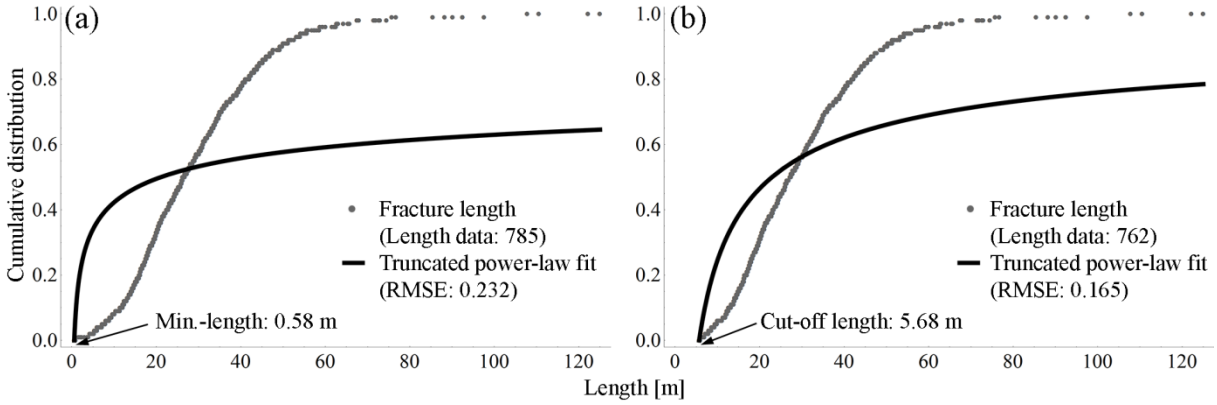

Fig. 1. Example for the correction of artificial censoring bias applying the "Lower uncensored cut-off length" option. Plotted is the cumulative distribution of the fracture lengths measured by application of the window sampling method to the field example (see below, section 4) and the fitted cumulative distribution function of a truncated power-law (Eq. 2). (a) shows the fit for all fracture lengths and (b) the fit excluding the fracture lengths below the lower uncensored cut-off length of 5.68 m.

2.3 Analysis of fracture lengths

The length distribution of fractures is analysed using their cumulative distribution. Three equations are currently provided to describe the fracture length distribution: (1) truncated power-law (Eq. 2), (2) lognormal (Eq. 3) and (3) exponential (Eq. 4). Although other distributions can also be found, these are the most commonly observed (e.g. Odling et al., 1999; Bonnet et al., 2001). Power-law relationships are often used to describe the distribution of fracture parameters such as length and aperture (e.g. Bonnet et al., 2001). The cumulative distribution function of a truncated power-law is given by Blum et al. (2005) and Riley (2005):

$$f(l) = 1 - \left(\frac{l}{l_0}\right)^{-E} \qquad (2)$$

where l is the fracture length, l_0 is the shortest observed fracture length and E is the power-law exponent. The lognormal distribution is also commonly used to describe fracture lengths (Priest and Hudson, 1981). Resolution effects (i.e. truncation bias) or the presence of a characteristic scale, for example associated to lithological layering, imposed on power-law distributed length data can give rise to lognormal distributions (Odling et al., 1999; Bonnet et al., 2001). The cumulative distribution function of a lognormal distribution is given by Priest and Hudson (1981):

$$f(l) = 0.5 + 0.5Erf\left(\frac{Ln(l) - \mu}{\sqrt{2\sigma^2}}\right) \quad (3)$$

where μ and σ are the mean and the standard deviation of the natural logarithm of l. Fracture lengths are best described by an exponential distribution when fractures are formed as a result of fracture growth under a uniform stress state (Dershowitz and Einstein, 1988) or are developed at early stages of deformation (Bonnet et al., 2001). The cumulative distribution function of an exponential distribution function is provided by Cruden (1977):

$$f(l) = 1 - e^{-\lambda l} \quad (4)$$

where λ is the rate parameter. The user can apply one of above distributions to the fracture length data or allow FraNEP to determine the best-fitting length distribution automatically.

The accuracy of the best fit is indicated by (1) the root mean squared error (RMSE) (Eq. 5), (2) the sum of squared errors (SSE) (Eq. 6) and (3) the maximum squared error (MSE) (Eq. 7) (Loague and Green, 1991). The RMSE is given by:

$$RMSE = \sqrt{\sum_{i=1}^{N}(P_i - O_i)^2 \Big/ N} \quad (5)$$

where n is the total number of measurements, P is the predicted/calculated value and O is the observed/measured value. The RMSE is commonly used to compare the best fits of different data. The SSE is a simplification of the RMSE and is given by:

$$SSE = \sum_{i=1}^{N}(P_i - O_i)^2 \quad (6)$$

For the automatic evaluation of the best fit the SSE is used, which is valid since the three distribution functions (Eqs. 2-4) are fitted to the same data. The MSE is given by:

$$MSE = (P_i - O_i)^2|_{i=1}^{N} \quad (7)$$

3. Program description

The methodology used to evaluate the characteristics of a fracture network based on trace-line maps is divided in three main steps: (I) data input, (II) sampling and (III) options for the analysis (Fig. 2).

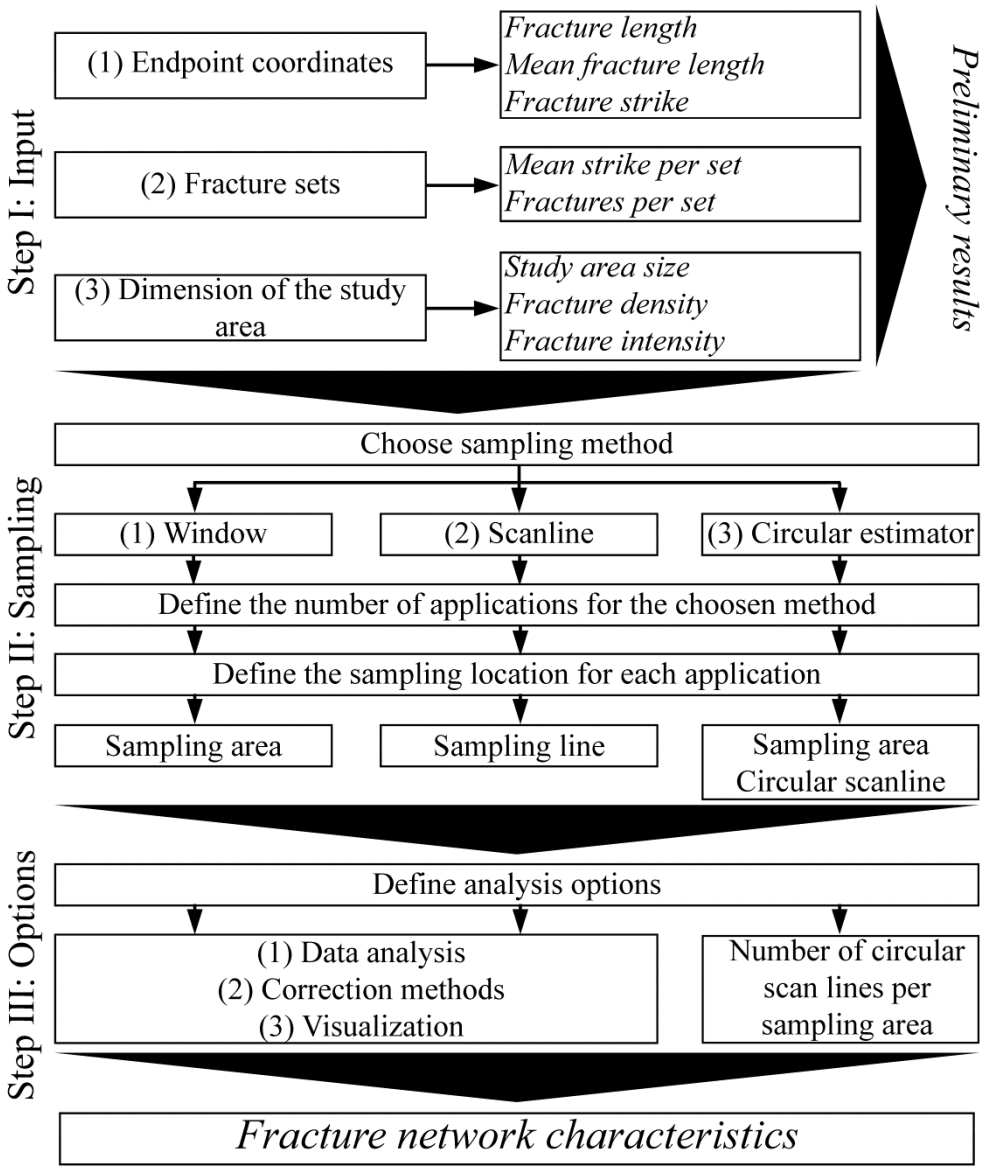

Fig. 2. Schematic methodology to evaluate the fracture-network characteristics using trace-line maps (Italics indicate results).

3.1. Step I: Input

The following information is required as program inputs: (1) endpoint coordinates of each fracture, (2) number of fracture sets as well as their strike spread (minimum and maximum value) and (3) dimension of the study area (Fig. 2; Fig. 3; Table 2). Endpoint coordinates are imported as points with coordinates (X1, Y1) and (X2, Y2). The length and strike of each fracture are automatically calculated using these two points. Summing up all lengths and dividing this total fracture length by the total number of fractures provides a first estimate of mean fracture length (Fig. 2; Table 2). Once the different fracture sets are defined, we automatically get the mean strike and the number of fractures for each set (Fig. 2; Table 2). If the definition of fracture sets is unclear, the input data can also be treated as one single set with strikes that range from 0° to 180°. The position and size of the study area is defined by the coordinates of its lower-left corner and the extension in the X- and Y-directions. Area size, fracture density and fracture intensity are calculated once the study area is defined (Fig. 2; Table 2). A definition of the study area is not necessarily required and can be skipped, if the size of the study area is unknown, or if data are missing from parts of the area, for example due to erosion, vegetation cover or surface alteration. The preliminary results calculated for fracture mean length, density and intensity should be always treated carefully.

FraNEP includes the possibility of generating and displaying a trace-line map from the imported fractures. To distinguish between different sets of fractures their strikes can be analyzed using a rose diagram plot, which is generated together with the aforementioned trace-line map. The rose diagram can be drawn with or without fracture-length weighting.

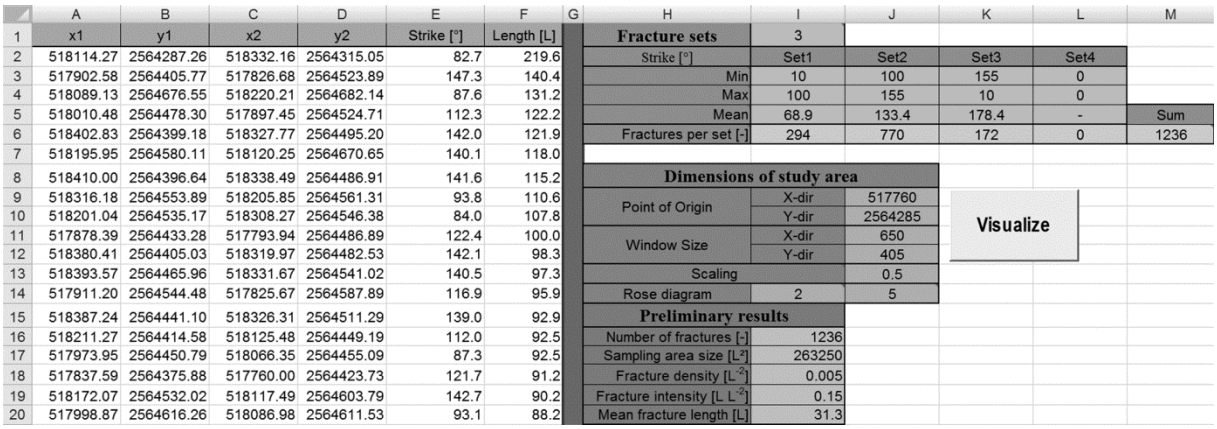

	A	B	C	D	E	F
1	x1	y1	x2	y2	Strike [°]	Length [L]
2	518114.27	2564287.26	518332.16	2564315.05	82.7	219.6
3	517902.58	2564405.77	517826.68	2564523.89	147.3	140.4
4	518089.13	2564676.55	518220.21	2564682.14	87.6	131.2
5	518010.48	2564478.30	517897.45	2564524.71	112.3	122.2
6	518402.83	2564399.18	518327.77	2564495.20	142.0	121.9
7	518195.95	2564580.11	518120.25	2564670.65	140.1	118.0
8	518410.00	2564396.64	518338.49	2564486.91	141.6	115.2
9	518316.18	2564553.89	518205.85	2564561.31	93.8	110.6
10	518201.04	2564535.17	518308.27	2564546.38	84.0	107.8
11	517878.39	2564433.28	517793.94	2564486.89	122.4	100.0
12	518380.41	2564405.03	518319.97	2564482.53	142.1	98.3
13	518393.57	2564465.96	518331.67	2564541.02	140.5	97.3
14	517911.20	2564544.48	517825.67	2564587.89	116.9	95.9
15	518387.24	2564441.10	518326.31	2564511.29	139.0	92.9
16	518211.27	2564414.58	518125.48	2564449.19	112.0	92.5
17	517973.95	2564450.79	518066.35	2564455.09	87.3	92.5
18	517837.59	2564375.88	517760.00	2564423.73	121.7	91.2
19	518172.07	2564532.02	518117.49	2564603.79	142.7	90.2
20	517998.87	2564616.26	518086.98	2564611.53	93.1	88.2

Fracture sets	3			
Strike [°]	Set1	Set2	Set3	Set4
Min	10	100	155	0
Max	100	155	10	0
Mean	68.9	133.4	178.4	-
Fractures per set [-]	294	770	172	0

Dimensions of study area		
Point of Origin	X-dir	517760
	Y-dir	2564285
Window Size	X-dir	650
	Y-dir	405
Scaling		0.5
Rose diagram	2	5

Preliminary results	
Number of fractures [-]	1236
Sampling area size [L²]	263250
Fracture density [L^{-2}]	0.005
Fracture intensity [L L^{-2}]	0.15
Mean fracture length [L]	31.3

Sum
1236

Fig. 3. Illustration of the "Input" worksheet. Columns "A" - "B" contain the endpoint coordinates of each fracture and columns "E" and "F" its automatically calculated strike and length. The highlighted section "Fracture sets" and "Dimension of study area" are reserved for the definition of different fracture sets and the studied area, respectively. The section "Preliminary results" provides first estimates for fracture density, intensity and mean length. The "Visualize"-button can be used to generate a trace-line map and a rose diagram plot.

Table 2. Input data and governing equations for the calculation of individual fracture and the preliminary fracture network characteristics (Fig. 2; Fig. 3).

Input	Parameter	Equation
Endpoint coordinates		
($X1_i$, $Y1_i$) ($X2_i$, $Y2_i$)	Length, l_i [L]	$l_i = \sqrt{(X2_i - X1_i)^2 + (Y2_i - Y1_i)^2}$
	Mean length, l_m [L]	$l_m = \frac{1}{N}\sum_{i=1}^{N} l_i$
	Strike, O_i [°]	$O_i = \tan^{-1}\left(\frac{X1_i - X2_i}{Y1_i - Y2_i}\right)$ $\quad 0° \leq O_i \leq 180°$
Fracture sets		
Set j $\quad O_{min}^j \leq O_i < O_{max}^j$	Mean strike, O_m^j [°]	$O_m^j = \frac{1}{N}\sum_{i=1}^{N} O_i$
	Fractures per set, N_j [-]	$N_j = \sum_{i=1}^{N} o_i$
Dimension of the study area		
Point of origin (X, Y) Extension (X-dir, Y-dir)	Study area size, A [L^2]	$A = X_{dir} \times Y_{dir}$
	Fracture density, p [L^{-2}]	$p = \frac{N}{A}$
	Fracture intensity, I [L L^{-2}]	$I = \frac{\sum_{i=1}^{N} l_i}{A}$

i denotes individual fractures, *j* denotes different fracture sets and L is an arbitrary unit of length.

3.2. Step II: Sampling

Three sampling methods can be applied to evaluate the characteristics of a fracture network: (1) scanline sampling, (2) window sampling and (3) circular estimator. A scanline is defined by the coordinates of its start- and endpoints (Fig. 4). The sampling areas for the application of the window sampling and circular estimator methods are selected by defining a point of origin (lower left corner) and the extension of the area in X- and Y-directions (Fig. 4). Fractures intersecting a boundary of the selected sampling area are considered censored and the intersection point is used to calculate the length of the censored fracture. The circular scanlines used by the circular estimator method are defined by their centres and radii (Fig. 4). Centres for circular scanlines are defined by their X- and Y-coordinates and can be placed either manually or randomly. The distance between the boundaries of a sampling area and the centres is equal to the radius plus a small constant value of 0.1 to avoid interaction between scanlines and boundaries. Sampling areas and/or scanlines can be placed anywhere within the study area. Although we apply each sampling method to the example study area only once, it is also possible to simultaneously apply up to 200 sampling areas/lines. The fracture network characteristics evaluated by the application of the window and scanline sampling methods are summarized in an extra worksheet for each analysis. Furthermore, the lengths, strikes and endpoints of the sampled fractures are provided in this worksheet. Since the circular estimator provides no information on fracture lengths and strike, the fracture network characteristics of all analyses are summarized in one worksheet.

	A	B	C	D	E	F	G	H	I	J	K	L	M	N	O	P
1		**Window sampling**					**Scanline sampling**						**Circular estimator**			
2	**Analysis**	Point of origin		Window size		Area [L²]	Start		End		Length [L]	Scanline strike [°]	Centre		Radius	Area [L²]
3		X	Y	X-dir	Y-dir		X	Y	X	Y			X	Y		
4	1	517835	2564355	500	300	150000.0	517835	2564355	518335	2564655	583.1	59.0			35	3848.5
5	2					0.0					0.0	180.0				0.0
6	3					0.0					0.0	180.0				0.0
7	4					0.0					0.0	180.0				0.0

Fig. 4. Illustration of the "Sampling" worksheet. Columns "B" - "E" are used to define the sampling areas required for the window sampling and circular estimator methods. "G" - "J" allow the definition of endpoint coordinates required for the scanline sampling method. "M" - "O" are reserved for the centre and radius of circular scanlines used by the circular estimator method.

3.3. Step III: Options

Three categories of options are available for the characterization of a fracture network. These options can be used to select (1) the correction methods, (2) the analysis performed with the acquired data and (3) the visualization of results (Fig. 5, Table 3).

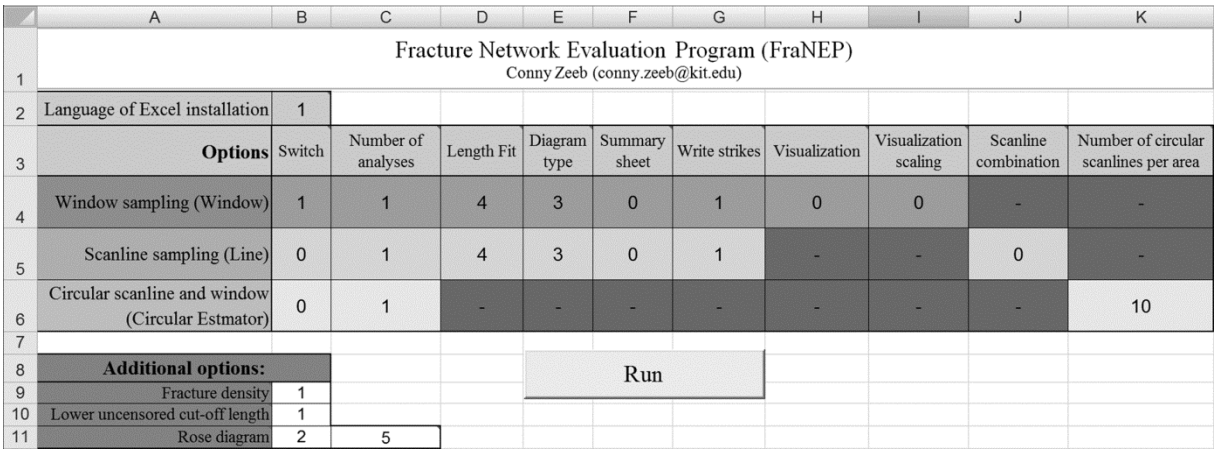

	A	B	C	D	E	F	G	H	I	J	K
1	Fracture Network Evaluation Program (FraNEP) Conny Zeeb (conny.zeeb@kit.edu)										
2	Language of Excel installation	1									
3	**Options**	Switch	Number of analyses	Length Fit	Diagram type	Summary sheet	Write strikes	Visualization	Visualization scaling	Scanline combination	Number of circular scanlines per area
4	Window sampling (Window)	1	1	4	3	0	1	0	0	-	-
5	Scanline sampling (Line)	0	1	4	3	0	1	-	-	0	-
6	Circular scanline and window (Circular Estmator)	0	1	-	-	-	-	-	-	-	10
7											
8	**Additional options:**				Run						
9	Fracture density	1									
10	Lower uncensored cut-off length	1									
11	Rose diagram	2	5								

Fig. 5. Illustration of the "Options"-worksheet. Dark gray cells marked by "□" indicate options that are not applicable for this sampling method.

Table 3. Options for (1) correction methods, (2) data analysis and (3) visualization of results. The symbols "+" and "–" indicate whether an option is applicable to the chosen sampling method or not.

Category	Option	Description	Window	Scanline	Circular estimator
(1) Correction methods	Fracture density	Reduces the overestimation of fracture density.	+	–	–
	Lower uncensored cut-off length	Corrects artificial censoring bias.	+	+	–
(2) Data analysis	Length fit	Defines the fitting for fracture lengths.	+	+	–
	Circular scanlines	Defines the total number of circular scanlines placed in each sampling area.	–	–	+
(3) Visualization	Diagram type	Creates a plot of sampled fracture lengths.	+	+	–
	Scanline combination	Combines the results from two and/or all scanlines.	–	+	–
	Write strikes	Write strikes in the output-sheets.	+	+	–
	Rose diagram	Plots the fracture strikes in a rose diagram.	+	+	–
	Visualization	Creates a trace-line map of the sampled fractures.	+	–	–

3.3.1. Correction methods

The option “*Fracture density*” accounts for fractures, which are only partly visible and therefore censored. The option applies a simple routine to reduce the overestimation of fracture density using window sampling by neglecting half of the censored fractures during the calculation.

The option “*Lower uncensored cut-off*” *length* corrects artificial censoring bias. All fractures with lengths below the shortest uncensored fracture are neglected to reduce the impact of artificially censored fractures on the evaluation of the length distribution.

3.3.2. Data analysis

The option “*Length fit*” must be chosen, if the user wants to evaluate the length distribution of a fracture network. The user can either manually apply one of the three provided distributions (truncated power-law, lognormal or exponential) to the fracture length data or allow FraNEP to evaluate the best fitting length distribution automatically.

The option “*Circular scanlines*” defines the number of circular scanlines applied to a sampling area. Rohrbaugh et al. (2002) suggested that a minimum of ten scanlines should be used to characterize a fracture network with the circular estimator method.

3.3.3. Visualization

The option “*Diagram type*” allows the visualization of the sampled fracture lengths as (a) a plot of the cumulative distribution and/or (b) a log-log plot of the cumulative number. Note that for the evaluation of the length distribution, the cumulative distribution is used.

The option “*Scanline combination*” joins the results from two consecutive and/or all applied scanlines.

The option “*Write strikes*” allows the reduction of computational times. This option can be used to skip the evaluation of fracture strikes, thus reducing the calculation time required for the analysis of large data sets.

The option “*Rose diagram*” creates a plot of fracture strikes in the form of a rose diagram with an adaptable bin size. A new worksheet is added for the data preparation and the visualization of the rose diagram. The plot shows the cumulative number or the sum of fracture lengths per bin.

The “*Visualization option*” creates a trace-line map of the fractures in the area analyzed by the window sampling method. The map is created in a new worksheet and a scaling coefficient is used to change the size of the map.

4. Example of application: Fracture networks in Jabal Akhdar (Oman)

A field case example from the Oman Mountains, which was already studied by Holland et al. (2009a), is used to illustrate the methodology of FraNEP. The study area is located at the southern flank of the Jabal Akhdar dome, the most prominent structure of the Oman Mountains (Fig. 6) (Glennie et al., 1973; Breton et al., 2004). The exposed rocks are mainly Mesozoic limestones with interbedded shales and marly layers, which were deposited on the southern Neothetyan continental margin from late Jurassic to upper Cretaceous times (Glennie et al., 1973; Breton et al., 2004). Closure of the Neotethyan Ocean during the early Cretaceous led to SSW directed obduction of the Semail Ophiolite and the volcano-sedimentary Hawasina nappes over the autochthonous carbonates (Glennie et al., 1973; Breton et al., 2004). Uplift and exhumation of the autochthonous carbonates and the formation of the Jabal Akhdar tectonic window is related to the development of the Makran subduction zone during the Tertiary and still ongoing (Breton et al., 2004). The complex geological history of the rocks is reflected by numerous sets of discontinuities, including faults of different sizes, fractures, veins, stylolites, bedding parallel slip surfaces and joints (e.g. Hilgers et al., 2006; Holland et al., 2009a; 2009b).

The available input data consists of a polyline shape file, which contains approximately 157 000 lineaments identified by manual interpretation of a Quickbird satellite image with a panchromatic resolution of 0.7 m (Holland et al., 2009b). The study area investigated here is a small part of this shape file and contains a total of 1236 lineaments. These lineaments correspond to veins, fractures and joints measured from an outcrop surface. Extensive ground truthing revealed that the vast

majority of the interpreted lineaments belong to a recent generation of joints. These joints were widened by erosion and filled with bright alluvium creating a good optical contrast to the dark grey carbonate rocks. Here we use the general term fractures, when referring to these lineament data, even if most of them are in fact joints.

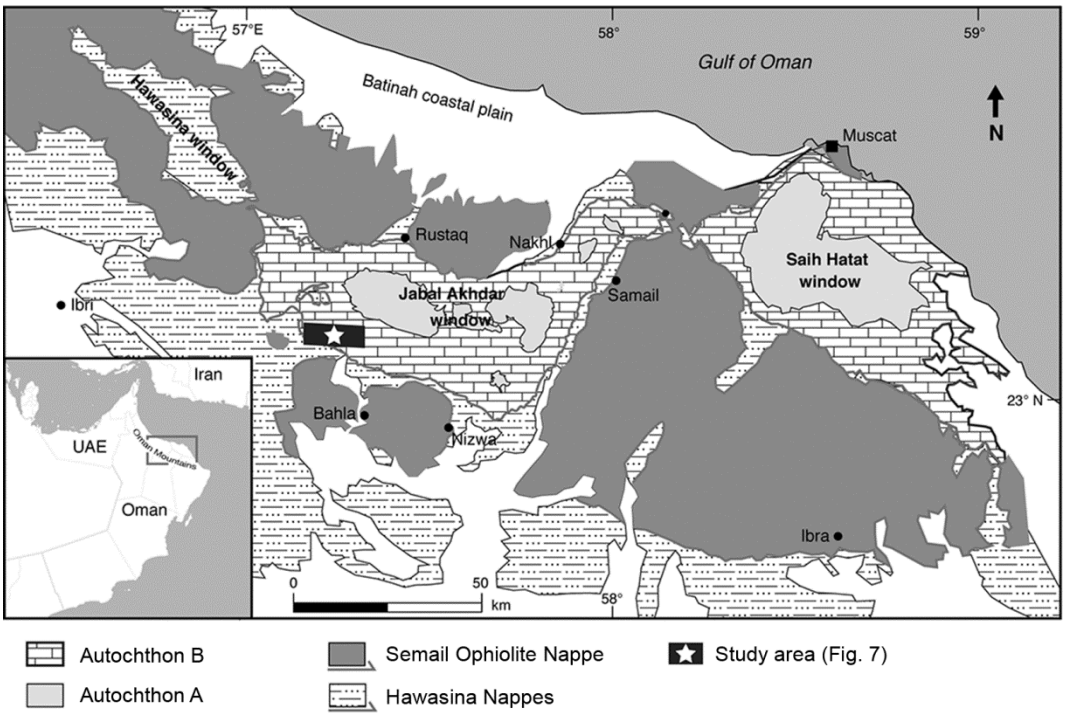

Fig. 6. Overview of the geology in the Oman Mountains and location of the study area in Fig. 7 (modified from Breton et al., 2004).

4.1. Input data and sampling

The endpoints of the fractures from the field example (Fig. 7) are given as UTM coordinates, which are imported to FraNEP. From the input the lengths and strikes of individual fractures are calculated, as well as a first estimate of mean fracture length (Table 4). Using the length-weighted rose diagram of the fracture strikes (Fig. 8), three main fracture sets can be identified. The spread of strikes as well as the mean strike and number of fractures per set are summarized in Table 4. The size of the study area and preliminary estimates of fracture density and intensity are also presented.

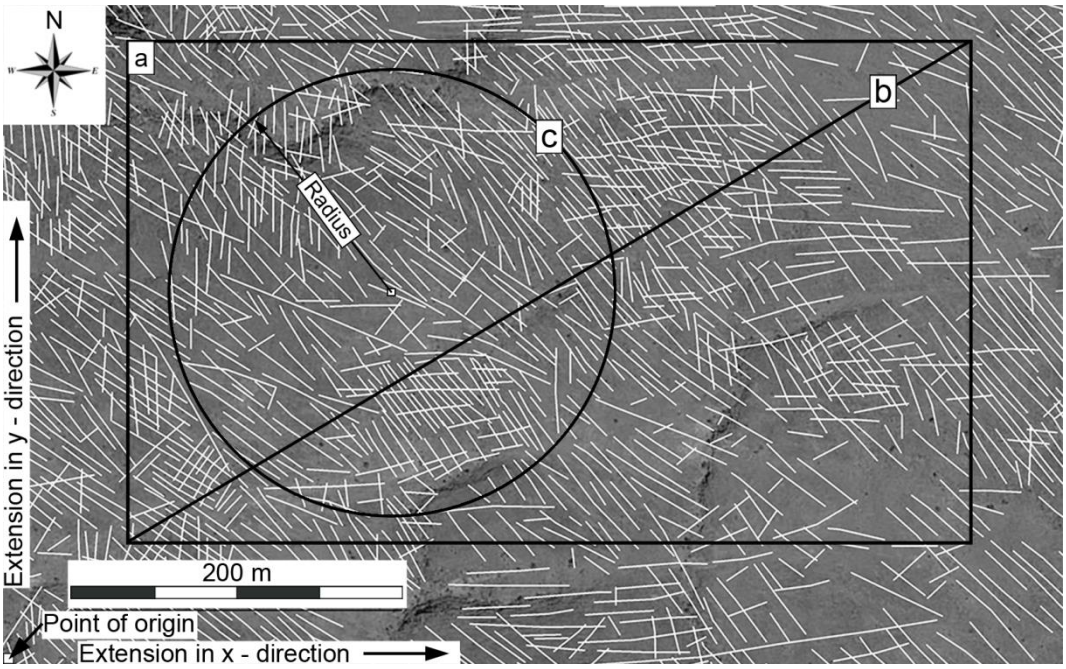

Fig. 7. Satellite image (modified from Google, GeoEye) and size of the study area at the southern flank of the Jabal Akhdar dome in the Oman Mountains (Holland et al., 2009b). Lineaments identified by manual interpretation are represented by white lines. (a) Sampling area analysed using the window sampling and circular estimator method, (b) sampling line analysed using the scanline sampling method and (c) example of a circular scanline. The UTM coordinates of the lower left corner are 40N 517744 2564259.

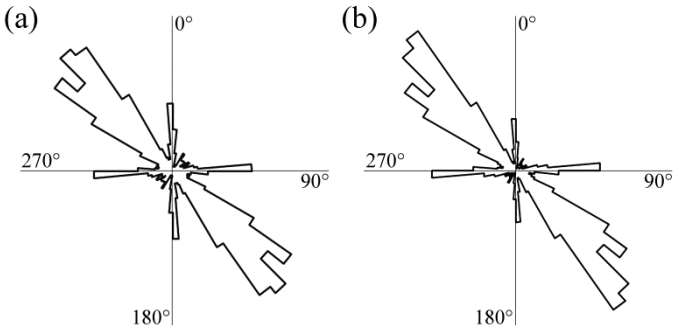

Fig. 8. Rose diagram (bin size of 5°) of the fracture strikes in Fig. 7, with (a) the cumulative-number plot and (b) the length-weighted plot.

Table 4. Input and preliminary results for the fracture network at Jabal Akhdar (Oman), with one fracture (i = 1) as an example for the calculation of fracture length and strike (Fig. 7).

Input		Parameter		Preliminary result
Endpoint coordinates [a]				
$X1_1$: 517830	$Y1_1$: 2564405	Length, l_i		66.7 m
$X2_1$: 517777	$Y2_1$: 2564445	Mean length, l_m		31.3 m
		Strike, O_i		127.2°
Fracture sets				
Set 1 $010° \le O_i < 100°$		Mean strike, O^j_m	Set 1	68.9°
			Set 2	133.4°
Set 2 $100° \le O_i < 155°$			Set 3	178.4°
		Fractures per set, N_j	Set 1	294
Set 3 $155° \le O_i < 010°$			Set 2	770
			Set 3	172
Dimension of the study area				
Point of origin (X, Y) [a]	517760 2564285	Study area size, A		2.63×10^5 m^2
Extension (X-dir, Y-dir)	650 m 405 m	Fracture density, p		0.005 m^{-2}
		Fracture intensity, I		0.15 m m^{-2}

[a] UTM coordinates.

4.2. Fracture network characteristics

In Fig. 7. the locations for the application of the window sampling (a), the scanline sampling (b), and the circular estimator (c) methods are shown. The definitions for the sampling areas and the scanline are summarized in Table 5 and a summary of the calculated fracture network characteristics in Table 6.

Table 5. Definition of the sampling areas/line locations for the application of the three sampling methods (Fig. 7).

Sampling method	Sampling location			
Window	Point of origin (X, Y) [a]		517835	2564355
	Extension (X-dir, Y-dir)		500 m	300 m
Scanline	Start point (X, Y) [a]		517835	2564355
	End point (X, Y) [a]		518335	2564655
Circular estimator	Sampling area	Point of origin (X, Y) [a]	517835	2564355
		Extension (X-dir, Y-dir)	500 m	300 m
	Coordinates centre (X, Y)			random
	Radius			140 m

[a] UTM coordinates.

Table 6. Fracture network characteristics of the Oman field example evaluated by the three sampling methods (Fig. 7). Fitted parameter 1 corresponds to E, μ or λ, and fitted parameter 2 to σ^2 (Eqs. 2-4).

Parameter		Window	Scanline	Circular
Sampled area [m²] or length of the scanline [m]		1.5×10^5	583	1.5×10^5
Number of fractures [-]		785	74	–
Fracture density [m^{-2}]		0.005	–	0.004
Fracture intensity [m m^{-2}] or fracture frequency (scanline) [m^{-1}]		0.15	0.13	0.17
Mean fracture length [m]		29.4	41.8	44.5
Number of censored fractures [-]		144	0	–
Number of fractures shorter than lower uncensored cut-off length [-]		23	0	–
Best fitted length distribution		lognormal	lognormal	–
Accuracy of the best fit	RMSE	0.014	0.053	–
	SSE	0.152	0.208	–
	MSE	0.001	0.011	–
Fitted parameter 1 (E, μ, λ)		μ = 3.287	μ = 3.706	–
Fitted parameter 2 (σ^2)		σ^2 = 0.545	σ^2 = 0.384	–

"–" Method provides no information.

Fig. 9 shows the cumulative distribution of the fracture lengths sampled by the scanline and window methods. The fitted cumulative distribution functions and the fitting accuracy for a truncated power-law (Eq. 2), a lognormal (Eq. 3) and an exponential (Eq. 4) function are also presented. For both sampling methods the best fit to the measured fracture lengths was found to follow a lognormal distribution. The strikes of the sampled fractures are presented as cumulative number and length-weighted rose diagrams in Fig. 10.

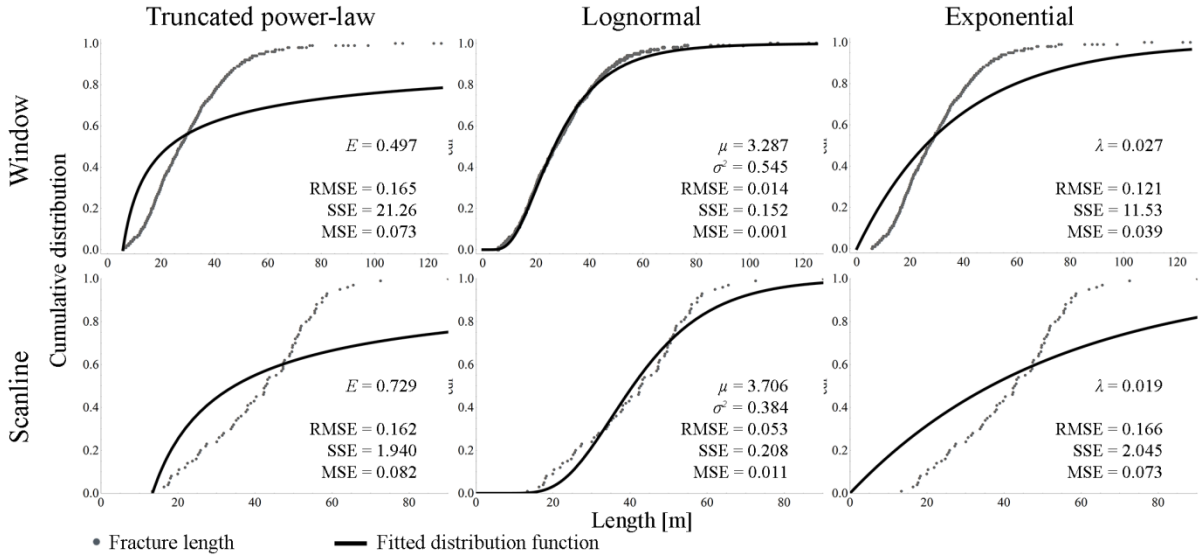

Fig. 9. Example illustrating the fit of a truncated power-law, lognormal and exponential function. Shown is the cumulative distribution of fracture lengths sampled by the scanline and window sampling methods. E, μ, σ2 and λ are the fitted parameters of the corresponding distribution functions (Eqs. 2-4). The accuracy of the fits is provided as RMSE, SSE and MSE.

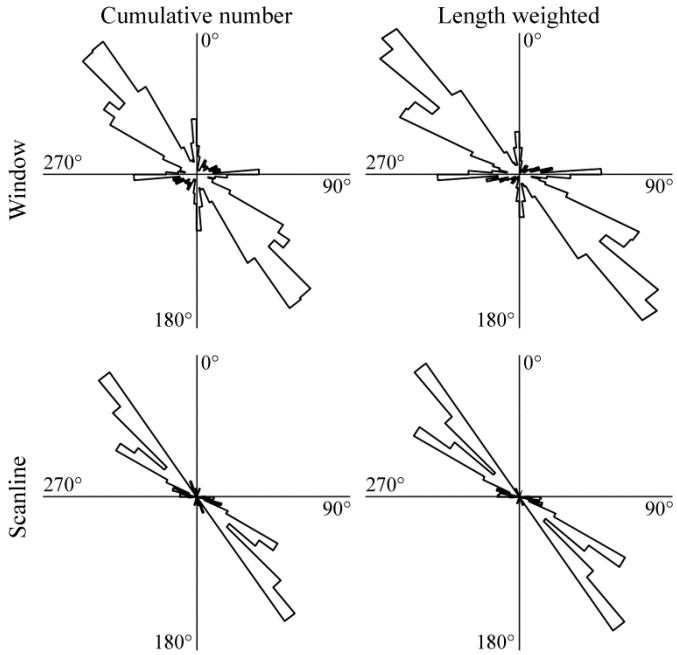

Fig. 10. Rose diagrams with a bin size of 5° showing the fracture strikes sampled by the scanline and window sampling methods.

4.3. Discussion of the results

The fracture network characteristics obtained with the three sampling methods are dissimilar, especially the estimate of the mean fracture length (Table 6). One possible explanation lies in the sampling methods themselves. For example, the probability of a fracture to intersect with a scanline is proportional to its length, with an increasing probability for longer fractures. The underrepresentation of short fractures explains the differences between the window and scanline sampling methods in fracture intensity and mean length (e.g. Priest, 1993). Following the guideline of Rohrbaugh et al. (2002) for the application of the circular estimator method, we found that the radius of the circular scanlines should be at least 45 m for the current study. For this radius, values of fracture density are similar to those obtained from window sampling. In contrast, values for fracture intensity and mean length differed significantly from those obtained by window and scanline sampling. For example, estimates of mean fracture length were >> 100 m. Applying additional circular scanlines (up to 100) to the sampling area did not help to improve the results. Increasing the radii of the circular scanlines provided more reliable results. Therefore, we applied the circular estimator method with a radius of 140 m (Table 6). This approach provided values for fracture density, intensity and mean length closer to those of the other two sampling methods (Table 6). Although it would be highly interesting to compare the capability of the three sampling methods in more detail, this is beyond the scope of this study. A more detailed comparison of sampling methods is provided, for example, by Rohrbaugh et al. (2002), Weiss (2008) and Belayneh et al. (2009).

5. Conclusions

The presented software FraNEP automatically analyzes the statistical properties of 2D fracture networks based on trace-line maps. For the input, each fracture has to be defined by the coordinates of its endpoints. Techniques such as automatic lineament detection from satellite images or aerial photographs can provide such fracture data. For the evaluation of the network characteristics three commonly used sampling methods are available: (1) scanline sampling, (2) window

sampling and (3) circular estimator. These methods can be applied to the entire study area or to specific sampling locations, if parts of the study area are obscured by erosion or vegetation. Hence, the most appropriate sampling method can be used to evaluate the most representative part of a study area.

FraNEP provides the main network statistics, which include the length and strike of each fracture, estimates for fracture density, intensity, mean length and length distribution, and information on the number of censored fractures. Rose diagrams with adjustable strike bin size provide information on fracture strikes and allow a quick classification of fracture sets. The strikes in each bin can be plotted either as their cumulative number or by the sum of their fracture lengths. The evaluation of the fracture length distribution is done either automatically, or by choosing one of three distribution functions (truncated power-law, lognormal and/or exponential). Existing software often uses histograms and probability density plots to describe fracture length distributions. In FraNEP the cumulative distribution function is used to determine the best fit, to avoid problems related to binning.

FraNEP was specifically developed in Visual Basic for Applications in Microsoft Excel™, which makes the program easy-to-use and enables a post-processing of the results without the need to export them to other software. Moreover, the program code is organized in modules, which makes it easy to extend FraNEP to personal and site-specific requirements.

Other software packages, such as those presented in the introduction, or even manual analysis of the Jabal Akhdar study area would have yielded results similar to those obtained with FraNEP. However, different software packages would have been required to characterize fracture networks by means of different sampling methods, whereas a manual analysis would have been very tedious and time-consuming. The advantage of FraNEP is that it offers a complete and easy-to-use combination of characterization techniques and tools. A major novelty is that three commonly used sampling methods are combined into a single software package. Therefore, FraNEP is a time-efficient tool for the characterization of fracture networks.

Acknowledgements

This study was carried out within the framework of DGMK (German Society for Petroleum and Coal Science and Technology) research project 718 "Mineral Vein Dynamics Modelling", which is funded by the companies ExxonMobil Production Deutschland GmbH, GDF SUEZ E&P Deutschland GmbH, RWE Dea AG and Wintershall Holding GmbH, within the basic research program of the WEG Wirtschaftsverband Erdöl- und Erdgasgewinnung e.V. We would like to acknowledge the companies for their financial support, their permission to publish these results and funding of the PhD grant to CZ and postdoctoral grant to EGR. We also would like to thank Franco Corona and Georg Schmitz from ExxonMobil Production Deutschland GmbH for their helpful advice. We are greatful to the helpful comments by the anonymous reviewers.

References

Becker, M. W., 2006. Potential for satellite remote sensing of ground water. Ground Water 44, 306-318. doi:10.1111/j.1745-6584.2005.00123.x

Belayneh, M. W., Matthäi, S. K., Blunt, M. J., Rogers, S. F., 2009. Comparison of deterministic with stochastic fracture models in water-flooding numerical simulations. AAPG Bulletin, 93, 1633-1648. doi:10.1306/07220909031

Berkowitz, B., 2002. Characterizing flow and transport in fractured geological media: A review. Advances in Water Resources 25, 861-884. doi: 10.1016/S0309-1708(02)00042-8

Bernard, S., 2002. Le logiciel MODFRAC: simulation de réseaux de fractures 2D et de l'écoulement associé (MODFRAC: a program for simulating steady-state flow in 2D random fracture networks). Geosciences DEA report (in French). University of Poitiers, France.

Blum, P., Mackay, R., Riley, M. S., Knight, J. L., 2005. Performance assessment of a nuclear waste repository: Upscaling coupled hydro-mechanical properties for far-field transport analysis. Journal of Rock Mechanics and Mining Sciences 42, 781-792. doi: 10.1016/j.ijrmms.2005.03.015

Blum, P., Mackay, R., Riley, M. S., 2009. Stochastic simulations of regional scale advective transport in fractured rock masses using block upscaled hydro-mechanical rock property data. Journal of Hydrology 369, 318-325. doi: 10.1016/j.jhydrol.2009.02.009

Bodin, J., Porel, G., Delay, F., Ubertosi, F., Bernard, S., de Dreuzy, J.-R., 2007. Simulation and analysis of solute transport in 2D fracture/pipe networks: The SOLFRAC program. Journal of Contaminant Hydrology 89, 1-28. doi: 10.1016/j.jeonhyd.2006.07.005

Bonnet, E., Bour, O., Odling, N. E., Davy, P., Main, I., Cowie, P., Berkowitz, B., 2001. Scaling of fracture systems in geological media. Reviews of Geophysics 39, 347-383. doi: 10.1029/1999RG000074

Breton, J.-P., Béchennec, F., Le Métour, J., Moen-Maurel, L., Razin, P. 2004. Eoalpine (Cretaceous) evolution of the Oman Tethyan continental margin: Insights from a structural field study in Jabal Akdhar (Oman mountains). GeoArabia 9, 1-18.

Casas, A. M., Cortés, A. L., Maestro, A., Soriano, M. A., Riaguas, A., Bernal, J., 2000. LINDENS: A program for lineament length and density analysis. Computers and Geosciences 26, 1011-1022. doi: 10.1016/S0098-3004(00)00017-0

Cruden, D. M., 1977. Describing the size of discontinuities. International Journal of Rock Mechanics and Mining Sciences 14, 133-137. doi: 10.1016/0148-9062(77)90004-3

Dershowitz, W. S., Einstein, H. H., 1988. Characterizing rock joint geometry with joint system models. Rock Mechanics and Rock Engineering 21, 21-51. doi: 10.1007/BF01019674

Ekneligoda, T. C., Henkel, H., 2010. Interactive spatial analysis of lineaments. Computers and Geosciences 36, 1081-1090. doi: 10.1016/j.cageo.2010.01.009

FracMan7, 2012. Golder Associates Inc., http://www.golder.com

Glennie, K.W., Boeuf, M.G.A., Hughes-Clarke, M.W., Moody-Stuart, M., Pilaar, W.F.H., Reinhardt, B.M., 1973. Late Cretaceous nappes in Oman Mountains and their geological evolution. AAPG Bulletin 57, 5-27.

Hilgers, C., Kirschner, D. L., Breton, J.-P., Urai, J. L., 2006. Fracture sealing and fluid overpressure in limestones of the Jabal Akhdar dome, Oman mountains. Geofluids 6, 168-184. doi: 10.1111/j.1468-8123.2006.00141.x

Holland, M., Urai, J. L., Muchez, P., Willemse, E. J. M., 2009a. Evolution of fractures in a highly dynamic thermal, hydraulic, and mechanical system - (I) Field observations in Mesozoic Carbonates, Jabal Shams, Oman Mountains. GeoArabia 14, 57-110.

Holland, M., Saxena, N., Urai, J. L., 2009b. Evolution of fractures in a highly dynamic thermal, hydraulic, and mechanical system - (II) Remote sensing fracture analysis, Jabal Shams, Oman Mountains. GeoArabia 14, 163-194.

Kulatilake, P. H. S. W., Wu, T. H., 1984. The density of discontinuity traces in sampling windows (technical note). International Journal of Rock Mechanics and Mining Sciences and Geomechanical Abstracts 21, 345-347.

Lacazette, A., 1991. A new stereographic technique for the reduction of scanline survey data of geologic features. Computers and Geosciences 17, 445-463. doi:10.1016/0098-3004(91)90051-E

LaPointe, P. R., 2002. Derivation of parent population statistics from trace length measurements of fractal populations. International Journal of Rock Mechanics and Mining Sciences 39, 381-388. doi:10.1016/S1365-1609(02)00021-7

Lee, C-H., Farmer, I., 1993. Fluid Flow in Discontinuous Rocks, Chapman & Hall, London, UK, 169pp.

Loague, K., Green, R. E., 1991. Statistical and graphical methods for evaluating solute transport models: Overview and application. Journal of Contaminant Hydrology 7, 51-73. doi: 10.1016/0169-7722(91)90038-3

Lyman, G. J., 2003. Rock fracture mean trace length estimation and confidence interval calculation using maximum likelihood methods. International Journal of Rock Mechanics and Mining Sciences 40, 825-832. doi:10.1016/S1365-1609(03)00043-1

Manzocchi, T., Walsh, J. J., Bailey, W. R., 2009. Population scaling bias in map samples of power-law fault samples. Journal of Structural Geology 31, 1612-1626. doi:10.1016/j.jsg.2009.06.004

Markovaara-Koivisto, M., Laine, E., 2012. MATLAB script for analyzing and visualizing scanline data. Computers and Geosciences 40, 185-193. doi: 10.1016/j.cageo.2011.07.010

Masoud, A. A., Koike, K., 2011. Auto-detection and integration of tectonically significant lineaments from SRTM DEM and remotely-sensed geophysical data. ISPRS Journal of Photogrammetry and Remote Sensing 66, 818-832. doi: 10.1016/j.isprsjprs.2011.08.003

Mauldon, M., 1998. Estimating mean fracture trace length and density from observations in convex windows. Rock Mechanics and Rock Engineering 31, 201-216. doi:10.1007/s006030050021

Mauldon, M., Dunne, W. M., Rohrbaugh Jr., M. B., 2001. Circular scanlines and circular windows: new tools for characterizing the geometry of fracture traces. Journal of Structural Geology 23, 247-258. doi: 10.1016/S0191-8141(00)00094-8

Neuman, S. P., 2005. Trends, prospects and challenges in quantifying flow and transport through fractured rocks. Hydrogeology Journal 13, 124-147. doi: 10.1007/sl0040-004-0397-2

Odling, N. E., Gillespie, P., Bourgine, B., Castaing, C., Chilés, J.-P., Christensen, N. P., Fillion, E., Genter, A., Olsen, C., Thrane, L., Trice, R., Aarseth, E., Walsh, J. J., Watterson, J., 1999. Variations in fracture system geometry and their implications for fluid flow in fractured hydrocarbon reservoirs. Petroleum Geoscience 5, 373-384. doi: 10.1144/petgeo.5.4.373

Pahl, P. J., 1981. Estimating the mean length of discontinuity traces. International Journal of Rock Mechanics and Mining Sciences & Geomechanics Abstracts 18, 221-228. doi: 10.1016/0148-9062(81)90976-1

Pérez-Claros, J. A., Palmqvist, P., Olóriz, F., 2002. First and second orders of suture complexity in ammonites: A new methodological approach using fractal analysis. Mathematical Geology 34, 323-343. doi:10.1023/A:1014847007351

Pickering, G., Bull, J. M., Sanderson, D. J., 1995. Sampling power-law distributions. Tectonophysics 248, 1-20. doi: 10.1016/0040-1951(95)00030-Q

Priest, S. D., Hudson, J. A., 1981. Estimation of discontinuity spacing and trace length using scanline surveys. International Journal of Rock Mechanics and Mining Sciences & Geomechanics Abstracts 18, 183-197. doi: 10.1016/0148-9062(81)90973-6

Priest, S. D., 1993. Discontinuity analysis for rock engineering, Chapman & Hall, London, UK, 473pp. doi: 10.1016/0926-9851(93)90044-Y

Priest, S. D., 2004. Determination of discontinuity size distributions from scanline data. Rock Mechanics and Rock Engineering 37, 347-368. doi:10.1007/s00603-004-0035-2

Riley, M. S., 2005. Fracture trace length and number distributions from fracture mapping. Journal of Geophysical Research, 110. doi: 10.1029/2004JB003164

Rohrbaugh Jr., M. B., Dunne, W. M., Mauldon, M., 2002. Estimating fracture trace intensity, density and mean length using circular scanlines and windows. AAPG Bulletin 86, 2089-2104. doi: 10.1306/61EEDE0E-173E-11D7-8645000102C1865D

Roy, A., Perfect, E., Dunne, W. M., Mckay, L. D., 2007. Fractal characterization of fracture networks: an improved box-counting technique. Journal of Geophysical Research 112, B12201. doi:10.1029/2006JB004582

Spillmann, T., Maurer, H., Willenberg, H., Evans, K. F., Heincke, B., Green, A. G., 2007. Characterization of unstable rock mass based on borehole logs and diverse borehole radar data. Journal of Applied Geophysics 61, 16-38. doi: 10.1016/j.jappgeo.2006.04.006

Terzaghi, R. D., 1965. Sources of error in joint surveys. Géotechnique 13, 287-304. doi: 10.1680/geot.1965.15.3.287

Weiss, M., 2008. Techniques for estimating fracture size: A comparison of methods. International Journal of Rock Mechanics and Mining Sciences, 45, 460-466. doi:10.1016/j.ijrmms.2007.07.010

Wilson, C. E., Aydin, A., Karimi-Farad, M., Durlofsky L. J., Sagy, A., Brodsky E. E., Kreylos O., Kellog, L. H., 2011. From outcrop to flow simulation: Constructing discrete fracture models from a LIDAR survey. AAPG Bulletin 95, 1883-1905. doi: 10.1306/03241108148

Xu, C., Dowd, P., 2010. A new computer code for discrete fracture network modelling. Computers & Geosciences 36, 292-301. doi: 10.1016/j.cageo.2009.05.012

Zeeb, C., Göckus, D., Bons, P. D., AlAjmi, H., Rausch, R., Blum, P., 2010. Fracture flow modelling based on satellite images of the Wajid sandstone, Saudi Arabia. Hydrogeology Journal 18, 1699-1712. doi:10.1007/s10040-010-0609-x

Zeeb, C., Gomez-Rivas, E., Bons, P. D., Blum, P., in press. Evaluation of sampling methods for fracture network characterization using outcrops. AAPG Bulletin